8-2021

Exact and Approximate Relaxation Techniques for Computational Guidance

Sheril Avikkal Kunhippurayil
Utah State University

EXACT AND APPROXIMATE RELAXATION TECHNIQUES FOR COMPUTATIONAL GUIDANCE

by

Sheril Avikkal Kunhippurayil

A dissertation submitted in partial fulfillment
of the requirements for the degree

of

DOCTOR OF PHILOSOPHY

in

Aerospace Engineering

Approved:

Matthew W. Harris, Ph.D. Major Professor	David Geller, Ph.D. Committee Member
Stephen A. Whitmore, Ph.D. Committee Member	Geordie Richards, Ph.D. Committee Member
Randy Christensen, Ph.D. Committee Member	D. Richard Cutler, Ph.D. Interim Vice Provost of Graduate Studies

UTAH STATE UNIVERSITY
Logan, Utah

2021

ABSTRACT

Exact and Approximate Relaxation Techniques for Computational Guidance

by

Sheril Avikkal Kunhippurayil, Doctor of Philosophy

Utah State University, 2021

Major Professor: Matthew W. Harris, Ph.D.
Department: Mechanical and Aerospace Engineering

The focus of this dissertation is in the development and application of relaxation techniques that enable efficient and real-time solution of complex computational guidance problems. Relaxations transform a non-convex constraint into a convex constraint and provides proof that the optimal solutions to the relaxed problem are optimal for the original problem. Unique contributions of this work include: 1) a relaxation technique for solving fixed final time problems between fixed points, 2) a performance analysis on the application of computational guidance for the Mars Ascent Vehicle, and 3) establishment of sufficient conditions for non-singularity of optimal control for problems on a smooth manifold with mixed constraints. The first result states that for annularly constrained linear systems, controllability is a sufficient condition for the problem to be solvable as a sequence of convex programs. The second result applies relaxations to an ascent problem. The third result is the most general result to date for problems with mixed constraints. It uses a minimum principle on manifolds with mixed contraints to analyze the problem in a geometric framework, and shows that strong observability of the dual system is sufficient for non-singularity.

(150 pages)

PUBLIC ABSTRACT

Exact and Approximate Relaxation Techniques for Computational Guidance

Sheril Avikkal Kunhippurayil

The focus of this dissertation is in the development and application of relaxation techniques that enable efficient and real-time solution of complex computational guidance problems. Relaxations transform a non-convex constraint into a convex constraint and provides proof that the optimal solutions to the relaxed problem are optimal for the original problem. Unique contributions of this work include: 1) a relaxation technique for solving fixed final time problems between fixed points, 2) a performance analysis on the application of computational guidance for the Mars Ascent Vehicle, and 3) establishment of sufficient conditions for non-singularity of optimal control for problems on a smooth manifold with mixed constraints. The first result states that for annularly constrained linear systems, controllability is a sufficient condition for the problem to be solvable as a sequence of convex programs. The second result applies relaxations to an ascent problem. The third result is the most general result to date for problems with mixed constraints. It uses a minimum principle on manifolds with mixed contraints to analyze the problem in a geometric framework, and shows that strong observability of the dual system is sufficient for non-singularity.

ACKNOWLEDGMENTS

First and foremost, I thank my adviser Dr. Matthew W. Harris. Dr. Matt has all the traits for an ideal supervisor – he is humble, kind, patient, and approachable. I thank him for sharing his knowledge on optimal control and for constantly pushing me in the right direction. I thank him for the many discussions we had – starting with optimal control, to Indian culture, and to life in general.

I owe an immeasurable debt of gratitude to my mother and father, Amritha and Haridas, for providing me with a great childhood and believing in me as I grew older. I thank my dear sisters – Kavitha, Sangeetha, and Saritha, for their unconditional love and support. I thank my dear wife and companion – Onima, for her love and friendship.

I thank all my wonderful friends for their love, support, and encouragement. Finally, I wish to acknowledge NASA MSFC for supporting this work in part through the grant 80NSSC20M0245.

Sheril Avikkal Kunhippurayil

CONTENTS

LIST OF FIGURES

CHAPTER 1

INTRODUCTION

Optimal control problems arise frequently not only in mechanics and aerospace engineering, but also in areas of management science and economics. Aerospace applications such as autonomous real-time control applications demand real-time optimization, i.e., convergence to a global optimum along with computational efficiency. Problems such as the planetary landing problem or the soft landing problem [1], the rendezvous problem [2], and the path planning problem for unmanned aerial vehicles [3] – all fall under this category.

However, these problems are naturally non-convex and not easy to solve in real-time. In the planetary landing problem, a spacecraft tries to land autonomously on the surface of the planet using thrusters, which produce a force vector that has an upper and non-zero lower bound on its magnitude. The non-zero lower bound makes the set of feasible controls non-convex. Similarly for the rendezvous problem, upper and lower bounds exist for the thrust magnitude resulting in a non-convex feasible set of controls. In the path planning problem for unmanned aerial vehicles, there are upper and lower bounds on the norm of the commanded velocity which makes the problem non-convex. In addition, solving these problems using nonlinear programming techniques can only guarantee convergence to a local optimum and can fail to find a feasible solution unless a feasible initial guess is provided by the user [4].

A computationally effective and practical approach is to transform these non-convex constraints into convex constraints through exact or approximate relaxations. An exact relaxation is the two-stage process of 1) relaxing the non-convex constraint to a convex form and 2) proving that the optimal solution to the relaxed problem is optimal for the original problem. Unlike approximate relaxations, exact relaxations do not involve any system dynamic perturbations. In the context of optimization-based control, exact relaxations were

first introduced by Behçet Açıkmeşe and Scott Ploen in 2007 for fuel optimal planetary landing [1] and they coined the term "lossless convexification" to such relaxations. These relaxations are useful since the relaxed problem can be solved using interior point methods (IPMs) [5–7] and customized IPM solvers [8]. The use of IPM algorithms guarantees convergence to the global optimum in polynomial time, meaning they can be solved in real-time. Current research with customized methods indicates orders of magnitude improvement in computation time [8–10].

Traditional guidance laws have been analytical. They were also simple in the sense that they require nominal algebraic operations for evaluating the closed-form guidance and control laws. However, for complex guidance and control problems that incorporate many state and control constraints, computational guidance offers significant increased capability with a simultaneous reduction in operational costs associated with guidance and control systems [11]. Computational guidance differs from traditional guidance in the sense that the generation of control commands relies extensively on onboard computation and the process of determining these commands is either model-based or data-based such that it does not require a specified reference state or trajectory.

The focus of this dissertation is in the development and application of relaxation techniques which are based in optimal and geometric control theory, and those that enable efficient, real-time solution of complex computational guidance problems. Relaxation techniques and computational guidance were first applied to the Mars landing problem in 2005 by Açıkmeşe and Scott Ploen – then staff members at the Jet Propulsion Laboratory (JPL). The work was extended by Blackmore et al. in 2010 for the case where landing at the desired point was not feasible [12]. Several other landing applications have also been considered [4, 13–15]. Later, the relaxation results were extended for nonlinear systems with annular control constraints [13], and linear systems with annular control contraints and linear state constraints [16]. While these relaxations are extremely powerful, a specific assumption precludes their application to fixed time transfers between fixed points. Also, the results have been proved only for certain specific classes of problems. Hence, many open

questions remain – some of them are listed below.

1. For annularly constrained linear systems,
   (a) Is there a relaxation that is applicable to the problem of fixed time transfer between fixed points?
   (b) If it exists, can the proof be done in finite dimensions?
2. Is computational guidance applicable to the Mars Ascent Problem? What advantages does it offer over traditional guidance schemes?
3. For problems on a smooth manifold with mixed constraints,
   (a) What are the sufficient conditions for non-singularity of optimal control?
   (b) Can singular solutions be characterized as system zeros/zero directions?

Chapters 4, 5, and 6 answer these questions, respectively. Now, we provide a brief description of the upcoming chapters.

Chapter 2: Background and Related Work

This chapter begins with a brief history of optimal control theory followed by its application to the development of analytical and computational guidance laws. The advantages of applying relaxation techniques and convex optimization are also discussed. Finally, a literature survey of the two problems of interest for this dissertation are presented.

Chapter 3: Elements of Optimal Control

This chapter primarily presents the necessary conditions for global optimality for two classes of problems – (i) a basic optimal control problem, and (ii) a problem on a smooth manifold with mixed constraints. The chapter also provides insight into some of the relevant tools from differential geometry.

Chapter 4: Lossless Convexification of Optimal Control Problems with Annular Control Constraints

The chapter presents new lossless convexification results for annularly constrained problems with linear dynamics. The work is unique because it addresses a specific category of problems – fixed time transfer between fixed points, and this was not done before. An attempt to provide the proof for relaxation in finite dimensions and its results are also presented.

Chapter 5: Application to Mars Ascent Guidance

This chapter presents an application of relaxation techniques and computational guidance to the Mars Ascent Vehicle – second stage guidance. The nominal and Monte Carlo performance results are compared to traditional guidance schemes such as Q-guidance (NASA's current choice) and LVLH-guidance (a PEG-like guidance).

Chapter 6: Strong Observability as a Sufficient Condition for Non-Singularity in Optimal Control with Mixed Constraints

This chapter presents sufficient conditions for non-singularity of optimal control for problems defined on a smooth manifold subject to mixed constraints. The results are applicable to time-invariant and time-varying systems, and subsume results of a previous work. The work is unique because it is the most general result to date. Applications to time optimal and fuel optimal problems are also presented. The chapter also provides a discussion on how to characterize singular solutions as zero directions of the system. Note that the zero directions result in zero output everywhere and are related to the observability properties of the system.

Chapter 7: Final Remarks

This chapter discusses some of the related open questions and challenges in the field of relaxations.

CHAPTER 2
BACKGROUND AND RELATED WORK

Optimal control theory is an outgrowth of the calculus of variations with a history stretching back over 360 years. The story begins with Galileo in 1638 when he posed two shape problems: the shape of a heavy chain suspended between two points (the catenary), and the shape of a wire such that a bead sliding along it under gravity traverses the distance between its end points in minimum time (brachistochrone). Galileo's conjectures on the solutions of his two problems were incorrect, and Newton in 1685 was the first to solve a shape problem - the nose shape of a projectile providing minimum drag - though he did not publish the result until 1694 [17]. In 1696, Johann Bernoulli challenged his contemporaries to solve the brachistochrone problem. Five mathematicians responded to the challenge including Johann's elder brother Jakob, Leibnitz, l'Hospital, Tschirnhaus, and Newton. Bernoulli published all their solutions together with his own in 1697 [17]. The competition aroused interest in this type of problem and was followed by a period of activity by a number of mathematicians. In 1744, Euler formulated the problem in general terms as of one finding the curve $x(t)$ over a time interval $a \leq t \leq b$, with given boundary conditions, which minimizes a cost J in integral form. He also stated a first order necessary condition for optimality.

Up to this point the solution techniques had been essentially geometric until in 1755 when Lagrange described an analytical approach, based on perturbations or "variations" of the optimal curve using his "undetermined multipliers" which led directly to Euler's necessary condition – now known as the "Euler-Lagrange equation". Euler readily adopted this approach and renamed the subject as "the calculus of variations" [17].

In 1786, Legendre studied the second variation and came up with a second-order necessary condition for optimality. Legendre derived it for scalar case, but was later extended to

the vector case by Clebsch and is now known as the Legendre-Clebsch condition. Meanwhile, Hamilton through his "principle of least action", had been reformulating the equations of mechanics as a variational principle and he introduced the function – now known as the "Hamiltonian function". These events were followed by contributions from Jacobi, Weierstrass, and Caratheodory until the general problem (now known as the problem of Lagrange) was solved. A notable contribution from Weierstrass are his necessary conditions for strong minima. These conditions were based on the topological fact that an optimal solution must terminate on the boundary of the extended reachable set formed by the competing curves and their integral costs [18]. As such, assumptions on the existence of control variations or normality assumptions were required. However, it was later established that any conditions that operate under these normality assumptions without qualification are not actually necessary [19]. The issue was first resolved in the calculus of variations by McShane in 1939 [20].

In the late 1950s, L. S. Pontryagin and his co-workers came up with the "Maximum Principle". An important novelty of Pontryagin's approach consists of liberating the variations along the optimal curves from the constricting condition that they must terminate at the given boundary. Instead, he considered variations that are infinitesimally near the terminal point and that generate a convex cone of directions locally tangent to the reachable set at the terminal point defined by the optimal trajectory [18]. In addition, an essential advantage of the maximum principle over the classical theorems in calculus of variations is the fact that this principle is applicable for any closed control set in an n-dimensional space, whereas calculus of variations is only applicable to an open set [21]. This set the scene for parameterizing the degrees of freedom implicit in Lagrange problem by considering constraints of the form $\dot{x}(t) = f(t, x(t), u(t))$, where parameters $u(t)$ or "controls" can be chosen at each $t \in (a, b)$, possibly restricted to some control set $\Omega \subset \mathbb{R}^m$, yielding the

optimal control problem:

$$\min \quad J = \int_a^b L(t, x(t), u(t))dt \tag{2.1}$$

$$\text{subj. to} \quad \dot{x}(t) = f(t, x(t), u(t)) \tag{2.2}$$

$$x(a) = x_0 \ , x(b) = x_f \tag{2.3}$$

$$u(t) \in \Omega \tag{2.4}$$

The necessary conditions for optimality for this problem were established by Pontryagin, which were based on the fact that the Hamiltonian that corresponds to the optimal trajectory must be maximal relative to the competing directions [18].

Soon after, the era of lunar exploration began and optimization techniques were heavily applied for developing guidance laws, especially for lunar powered descent. These guidance laws were purely analytical in nature. In 1964, Meditch applied the Pontryagin's maximum principle to develop a minimum fuel thrust program for the terminal phase of a lunar soft landing mission [22]. He proved that no singular solutions existed for the problem and with the help of a switching function, he was able to show that the optimal thrust program consisted of either full thrust from the initiation of the mission until touchdown, or a period of free-fall followed by full thrust until touchdown. In 1967, Hull developed thrust programs for minimum fuel consumption during vertical take-off and landing manuever of a rocket in vacuum which were applicable to an arbitrary central gravitational field [23]. He employed a linear integral technique developed by Miele, which is based on the application of Green's theorem to extremization of linear integrals. Later in 1969, the Apollo Lunar Module landed on the moon using the Apollo powered descent guidance (APDG) law, which is considered one of the many technological innovations of the time that delivered the ultimate success. This guidance law computed a commanded thrust acceleration vector which was defined as a quartic function of time [24]. Using the current position and velocity vector as the initial condition, the coefficients of the quartic polynomial were uniquely determined by meeting the targeted final position, velocity, and thrust acceleration at a specified final

time. Another powered guidance law developed at the same time is the E-guidance law [25], where the commanded thrust acceleration was defined by a linear polynomial of time, and the targeting condition is specified by the final position and velocity at the prescribed final time. Eventually, it was discovered that the E-guidance law is a special case of APDG [26]. Both APDG and E-guidance laws have simple and elegant closed-form solutions, and they still represent a useful technology more than 50 years old.

However, in recent years, with the advances in the computational technology, there is an emerging and accelerating trend to replace these traditional closed-form guidance and control laws with numerical algorithms. This approach was given the name "computational guidance and control" (CG&C) by Ping Lu [11]. In contrast to the traditional guidance and control, CG&C differs in the following: (i) the generation of guidance and control commands relies extensively on onboard computation, often involving iterations, and (ii) the process of determining guidance and control commands is model-based or data-based, and it does not require a specified reference trajectory, gain tuning, or extensive offline mission, or system-dependent designs [11].

Now, to solve an optimal control problem, one could use either the indirect or direct method. The former applies the optimal control theory to derive the necessary conditions and then solve the resulting two-point boundary value problem (TPBVP). The latter discretizes the original continous-time problem into a nonlinear programming (NLP) problem, which is then solved by an NLP algorithm. However, the TPBVP is known to be highly sensitive to initial guesses and NLP problems are non-deterministic polynomial-time hard (NP-hard), which means that the amount of computation required to solve the problem will not be limited by a bound determinable a priori [27]. As a result, convex optimization problems have gained popularity since they are computationally tractable in the sense that they can be solved in polynomial-time with the help of IPMs [6]. An optimal control problem with linear dynamics, affine equality constraints, inequality constraints formed by convex functions, and a convex cost is classified as a convex optimal control problem.

Over the last 15 years, convex optimization has been applied to a wide range of spacecraft applications. These include the application of convex optimization in the Mars precise landing problems with nonconvex constraints on the thrust magnitude [1,12,28,29]. Highly nonlinear problems such as spacecraft rendezvous and proximity operations with the target spacecraft in any Keplerian orbit were solved by successive second order cone programming (SOCP) [2,30,31]. Convex optimization has also found applications in rapidly designing descent trajectories for asteroid landing [32,33].

However, most spacecraft applications are naturally nonconvex. Nonconvexity may arise if the objective function and/or the constraints are nonconvex. One source of convexity is due to nonlinear dynamics which is true for many spacecraft applications. Since optimal control problems are infinite-dimensional, they must be discretized in order to be solved. After descretization, the nonlinear dynamics will become nonlinear algebraic equality constraints and become the major sources of nonconvexity. Hence, a number of techniques were developed to reformulate the nonconvex problem into a convex problem. These include equivalent transformations, change of variables, successive linearization, successive approximation, and relaxations [27].

We define relaxation as the process in which a non-convex constraint is transformed into a convex constraint. Throughout this work, the terms – exact relaxation and lossless convexification are used synonymously. The interest of this research is primarily focused towards relaxing the following two major categories of non-convex problems: (i) problems with annular constraints, and (ii) problems on smooth manifolds with mixed constraints. A brief survey of the existing literature on these specific problems is given in the following subsections.

2.1 Problems with Annular Constraints

Problems with annular constraints are relevant as many guidance problems fall under this category including the rocket landing problem. Rockets with chemical propulsion systems do not perform reliably under a certain thrust level, and hence the guidance system is responsible for generating thrust commands with a magnitude constrained between a

non-zero lower bound and an upper bound. Such constraints introduce nonconvexity to the problem. This problem was first studied by Behçet Açıkmeşe and Scott Ploen in 2007 for Mars entry, descent, and landing [1]. They developed computational guidance schemes for Mars landing, wherein they formulated the problem as a non-convex optimization problem, transformed it to a convex form, and solved it using convex solvers. In 2011, Açıkmeşe and Blackmore presented results for lossless convexification of optimal control problems with a convext cost, linear dynamics, and an annular control constraint [4]. The proof was based on two conditions: system controllability and an orthogonality condition. However, the orthogonality condition prevented the relaxation results to be applied for fixed final time problems between fixed points. A problem discussed in [4] is the planetary soft landing problem, wherein an autonomous spacecraft lands at a prescribed location on the planet surface with zero relative velocity. The constraint set in this problem is non-convex since the magnitude of the control vector is bounded above and below with a non-zero lower bound.

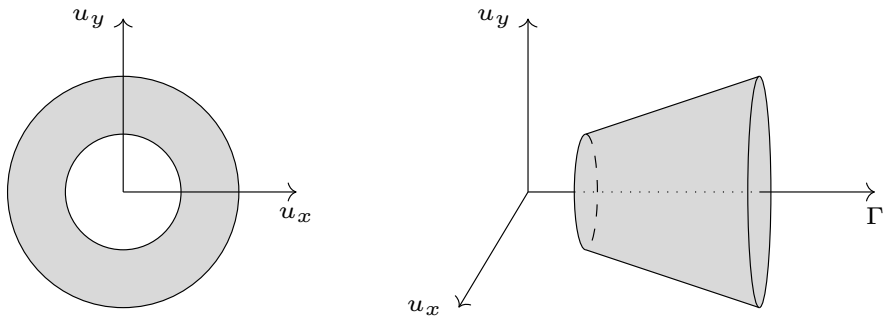

Fig. 2.1: Relaxation of the annular control constraint

The annulus in Figure 2.1 represents the actual non-convex control set in the (u_x, u_y) space. After the relaxation, this non-convex annular space is lifted to a convex cone in the (u_x, u_y, Γ) space, where Γ is a slack variable.

In 2012, Blackmore et al. extended the results for problems with continuous-time nonlinear dynamics and annular control constraints [13]. Here again a controllabilty condition was required for the relaxation and the results were applicable only to free final time prob-

lems. Later in 2014, Harris, and Açıkmeşe presented relaxation results for problems with linear dynamics, annular control constraint, and linear state constraints. For time-varying systems, the proof required the state space be strongly controllable, A-invariant and an orthogonality condition. For time-invariant systems, the state space required to be strongly controllable. Again the results were applicable to free final time problems.

Note that upon relaxation, the resulting convex problem is still an infinite-dimensional optimal control problem. This difficulty is overcome by considering direct numerical methods to compute the optimal solutions, where the original infinite-dimensional control problem is approximated by a finite-dimensional parameter optimization problem, i.e., the problem is discretized in time [34–36]. Since the resulting parameter optimization problem is convex, it can be solved to global optimality in polynomial time with an a priori known upper bound on the number of mathematical operations needed [5, 6, 37].

However, in all of the previous works, the proofs for the relaxation were done for the infinite-dimensional problem and no attempt to provide the same for the discrete-time problem were discussed. Problems with annular constraints are commonly encountered but yet they pose a very specific problem. A more general problem is discussed in the next section.

2.2 Problems on Smooth Manifolds with Mixed Constraints

Problems on smooth manifolds with mixed constraints appear in the real-time control of mechanical and aerospace systems that are highly constrained by operational, environmental, and mission constraints. One such problem is the atmospheric reentry of the space shuttle [38–40]. The problem is challenging because of nonlinear dynamics and a heating constraint. To ensure structural safety of the vehicle during reentry, it is crucial to limit the atmospheric heating on the shuttle wing leading edge. The heating constraint is a mixed constraint that is a function of the states and the control. Another particularly relevant example is that of planetary descent [1, 41]. Consider the scenario wherein a spacecraft is powered with a chemical propulsion system such that the thrust magnitude is constrained between a non-zero lower bound and an upper bound, and the mission requires

the spacecraft to approach the landing site at a specific angle. As noted before, such annular constraints on the thrust levels make the problem non-convex. Also, state constraints such as the glide slope constraint introduce additional complexity to the problem. Another trajectory optimization problem that falls into this category is the rendezvous problem of spacecraft in LEO [2] with a constant altitude constraint.

Optimization problems on manifolds also appear in other fields of engineering – particularly robotics. These include generating collision-free trajectories for quadrotors [42, 43], vision-based trajectory optimization for robots with camera orientation constraints [44, 45], and trajectory planning for free-floating robotic spacecraft [46] to name a few.

In many practical scenarios, it is beneficial to know a priori that the optimum controls to the problem are on the boundary of the control set. This simplifies the controller design, enables relaxations, and helps to choose an appropriate numerical method. In this context, if the controls are not on the boundary, then the solution is said to be singular.

The requirement for non-singularity is related to the idea of lossless convexification. In [16], Harris and Açıkmeşe presented sufficient conditions for non-singularity of optimal control for a particular class of annularly constrained problems. The problem included an annular control constraint, a convex control contraint, and linear state contraints. The problem, however, did not include mixed constraints explicitly. Moreover, the analysis was done in Euclidean space and their method of proof required a specific coordinate representation. The authors utilized the idea of "friends" from linear systems theory [47] to replace the linear state constraint with a mixed constraint. This reformulation was used to arrive at the proof for the relaxation that they introduced in the paper [16].

As such, it would be beneficial to define the problem with mixed constraints in a geometric intrinsic framework using the notion of smooth manifolds and generalize the results of Harris and Açıkmeşe [16] in a coordinate-independent setting. It is also important to note that the proof for lossless convexification in [16] required the system to be strongly controllable on a reduced state space defined by the state constraints.

A closely related idea to strong controllability or strong observability of the system is that of a system zero. The non-existence of zeros, and zero directions is equivalent to strong observability. Also, results from [16] indicate that strongly observable systems do not permit singular solutions. This suggests that the singular solutions can be characterized as zero directions of the system.

2.3 Summary

Optimization problems have been studied for centuries but optimal control was developed in the late 1950s. Starting with the lunar exploration era, a number of analytical guidance laws based on optimal control have been developed including the APDG and the E-guidance laws. However, with the advent of high speed computing, more effecctive computational guidance laws are being developed to exploit the powerful techniques of convex optimization. This relative ease of solving convex problems demanded the need for relaxation techniques.

Açıkmeşe, Ploen, Blackmore, and Harris have made some significant contributions to the field of relaxations. They presented new mathematical results for problems with linear and nonlinear dynamics, nonconvex control constraints, and linear systems evolving on manifolds. However, the results are inapplicable to fixed time problems between fixed points.

Sufficient conditions for non-singularity of optimal control for problems with state constraints defined in Euclidean space have been studied by Harris and Açıkmeşe [16]. However, the results were confined to linear systems evolving on linear manifolds and required a specific coordinate representation.

CHAPTER 3

ELEMENTS OF OPTIMAL CONTROL

3.1 Introduction

This chapter emphasizes the main mathematical results related to optimal control theory which are critical to the development of results presented in this work. The chapter is organized as follows. Section 3.2 introduces the mathematical notation. Section 3.3 describes the basic optimal control problem defined in Euclidean space and states the standard conditions of Pontryagin. Section 3.4 recalls some basic tools from differential geometry concerning flows of vector fields over a smooth manifold which are essential in defining an optimal control problem in a geometric intrinsic framework. Section 3.5 re-interprets the minimum principle in the geometric language of manifolds. Finally, in section 3.6 a problem on a smooth manifold subject to mixed contraints is defined and the necessary conditions for optimality are stated.

3.2 Nomenclature for the Chapter

A function $f \in C^n$ if its first n derivatives exist and are continuous; $\mathbb{R}$ is the set of real numbers; $\mathbb{R}^n$ is the n-dimensional real vector space; Z is the set of positive integers; $||v||$ is the 2-norm of the vector v; a condition is said to hold almost everywhere in the interval $[a, b]$, a.e. $[a, b]$, if the set of points in $[a, b]$ where this condition fails to hold is measure zero; the function $x(\cdot)$ evaluated at t is denoted by $x(t)$; the time derivative of a function is denoted by dx/dt or an overdot as $\dot{x}$; the partial of ϕ with respect to vector $x \in \mathbb{R}^n$ is denoted $\nabla_x \phi$ and is a column vector.

3.3 Basic Optimal Control Problem

In this section, we introduce the basic optimal control problem and state the necessary conditions for global optimality. The primary references for this section are the original

work by Pontryagin [21] and its more recent interpretation by Liberzon [48]. In general, an optimal control problem is one of finding a control trajectory $u(\cdot)$ and an associated state trajectory $x(\cdot)$ such that a given objective or performance index is minimized over a finite time interval $[t_0, t_f]$. A number of different constraints can be imposed on the problem but here we consider a problem with only pure control constraints. Hence we call it the basic optimal control problem (BOCP). The problem is mathematically described below.

$$\begin{aligned} \min \quad & J = \phi(t_f, x_f) + \int_{t_0}^{t_f} \ell(t, x(t), u(t))\, dt \\ \text{subj. to} \quad & \dot{x}(t) = f(t, x(t), u(t)),\ x(t_0) = x_0 \\ & u(t) \in \Omega, \quad \psi(t_f, x_f) = 0. \end{aligned} \tag{BOCP}$$

The system dynamics are described by the ordinary differential equations

$$\dot{x}(t) = f(t, x(t), u(t)), \quad x(t_0) = x_0. \tag{3.1}$$

The system state belongs to the set of absolutely continous functions with $x(t) \in \mathbb{R}^n$. It is assumed that $f(\cdot,\cdot,\cdot) \in \mathcal{C}$ and $f(\cdot,\cdot,\omega) \in \mathcal{C}^1$ for each fixed ω, i.e., it is continuous in all arguments and continuously differentiable with respect to the first and the second. The control input is assumed to belong to the set of bounded measurable functions with $u(t) \in \Omega \subset \mathbb{R}^m$, where Ω is the control constraint set. Both $x(t)$ and $u(t)$ are defined on the interval $[t_0, t_f]$ where t_0 is the initial time, and t_f is the final time. The final time can be free or fixed. The terminal constraint is given by $\psi(t_f, x_f) = 0$. The objective is to minimize the sum of the terminal cost $\phi(t_f, x_f)$ and the running cost $\ell(t, x(t), u(t))$.

Before stating the necessary conditions for optimality, we define the Hamiltonian and the endpoint functions as the following

$$H(t, x, u, p, p_0) = p_0 \ell(t, x, u) + p^T f(t, x, u) \tag{3.2}$$

$$G(t_f, x_f, p_0) = p_0 \phi(t_f, x_f) + \xi^T \psi(t_f, x_f). \tag{3.3}$$

Now we state the necessary conditions for the BOCP.

Theorem 3.1. *Let u be an optimal control and x be the corresponding optimal trajectory. Then there exist a constant $p_0 \in \{0, 1\}$, a function $p : [t_0, t_f] \to \mathbb{R}^n$, and a constant ξ such that the following relations hold almost everywhere in $[t_0, t_f]$:*

(i) *the non-triviality condition*

$$(p_0, p(t)) \neq 0 \quad \forall t \in [t_0, t_f] \tag{3.4}$$

(ii) *the differential equations*

$$\begin{aligned} \dot{x}(t) &= \nabla_p H(t, x, u, p, p_0) \\ \dot{p}(t) &= -\nabla_x H(t, x, u, p, p_0) \end{aligned} \tag{3.5}$$

(iii) *the pointwise minimum condition*

$$u(t) \in \arg\min_{\omega \in \Omega} H(t, x, u, p, p_0), \quad a.e.\ t \in [t_0, t_f] \tag{3.6}$$

(iv) *and, the transversality conditions*

$$\begin{aligned} H(t_f) &= -\nabla_{t_f} G(t_f, x_f, p_0) = -p_0 \nabla_{t_f} \phi(t_f, x_f) - \xi^T \nabla_{t_f} \psi(t_f, x_f) \\ p(t_f) &= \nabla_{x_f} G(t_f, x_f, p_0) = p_0 \nabla_{x_f} \phi(t_f, x_f) + \xi^T \nabla_{x_f} \psi(t_f, x_f). \end{aligned} \tag{3.7}$$

Remark 3.1. *For time-invariant systems, the Hamiltonian is a constant along the optimal trajectory.*

While most optimal control problems can be analyzed in Euclidean space, setting up the problem in a geometric intrinsic framework provides key benefits. Primarily, this elucidates the intrinsic role of the costate and provides a geometric re-interpretation of the minimum principle. As we shall see later in chapter 6, this aids in leveraging geometric control concepts leading to sufficient conditions that are weaker and those that are more easily

satisfied. The next section introduces basic concepts from differential geometry that are essential for setting up the problem in a geometric intrinsic framework and re-interpreting the mininum principle.

3.4 Tools from Differential Geometry

The purpose of this section is to review some basic concepts in differential geometry, thereby introducing notations and fundamental results concerning smooth manifolds and vector fields. These results are standard and well-known, and the reader is encouraged to refer to classical texts such as [49–52] for further details.

3.4.1 Open Sets and Continuous Mappings in $\mathbb{R}^n$

We call a subset $U \subseteq \mathbb{R}^n$ open if for every point $x \in U$, there exist a real number $\epsilon > 0$ such that the open ball $B_\epsilon(x)$ defined by

$$B_\epsilon(x) = \{y \in \mathbb{R}^n : \|x - y\| < \epsilon\} \tag{3.8}$$

is contained in U. If we consider a set $X \subseteq \mathbb{R}^n$, a subset $V \subseteq X$ containing a point $x \in X$ is a neighborhood of x if there is an open subset $U \subseteq V$ with $x \in U$. If V itself is open, we call V an open neighborhood. Now, the collection of all open subsets of X define a topology on X and a set together with a topology is called a topological space. A topological space X is called Hausdorff if any two distinct points in X have open neighborhoods that do not intersect.

Given two topological spaces $X \subseteq \mathbb{R}^n$ and $Y \subseteq \mathbb{R}^m$, a map $f : X \to Y$ is defined to be continuous if for every open set $U \subseteq Y$, the subset $f^{-1}(U)$ is open in X. A continuous map $f : X \to Y$ is a homeomorphism if it is a bijection (one to one and onto) and it's inverse f^{-1} is continuous as well.

A map $f : X \to Y$ is called smooth if for each $x \in X$ there exist an open subset $U \subseteq \mathbb{R}^n$ and a smooth map $F : U \to \mathbb{R}^m$ that coincides with f on all of $X \cap U$, i.e. $F_{X \cap U} = f$. A smooth map $f : X \to Y$ is a diffeomorphism if it is a bijection and its inverse f^{-1} is smooth

as well. Thus, every diffeomorphism is a homeomorphism, but the converse is not true.

3.4.2 The Notion of a Differentiable Manifold

Now we want to introduce the notion of an intrinsic geometry without making reference to an Euclidean space. This leads us to the concept of manifolds which has taken center stage in mathematics, especially in topology and geometry, ever since its introduction in the twentieth century.

Before we introduce the notion of a differentiable manifold, we recall the definition for a topological manifold X of dimension k. It is a topological space which is Hausdorff, has a countable basis with an open covering $X = \bigcup_{\alpha \in Z} U_\alpha$, and corresponding coordinate maps $\varphi_\alpha : U_\alpha \to \varphi_\alpha(U_\alpha)$ which are homeomorphisms of U_α to open subsets $\varphi_\alpha(U_\alpha) \subset \mathbb{R}^k$. The pair $(U_\alpha, \varphi_\alpha)$ is called a coordinate chart or a coordinate neighborhood. A family of such charts $\mathscr{U} = \{(U_\alpha, \varphi_\alpha)\}$ whose domain covers X is called an atlas for X.

To each point q that lies in a coordinate neighborhood (U, φ), we assign the k coordinates $x_1(q), ..., x_k(q)$ of its image $\varphi(q)$ in $\mathbb{R}^k$, where each $x_i(q)$ is a real-valued function on U. If q lies also in a second coordinate neighborhood (V, ψ), then it has coordinates $y_1(q), ..., y_k(q)$ in this neighborhood. Figure 3.1 shows the coordinate neighborhoods (U, φ) and (V, ψ) on a two-dimensional sphere (S^2). Since φ and ψ are homeomorphisms, the function

$$\psi \circ \varphi^{-1} : \varphi(U \cap V) \to \psi(U \cap V) \tag{3.9}$$

defines a homeomorphism with the domain and range being the two open subsets of $\mathbb{R}^k$ which corresponds to the points of $U \cap V$ by the two coordinate maps φ and ψ respectively. In coordinates, $\psi \circ \varphi^{-1}$ is given by continuous functions

$$y_i = h_i(x_1, ..., x_k), \quad i = 1, ..., k, \tag{3.10}$$

giving the y-coordinates of each $q \in U \cap V$ in terms of its x-coordinates. Similarly, $\varphi \circ$

ψ^{-1} gives the inverse mapping which expresses the x-coordinates as functions of the y-coordinates

$$x_i = g_i(y_1, ..., y_k), \quad i = 1, ..., k. \tag{3.11}$$

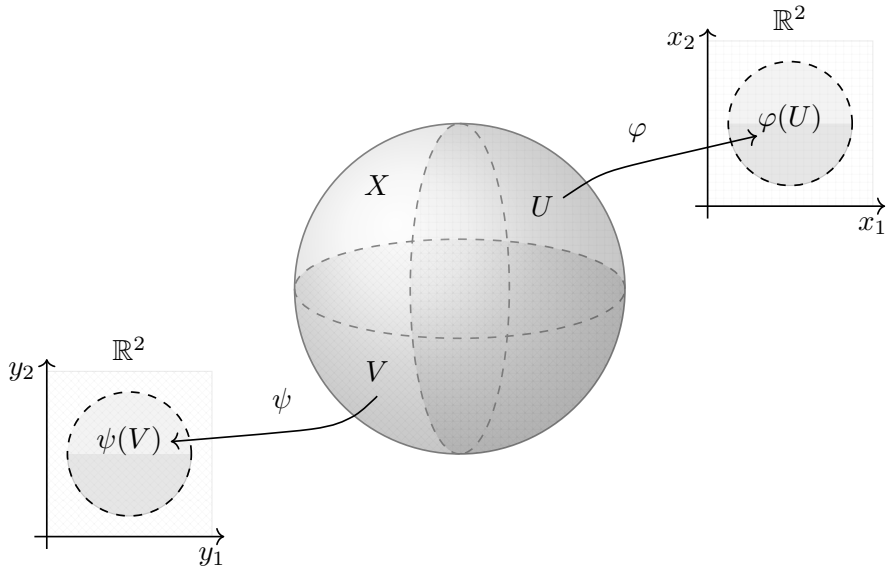

Fig. 3.1: The open sets U (right hemisphere) and V (lower hemisphere) on S^2 are mapped onto open discs $\varphi(U)$ and $\psi(V)$ in $\mathbb{R}^2$ through the coordinate maps φ and ψ respectively

The fact that $\psi \circ \varphi^{-1}$ and $\varphi \circ \psi^{-1}$ are homeomorphisms and are inverse to each other is equivalent to the continuity of $h_i(x)$ and $g_j(y)$, together with the identities

$$\begin{aligned} h_i(g_1(y), ..., g_k(y)) &= y_i, \quad i = 1, ..., n, \\ g_j(h_1(x), ..., h_k(x)) &= x_j, \quad j = 1, ..., n. \end{aligned} \tag{3.12}$$

Thus, every point of a topological manifold X lies in a collection of coordinate neighborhoods, but whenever two neighborhoods intersect, we have continuous functions $h_i(x)$ and $g_j(y)$, also known as transition functions, that give the change of coordinates. The basic idea that leads to differentiable manifolds is to try to select a family or subcollection of neighborhoods so that the change of coordinates is always given by differentiable functions.

We call two neighborhoods (U, φ) and (V, ψ) smooth-compatible or $\mathcal{C}^\infty$-compatible if $U \cap V$ nonempty implies that the functions $h_i(x)$ and $g_j(y)$ are $\mathcal{C}^\infty$. This is equivalent to requiring $\psi \circ \varphi^{-1}$ and $\varphi \circ \psi^{-1}$ to be diffeomorphisms of the open subsets $\varphi(U \cap V)$ and $\psi(U \cap V)$ of $\mathbb{R}^k$. Therefore, a differentiable manifold or smooth manifold is a topological manifold if for the atlas $\mathscr{U} = \{(U_\alpha, \varphi_\alpha)\}$, the transition functions are diffeomorphisms of their corresponding open sets in $\mathbb{R}^k$. Hereafter, we will use X to denote a smooth manifold of dimension k.

3.4.3 Tangent and Cotangent Spaces

With the above notion of a smooth k-dimensional manifold X, we can now define the tangent space and cotangent space attached to a point $q \in X$. Before doing so, we recall differentiable functions and mappings on smooth manifolds.

A function $f : X \to \mathbb{R}$ is called differentiable if for all coordinate maps $\varphi : U \to \varphi(U)$, we have $f \circ \varphi^{-1} : \varphi(U) \to \mathbb{R}$ to be a C^∞ function defined on the open set $\varphi(U) \subset \mathbb{R}^k$.

Consider a smooth manifold Y of dimension l. A mapping $F : X \to Y$ is called smooth if for every $q \in X$, there exist coordinate neighborhoods (U, φ) of q and (V, ψ) of $F(q)$ with $F(U) \subset V$ such that $\psi \circ F \circ \varphi^{-1} : \varphi(U) \to \psi(V)$ is $\mathcal{C}^\infty$.

Tangent Spaces

Intuitively, a tangent vector at a point $q \in X$ can be considered as a derivative operator or derivation acting on a locally defined $\mathcal{C}^\infty$ function around q. To make this connection evident, we define a curve θ lying in X and passing through q as a differentiable mapping $\theta(t) : (-\epsilon, \epsilon) \to X$ with $\epsilon > 0$ and $\theta(0) = q$, and $\mathcal{C}^\infty(q)$ as the set of $\mathcal{C}^\infty$ functions locally defined around q. Now, the tangent vector to the curve θ at $t = 0$ is a function given by $\dot{\theta}(0) = \zeta : \mathcal{C}^\infty(q) \to \mathbb{R}$, such that

$$\zeta(f) = \frac{d}{dt}(f \circ \theta)\Big|_{t=0} \tag{3.13}$$

where $f \in \mathcal{C}^\infty(q)$. The space of all tangent vectors at q gives the tangent space of X at q,

denoted by T_qX (see Figure 3.2). More formally, we define the tangent space T_qX to be the set of all mappings $\zeta : \mathcal{C}^\infty(q) \to \mathbb{R}$ satisfying for all $\alpha, \beta \in \mathbb{R}$ and $f, g \in \mathcal{C}^\infty(q)$ the two conditions

$$\zeta(\alpha f + \beta g) = \alpha(\zeta f) + \beta(\zeta g) \quad \text{(linearity)}, \tag{3.14}$$

$$\zeta(fg) = (\zeta f)g(q) + f(q)(\zeta g) \quad \text{(Leibniz rule)}. \tag{3.15}$$

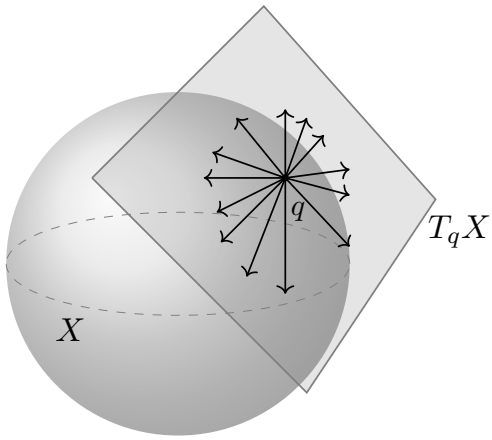

Fig. 3.2: Tangent space at q of S^2

Lemma 3.1. *T_qX is a k-dimensional space, i.e., dim(T_qX)=dim(X).*

Proof. Consider a coordinate chart (U, φ) such that $q \in U$ and $\varphi(q) = x_0$. Let the coordinates of the map φ be $x_1(q), ..., x_k(q)$ which are real valued functions in U. Then, we know that $\forall f \in \mathcal{C}^\infty(q)$, there exist a function $\hat{f} = f \circ \varphi^{-1} : \varphi(U) \to \mathbb{R}$ which expresses f in local coordinates relative to (U, φ). Let $\theta(t) : (-\epsilon, \epsilon) \to U$ be a curve in U with $\theta(0) = q$ and let

$\varphi \circ \theta(t) = (x_1(t), ..., x_k(t))$. Then,

$$\begin{aligned}
\zeta(f) &= \frac{d}{dt}(f \circ \theta)\Big|_{t=0} \\
&= \frac{d}{dt}((f \circ \varphi^{-1}) \circ (\varphi \circ \theta))\Big|_{t=0} \\
&= \frac{d}{dt}(\hat{f}(x_1(t), ..., x_k(t)))\Big|_{t=0} \\
&= \dot{x}_1(0)\frac{\partial \hat{f}}{\partial x_1}\Big|_{x_0} + ... + \dot{x}_k(0)\frac{\partial \hat{f}}{\partial x_k}\Big|_{x_0}.
\end{aligned}$$

Let $\frac{\partial f}{\partial x_i}\Big|_q = \frac{\partial \hat{f}}{\partial x_i}\Big|_{x_0} : \mathcal{C}^\infty \to \mathbb{R}$ be the differentiation with respect to the i^{th} coordinate using the coordinate chart (U, φ). Then, the tangent vector at q given by

$$\zeta(\cdot) = \dot{x}_1(0)\frac{\partial(\cdot)}{\partial x_1}\Big|_q + ... + \dot{x}_k(0)\frac{\partial(\cdot)}{\partial x_k}\Big|_q, \tag{3.16}$$

is a linear combination of the terms $\frac{\partial}{\partial x^i}\Big|_q$. These gradients are linearly independent since $\frac{\partial}{\partial x_i}\Big|_q x^j = \delta_{ij}$. Therefore, the tangent space T_qX is a k-dimensional space spanned by $\left\{\frac{\partial}{\partial x_i}\Big|_q\right\}$, where $i = 1, ..., k$. □

Remark 3.2. *The basis* $\left\{\frac{\partial}{\partial x_i}\Big|_q\right\}$ *to the tangent space* T_qX *at* q *depends on the selection of the coordinate neighborhood that contains* q*. In other words, to each coordinate neighborhood* (U, φ) *on* X*, there corresponds a natural basis* $\frac{\partial}{\partial x_1}\Big|_q, ..., \frac{\partial}{\partial x_k}\Big|_q$ *for every* $q \in U$*.*

A concept closely tied to the idea of tangent spaces is that of a vector field. Before defining a vector field, we introduce the tangent bundle. Loosely speaking, the tangent bundle of X is the union of tangent spaces attached to every $q \in X$, given by

$$TX := \bigcup_{q \in X} T_qX. \tag{3.17}$$

More precisely, we define the tangent bundle as follows. Let $\pi : TX \to X$ be the projection function. Now, TX is a tangent (vector) bundle if $\forall\, q \in X$,

(i) $\pi^{-1}(q)$ has a vector space structure,

(ii) there exist a local trivialization, i.e., an open neighborhood U such that the map $g_U : \pi^{-1}(U) \to U \times \mathbb{R}^k$ is a diffeomorphism, and the restriction of g at q, given by $g_q : \pi^{-1}(q) \to \mathbb{R}^k$ is an isomorphism of vector spaces.

The local trivialization of TX over the open set U is analogous to choosing k local sections s_i such that $\{s_i(q)\}$ form a basis for $\pi^{-1}(q)\ \forall\ q \in U$. A section is a continuous map $F : U \to \pi^{-1}(q)$ such that $\forall\ q \in U,\ \pi \circ F(q) = q$. Finally, we define a vector field on X as every smooth section of the tangent bundle, i.e., every smooth function $F : X \to TX$ such that $F(q) \in T_qX$.

Cotangent Spaces

The cotangent space to X at q, denoted by T_q^*X, is the dual space to T_qX. It is a vector space of dimension k and is defined as the set of all linear mappings $\sigma_q : T_qX \to \mathbb{R}$. The elements of a cotangent space are called cotangent vectors, or simply covectors.

Recall that tangent vectors are linear functions mapping locally defined functions at q, i.e., $\mathcal{C}^\infty(q)$ to real numbers. Now, cotangent vectors are linear functions mapping tangent vectors to real numbers. Therefore, cotangent spaces can be considered as an equivalence class of local functions whose directional derivative with respect to any tangent vector is the same, i.e., $T_q^*X = \mathcal{C}^\infty(q)/\sim$, where $f \sim g$ if and only if $\zeta f = \zeta g\ \ \forall\ \zeta \in T_qX$.

We write the equivalence class of $f \in \mathcal{C}^\infty(q)$ in T_q^*X by df, called the differential of f. This matches with $f : U \to \mathbb{R}$ and $df\Big|_q = f_*\Big|_q : TqX \to \mathbb{R}$ for differential of smooth mappings, where f_* denotes the push forward. The dual basis for $\left\{\frac{\partial}{\partial x_i}\right\}$ of T_qX is $\{dx_i\}$ such that $dx_i\big(\frac{\partial}{\partial x_j}\big) = \frac{\partial}{\partial x_j}x_i = \delta_{ij}$. We also define the cotangent bundle as the union

$$T^*X := \bigcup_{q \in X} T_q^*X \tag{3.18}$$

Combining the local coordinates $x_1, ..., x_k$ on X with local coordinates on T_q^*X relative to the basis $dx_1, ..., dx_k$, we obtain the local coordinates on the cotangent bundle T^*X known

as canonical coordinates.

Finally, we define the Hamiltonian H as any arbitrary smooth function on the contangent bundle. Then the differential dH of the Hamiltonian gives a covector on T^*X at each point. To each such covector, we can then associate a tangent vector at each point of T^*X. Doing so, we obtain a vector field on T^*X, called the Hamiltonian vector field.

3.5 Re-interpreting the Minimum Principle

The purpose of this section is to reformulate our optimal control problem and the minimum principle (Theorem 3.1) in the geometric language of manifolds. Besides providing a higher level of generality, it clarifies the intrinsic meaning of the adjoint vector (costate), thereby elucidating the essence of minimum principle even in the familiar setting of problems in $\mathbb{R}^n$.

Consider the control system given by

$$\dot{x}(t) = f(t, x(t), u(t)) \tag{3.19}$$

whose state $x(t)$ evolves on a k-dimensional manifold X and whose control $u(t)$ takes values in some control set Ω. For its solution $x(\cdot)$ to evolve in X, the velocity vector must be tangent to X. Hence, we see that the state vector evolves in X while the velocity vector evolves in the tangent bundle TX. Therefore, we define the continuous mapping $f : \mathbb{R} \times X \times \mathbb{R}^m \to TX$ as a vector field on X such that $f(t, x(t), u(t)) \in T_{x(t)}X$, and which is smooth with respect to $(t, x(t))$.

Remark 3.3. *To be coherent, hereafter, we denote a point on the manifold by $x(t)$, as opposed to q, used in the preceding section.*

Now we want to determine the space that the costate $p(t)$ belongs to. Refering to our earlier definition of the Hamiltonian (Eq. 3.2), $p(t)$ appears in an inner product with the vector field $f(\cdot, \cdot, \cdot)$. Thus, we see that the intrinsic role of the costate $p(t)$ is that of a covector and hence, it should belong to the cotangent space. This becomes clear as we analyze how covectors propagate along a flow induced by a dynamical system on X.

Let $\tau > 0$ and $\Phi_\tau : X \to X$ be a $\mathcal{C}^1$ map that is obtained by flowing forward for τ units of time along the trajectory of the system (Eq. 3.5) corresponding to some fixed control $u(\cdot)$. First, we discuss the transformation that Φ_τ induces on tangent vectors. Let $x(t) \in X$ and ζ be a tangent vector at $x(t)$. We know that ζ is tangent to some curve $\theta(\alpha)$ in X passing through $x(t)$, such that $\theta(0) = x(t)$. The image $\Phi_\tau(\theta(\cdot))$ of this curve under the map Φ_τ is a curve in X, which passes through $\Phi_\tau(x(t))$, as illustrated in Figure 3.3. Define the tangent vector at $\Phi_\tau(x(t))$ associated with this new curve as

$$d\Phi_\tau|_{x(t)}(\zeta) = \frac{d}{d\alpha}\Big|_{\alpha=0}(\Phi \circ \theta) \tag{3.20}$$

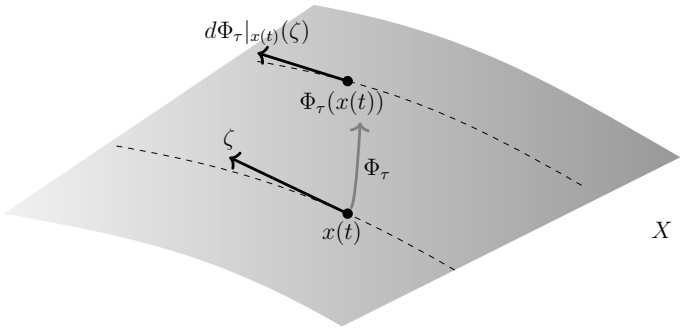

Fig. 3.3: Tangent vectors propagating forward

The above quantity depends only on the vector ζ and not on the choice of a particular curve $\theta(\cdot)$. Therefore, we obtain a linear map

$$d\Phi_\tau|_{x(t)} : T_{x(t)}X \to T_{\Phi_\tau(x(t))}X \tag{3.21}$$

called the derivative or differential of Φ_τ at $x(t)$. We see that the derivative map $d\Phi_\tau$ pushes the tangent vectors forward in the direction of action of the original map Φ_τ on X. The infinitesmal transformation induced by $d\Phi_\tau$ is the variational equation given below, which

arises in the proof of the minimum principle.

$$\dot{\zeta} = f_x \zeta \tag{3.22}$$

where f_x is calculated along the optimal trajectory.

Now we consider the case of a covector, denoted by $p|_{x(t)}$ such that $p|_{x(t)}(\zeta) \in \mathbb{R}$ for each $\zeta \in T_{x(t)}X$. For the same map $\Phi_\tau : X \to X$, we try to define a linear function $p|_{\Phi_\tau(x(t))}$ on $T_{\Phi_\tau(x(t))}X$. In order to do so, we need to assign a value $p|_{\Phi_\tau(x(t))}(\eta)$ for every $\eta \in T_{\Phi_\tau(x(t))}X$. We could assume that $p|_{\Phi_\tau(x(t))}(\eta)$ equals the value of $p|_{x(t)}$ on the preimage of η under the map Φ_τ. However, this preimage is not well defined unless the map Φ_τ is invertible. Therefore, there is no apparent candidate map for propagating covectors along Φ_τ similarly to how the derivative map $d\Phi_\tau$ acts on tangent vectors. Therefore, we need to pull covectors back, i.e., given a covector $p|_{\Phi_\tau(x(t))}$ on $T_{\Phi_\tau(x(t))}X$, define a covector $p|_{x(t)}$ on $T_{x(t)}X$ by

$$p|_{x(t)}(\zeta) := p|_{\Phi_\tau(x)}(d\Phi_\tau|_{x(t)}(\zeta)) \tag{3.23}$$

Also note that the adjoint equation $\dot{p}(t) = -(f_x)^T p(t)$ is the infinitesmal version of Eq.3.5 written in local coordinates. Finally, we define the Hamiltonian as

$$H(t, x(t), u(t), p(t)) = p|_{x(t)}(f(t, x(t), u(t))). \tag{3.24}$$

This further aligns with our earlier statement of the Hamiltonian being a function on the cotangent bundle.

3.6 Optimal Control Problem on a Smooth Manifold with Mixed Constraints

In this section, we define an optimal control problem on a smooth manifold with mixed constraints. Due to the mixed constraints and the manifold, the standard result of Pontryagin [21] is inapplicable. The necessary conditions stated here have been derived by Bonalli [53]. This was done by embedding the manifold and the related vector fields into an Euclidean space of appropriate dimension and subsequently exploiting a maximum principle

theorem for problems with mixed constraints by Dmitruk [54].

We define the problem as the following

$$\begin{aligned} \min \quad & J = \phi(t_f, x_f) + \int_{t_0}^{t_f} \ell(u(t))\, dt \qquad \text{(OCPMC)} \\ \text{subj. to} \quad & \dot{x}(t) = f(t, x(t), u(t)),\ x(t_0) = x_0 \\ & h_e(t, x(t), u(t)) = 0,\ h_i(t, x(t), u(t)) \leq 0 \\ & \psi(t_f, x_f) = 0. \end{aligned}$$

A number of technical assumptions on the problem data must be made such as smoothness [53]. Note that the system evolves intrinsically on the manifold X, i.e., the dynamics are given by the function $f : \mathbb{R} \times X \times \mathbb{R}^m \to TX$. Furthermore, the control constraints must satisfy a rank condition so that they are regular and the non-triviality condition can be strengthened [55, 56].

Before stating the principle, we define the Hamiltonian, Lagrangian, and endpoint functions as the following

$$H(t, x, u, p, p_0) = p_0 \ell(u) + p^T f(t, x, u) \tag{3.25}$$

$$L(t, x, p, u, p_0, \nu_h, \nu_k) = H(t, x, u, p, p_0) + \nu_{h_e}^T h_e(t, x, u) + \nu_{h_i}^T h_i(t, x, u) \tag{3.26}$$

$$G(t_f, x_f, p_0) = p_0 \phi(t_f, x_f) + \xi^T \psi(t_f, x_f). \tag{3.27}$$

Theorem 3.2. *Let u be an optimal control and x be the corresponding optimal trajectory. Then, there exist a constant $p_0 \geq 0$, an absolutely continuous curve $p : [t_0, t_f] \to T^*X$ for which $p(t) \in T^*_{x(t)}X$ and $(p_0, p(t)) \neq 0$, bounded functions with $\nu_{h_e}(t) \in \mathbb{R}^{r_{h_e}}$ and $\nu_{h_i}(t) \in \mathbb{R}^{r_{h_i}}$ where $\nu_{h_i} \geq 0$ such that the following relations hold almost everywhere in $[t_0, t_f]$:*

(i) *the differential equations*

$$\begin{aligned} \dot{x}(t) = &\quad \nabla_p L(t, x, p, u, p_0, \nu_{h_e}, \nu_{h_i}) \\ \dot{p}(t) = &-\nabla_x L(t, x, p, u, p_0, \nu_{h_e}, \nu_{h_i}) \end{aligned} \tag{3.28}$$

(ii) *the Hamiltonian minimum condition*

$$H(t, x, u, p, p_0) \leq H(t, x, \omega, p, p_0) \tag{3.29}$$

for every admissible ω.

(iii) *the stationary condition*

$$\nabla_u L(t, x, p, u, p_0, \nu_{h_e}, \nu_{h_i}) = 0 \tag{3.30}$$

(iv) *the complementary slackness condition*

$$\nu_{h_i}^T h_i(t, x, u) = 0 \tag{3.31}$$

(v) *the transversality conditions*

$$p_f - p_0 \nabla_{x_f} \phi(t_f, x_f) \ \perp \ T_{x_f} X_f \tag{3.32}$$

and, if the final time t_f *is free,*

$$H(t_f, x_f, u_f, p_f, p_0) = -p_0 \nabla_{t_f} G(t_f, x_f, p_0) \tag{3.33}$$

The transversaility conditions stated above can also be written in the form

$$\begin{aligned} H(t_f) &= -p_0 \nabla_{t_f} \phi(t_f, x_f) - \xi^T \nabla_{t_f} \psi(t_f, x_f) \\ p(t_f) &= \ \ p_0 \nabla_{x_f} \phi(t_f, x_f) + \xi^T \nabla_{x_f} \psi(t_f, x_f). \end{aligned} \tag{3.34}$$

3.7 Summary

The chapter began with the introduction of a basic optimal control problem and stating its necessary conditions for optimality. Some of the important tools from differential geometry such as the notion of a smooth manifold, tangent and cotangent spaces, and vector fields were then introduced. This was followed by a re-interpretation of the minimum principle in the geometric language of manifolds. Finally, the necessary conditions for problems on smooth manifolds subject to mixed constraints were stated.

CHAPTER 4
LOSSLESS CONVEXIFICATION OF OPTIMAL CONTROL PROBLEMS WITH ANNULAR CONTROL CONSTRAINTS

4.1 Introduction

This chapter analyzes a class of optimal control problems with an annular control constraint. Annular control constraints appear in many real-time control applications that involve systems with complex actuator models – particularly in the entry, descent, and landing of spacecraft with chemical thrusters [1, 12, 41, 57]. Chemical thrusters fail to operate reliably under a certain thrust level, thereby introducing a non-zero lower bound on the thrust magnitude. This lower bound is non-convex, and as such, the resulting trajectory optimization problems are difficult to solve. Existing nonlinear programming based trajectory optimization methods do not guarantee convergence to solutions (optimal or feasible) making them inappropriate for real-time applications. If, however, the problem can be written in a convex form, then powerful interior point methods can be customized to find globally optimal solutions in polynomial-time. This is the approach taken by SpaceX in their rocket landings [58].

The term lossless convexification refers to the two-stage process of 1) relaxing the annular, non-convex constraint to a convex form and 2) proving optimal solutions for the relaxed problem are also optimal for the original problem. These relaxation techniques have been studied extensively for annularly constrained linear systems [4], nonlinear systems [13], and linear systems with explicit state constraints and additional control inequalities [16]. Each of these proofs requires an assumption on the gradient of the final point. In general, the assumption cannot be verified a priori since it depends on the optimal solution. However, one special case where it can be verified a priori is the free final time transfer between fixed points, which is assumed directly in [13]. The proofs also have in common controllabil-

ity/observability assumptions. In [4], controllability of the linear system (observability of the dual system) is assumed. In [13], controllability of the system linearized about each extremal is assumed. In [16], strong controllability is assumed.

As noted before, the primary motivation for this work is real-time optimization. Within the domain of spaceflight, the real-time calculation of trajectories is called guidance. Traditional guidance algorithms, dating back to the 1950s, are simple and analytical in nature. Examples include Apollo lunar descent guidance [24–26, 59], the Iterative Guidance Mode (IGM) for Saturn V ascent [60, 61], and Powered Explicit Guidance (PEG) for Shuttle [62, 63]. However, with improved computing power and algorithms, computational guidance laws (especially ones based on convex optimization) are becoming popular [2, 11, 27, 30, 32, 33, 64]. Notably, in the last few decades, the computational speed-up due to algorithmic advances exceeds that due to hardware improvements by a factor of two for some problem classes [65]. Within a computational guidance framework, more difficult problems involving systems with practical limitations or constraints can be solved such as the powered rocket landing problem with velocity bounds [29], problems with linear state constraints [14], problems with quadratic state constraints [15], and problems with integer-type control constraints [66, 67].

Even when the problem can be rendered convex, customization is required to accelerate solve times [8–10] to levels sufficient for use onboard radiation-hardened flight processors. These customizations exploit problem structure, sparsity, and memory allocation. The efficacy of this relax and customize approach to the problem of powered rocket landing has been successfully demonstrated through bench testing on a flight computer [68], flights tests [69–71], and the SpaceX landings [58]. Regarding the flight computer tests [68], tests were carried out on a 200 MHz RAD750 in the flight software testbed at NASA JPL. Solution times of milliseconds on a 3.4 GHz desktop processor corresponded to solution times of approximately one second on the flight computer with customized code, which is considered appropriate for a real-time guidance, navigation, and control system. During testing and simulation for the above demonstrations, it was observed that the relaxations

work even at times that are not the fuel optimal times. This observation and the removal of the assumption on the gradient of the final point motivate the results of this work.

To briefly summarize the previous theoretical results: In [4], the sufficient condition for convexification required two assumptions: system controllability (Condition 1 of their paper) and an orthogonality condition on the gradient of the final point (Condition 2 of their paper). *These assumptions preclude convexification for fixed final time problems between fixed points.*

In [13], free final time problems were considered as well as a controllability condition (Condition 1 of their paper). *These assumptions preclude convexification for fixed final time problems between fixed points.*

In [16], linear systems evolving on a linear manifold were considered. For time-invariant systems with free final time, a strong controllability assumption was made (Criterion 1.i of their paper). For time-varying systems, assumptions on strong controllability and the gradient of the final point were made (Criterion 1.ii of their paper). *These assumptions preclude convexification for fixed final time problems between fixed points.*

To summarize, the three most significant theoretical contributions involve a controllability condition plus a second condition (at the final point or free final time). A key result of this work is that for time-invariant systems the second condition is not needed (within the setting of [4]). Moreover, since controllable systems are dense in the space of LTI systems, uncontrollable systems can be 'approximately convexified.' The main contributions of the work are:

1. Conditions for the standard convexification to hold that are applicable to both free and fixed final time problems (see Theorem 4.1, Corollary 4.2, and Theorem 4.2).

2. A sufficient condition for the standard convexification to hold for all final times between the minimum time and optimal time (see Theorem 4.3).

3. Establishment of controllability as a sufficient condition for solving the general fixed time problem as a sequence of convex programs (see Theorem 4.4).

The remainder of the chapter is organized as follows. Section 4.2 introduces the mathematical notation. Section 4.3 describes the problem of interest, which is an optimal control problem with an annular control constraint. Section 4.4 provides the mathematical analysis of the problem. The main result of the paper is presented in Section 4.5, which proves controllability to be a sufficient condition for solving fixed final time and fixed end point problems. The section also provides a brief background on reachable sets and minimum time problems. Section 4.6 describes the numerical solution procedure. Section 4.7 illustrates the application of the new convexification results to some standard problems in optimal control. A Mars powered descent guidance example is also presented. In section 4.8, an attempt to provide the proof for relaxation in finite dimensions is presented. Finally, Section 4.9 concludes the chapter.

4.2 Nomenclature for the Chapter

The following is a partial list of notation used; a function $f \in C^n$ if its first n derivatives exist and are continuous; $\mathbb{R}$ is the set of real numbers; $\mathbb{R}^n$ is the n-dimensional real vector space; $||v||$ is the 2-norm of the vector v; a condition is said to hold almost everywhere in the interval $[a, b]$, a.e. $[a, b]$, if the set of points in $[a, b]$ where this condition fails to hold is measure zero; the time derivative of a function is denoted with an over-dot, i.e. $dx(t)/dt = \dot{x}(t)$; the boundary of a set S is denoted by ∂S, and the interior of the set by int$S$. The open ball centered at p with radius r is $B_r(p)$.

4.3 Problem Description

The primary problem of interest is that of minimizing the control effort required to transfer a linear time-invariant system between fixed points subject to an annular control

constraint. The problem is described mathematically below in P0.

$$\begin{aligned} \min \quad & J = \textstyle\int_{t_0}^{t_f} \ell(g(u(t)))\, dt \\ \text{subj. to} \quad & \dot{x}(t) = Ax(t) + Bu(t) \\ & x(t_0) = x_0, \;\; x(t_f) = x_f \\ & u(t) \in U_0 = \{\omega : 0 < \rho_1 \leq g(\omega) \leq \rho_2\} \end{aligned} \tag{P0}$$

The initial time is t_0. The final time is t_f. The system state $x : [t_0, t_f] \to \mathbb{R}^n$ belongs to the set of absolutely continuous functions. The control $u : [t_0, t_f] \to U_0 \subset \mathbb{R}^m$ belongs to the set of bounded measurable functions with $\rho_1, \rho_2 \in \mathbb{R}$. The objective is to minimize the control effort given by $\ell : [\rho_1, \rho_2] \to \mathbb{R}$ where $g : \mathbb{R}^m \to \mathbb{R}$. The system dynamics are described by the linear differential equations where A and B are constant matrices. It is assumed that g is convex and that ℓ is convex, strictly increasing, and positive on its domain. The objective function is then convex. For the moment, the final time can be free or fixed. The least final time for which the problem is feasible is called the minimum time. The final time for which P0 achieves a global minimum is called the optimal time. The primary challenge in solving P0 is the non-convex control constraint U_0.

The problem P1 below is the standard relaxation of P0. It is obtained by introducing a new variable Γ and reformulating the control constraint.

$$\begin{aligned} \min \quad & J = \textstyle\int_{t_0}^{t_f} \ell(\Gamma(t))\, dt \\ \text{subj. to} \quad & \dot{x}(t) = Ax(t) + Bu(t) \\ & x(t_0) = x_0, \;\; x(t_f) = x_f \\ & (u(t), \Gamma(t)) \in U_1 = \{(\omega, \Omega) : \rho_1 \leq \Omega \leq \rho_2, \text{ and } g(\omega) \leq \Omega\}. \end{aligned} \tag{P1}$$

The control set U_1 is a convex relaxation of U_0, but because it is a relaxation, solutions of P1 may not be feasible for P0. If it so happens that $g(u(t)) = \Gamma(t)$ almost everywhere, then solutions of P1 are solutions of P0. This leads to the definition of *lossless convexification*.

Definition 4.1. *P1 is a lossless convexification of P0 if for every* (u, Γ) *solving P1 it follows that* $g(u(t)) = \Gamma(t)$ *almost everywhere.*

From this definition and inspection of the problems follows a necessary and sufficient condition, albeit one that is not checkable a priori.

Lemma 4.1. *Let* (u, Γ) *be a solution of P1. Lossless convexification holds if and only if* $g(u(t)) \geq \rho_1$ *almost everywhere. Equivalently, it fails if and only if* $g(u(t)) < \rho_1$ *on a set of positive measure.*

Proof. To prove the forward implication, suppose convexification holds. Then $g(u(t)) = \Gamma(t) \geq \rho_1$. To prove the backward implication, suppose $g(u(t)) \geq \rho_1$. Then the objective is minimized by picking $\Gamma(t)$ as small as possible, i.e., $\Gamma(t) = g(u(t))$. □

This leads to the definition of the *hairline case*.

Definition 4.2. *Let* (u, Γ) *be a solution of P1. The hairline case is when* $g(u(t)) = \rho_1$ *almost everywhere.*

Lossless convexification holds in the hairline case according to the above theorem. However, any change in problem data that causes $g(u(t))$ to decrease on a set of positive measure will make convexification fail.

4.4 Mathematical Results

Problem P1 is now analyzed mathematically leading to some new results. According to Theorem 3.1, if (x, u, Γ) is optimal for P1 then there exist a scalar $p_0 \in \{0, 1\}$, a function

$p : [t_0, t_f] \to \mathbb{R}^n$, and a scalar ν such that the following hold.

$$0 \neq (p_0, p) \tag{4.1}$$

$$H(t) = p_0 \ell(\Gamma(t)) + p(t)^T (Ax(t) + Bu(t)) = -\nu \tag{4.2}$$

$$\dot{p}(t) = -A^T p(t) \tag{4.3}$$

$$u(t) \in \arg\min_{\omega} p^T B\omega \quad \text{s.t. } g(\omega) \leq \Gamma \tag{4.4}$$

$$\Gamma(t) \in \arg\min_{\Omega} p_0 \ell(\Omega) \ \text{ s.t. } \rho_1 \leq \Omega \leq \rho_2 \ , \ g(u) \leq \Omega \tag{4.5}$$

The first condition is called the non-triviality condition. The second condition states that the Hamiltonian H is a constant. It is zero when the final time is free and possibly non-zero when the final time is fixed. The third condition is the adjoint system. The fourth and fifth conditions are the pointwise minimum conditions.

A sufficient condition for lossless convexification is stated below. In general, it cannot be checked a priori.

Lemma 4.2. *If $p^T(t)B$ is non-zero almost everywhere, then lossless convexification holds.*

Proof. If $p^T(t)B$ is non-zero, then the optimal point is on the boundary of the feasible set in Eq. (4.4), i.e., $g(u(t)) = \Gamma(t)$ almost everywhere. □

In other words, convexification holds if the solution is non-singular. Conversely, if convexification fails, then the solution is singular. However, if the solution is singular, convexification may or may not hold. This leads to another result for free final time problems.

Corollary 4.1. *If (A, B) is controllable and the final time is free, then lossless convexification holds.*

Proof. Suppose convexification fails such that $p^T(t)B = 0$ on a set of positive measure. Because p is analytic and (A, B) is controllable, $p(t) = 0$ on this set [4]. Because the final time is free, the Hamiltonian must be zero, which can only happen if $p_0 = 0$ since ℓ is positive. This violates the non-triviality condition. Therefore, the problem is non-singular and lossless convexification holds. □

The following sufficient condition is true for all cases except the hairline case. This condition and its corollary are new results.

Theorem 4.1. *Let (u, Γ) be a solution of P1. If (A, B) is controllable and $g(u(t)) > \rho_1$ on a set of positive measure, then convexification holds.*

Proof. There are two cases.

Case 1: Suppose the final time is free. Then the above corollary applies and lossless convexification holds.

Case 2: Suppose the final time is fixed and convexification fails. Then on a set of positive measure, $p^T(t)B = 0$ and $p(t) = 0$ because of controllability. The Hamiltonian reduces to $H(t) = \ell(\Gamma(t)) = constant$ almost everywhere. From Lemma 4.1, we know that there is some time where $g(u(t)) < \rho_1$. Minimizing the Hamiltonian implies $\Gamma(t) = \rho_1$ almost everywhere since ℓ is strictly increasing. Thus, $g(u(t)) \leq \rho_1$ almost everywhere, which is a contradiction. □

This proof leads to a very useful corollary.

Corollary 4.2. *Let (u, Γ) be a solution of P1. Suppose (A, B) is controllable. Lossless convexification fails if and only if $g(u(t)) \leq \rho_1$ almost everywhere and $g(u(t)) < \rho_1$ on a set of positive measure.*

For free final time problems, we have an a priori checkable sufficient condition: controllability. For fixed final time problems, we now derive another checkable condition from this corollary for the common situation where $g(u(t)) = ||u(t)||$. Recall that the state equation can be written as

$$x_f - \Phi(t_f, t_0)x_0 = \int_{t_0}^{t_f} \Phi(t_f, t)Bu(t)dt, \tag{4.6}$$

where Φ is the state transition matrix, or matrix exponential. Norming each side and assuming convexification fails, i.e., $||u(t)|| \leq \rho_1$, then

$$\begin{aligned} ||x_f - \Phi(t_f, t_0)x_0|| &= || \int_{t_0}^{t_f} \Phi(t_f, t)Bu(t)dt|| && (4.7)\\ &\leq \int_{t_0}^{t_f} ||\Phi(t_f, t)Bu(t)||dt && (4.8)\\ &\leq \int_{t_0}^{t_f} ||\Phi(t_f, t)B||\, ||u(t)||dt && (4.9)\\ &\leq \rho_1 \int_{t_0}^{t_f} ||\Phi(t_f, t)B||dt. && (4.10) \end{aligned}$$

We define the following

$$\begin{aligned} F(t_f) &= ||x_f - \Phi(t_f, t_0)x_0||, \\ G(t_f) &= \rho_1 \int_{t_0}^{t_f} ||\Phi(t_f, t)B||dt, \end{aligned} \tag{4.11}$$

so that a checkable condition for the fixed final time problem can be stated.

Theorem 4.2. *Suppose that (A, B) is controllable and $g(u(t)) = ||u(t)||$. If $F(t_f) > G(t_f)$, then convexification holds.*

Proof. The proof follows from the analysis above and Corollary 4.2. □

Conceptually, convexification is guaranteed when the boundary conditions belong to the open, non-convex set whose complement is the closed ellipsoid defined by F and G. As an example, consider problems that terminate at the origin. The ellipsoid is then centered at the origin and given by

$$x_0^T \Phi^T(t_f, t_0)\Phi(t_f, t_0)x_0 \leq \left(\rho_1 \int_{t_0}^{t_f} ||\Phi(t_f, t)B||dt\right)^2, \tag{4.12}$$

which can easily be calculated for given problem data.

We now prove that for fixed final time problems, convexification holds for all final times between the minimum time and the optimal time.

Theorem 4.3. *Suppose* (A, B) *is controllable. Let* t_1 *be the minimum time and* t_2 *be the optimal time. If the optimal cost* $J(t_f) = \int_{t_0}^{t_f} \ell(g(u(t)))dt$ *decreases strictly on* $[t_1, t_2]$*, then convexification holds for any* $t_f \in [t_1, t_2]$*.*

Proof. Because the objective is strictly decreasing, one can deduce that $\nu \geq 0$ and that the Hamiltonian is a non-positive constant [55]. Suppose convexification fails such that $p^T(t)B$ is zero on a set of positive measure. Because (A, B) is controllable, $p(t) = 0$ on this set. The Hamiltonian then reduces to

$$p_0 \ell(\Gamma) + \nu = 0. \tag{4.13}$$

The scalar p_0 is non-negative and $\ell(\Gamma)$ is positive such that the both terms are non-negative. Equality holds only when $p_0 = \nu = 0$, but this violates the non-triviality condition. □

4.5 Main Result

The sufficient condition in Theorem 4.2 is quite conservative because it involves several approximations. Also, Theorem 4.3 is only applicable to final times between the minimum time and the optimal time. In this section, we show that controllability is a sufficient condition to solve P0 as a sequence of convex programs for any fixed final time. To do so, several facts related to reachable sets and minimum time problems are needed.

Define the point $w_f := x_f - \Phi(t_f, t_0)x_0$ and the reachable set as

$$\mathcal{R}(t_0, t_f, U) := \{\int_{t_0}^{t_f} \Phi(t_f, t)Bu(t)dt, \ \forall u(t) \in U\}, \tag{4.14}$$

where U is a compact set of all admissible controls. It is clear that $w_f \in \mathcal{R}(t_0, t_f, U)$ is required for any optimal control problem, no matter the objective, to be feasible. It is known that the reachable sets are compact, convex, and continuous in both time arguments (see Lemmas 12.1 and 12.2 in [72]).

Definition 4.3. *A reachable set is expanding if for all* $t_1 < t_2$*,* $\mathcal{R}(t_0, t_1, U) \subset \text{int } \mathcal{R}(t_0, t_2, U)$*.*

Lemma 4.3. *Suppose U is compact, convex, and $0 \in \operatorname{int} U$. The reachable set is expanding if and only if (A, B) is controllable. If the reachable set is expanding, then t_f is the minimum time if and only if $w_f \in \partial\mathcal{R}(t_0, t_f, U)$.*

Proof. See Corollary 17.1 and Theorem 17.3 of [72]. Also see Theorem 1 on page 301 of [18]. □

An illustration of the expanding reachable set and its connection with the minimum time is given in Fig. 4.1.

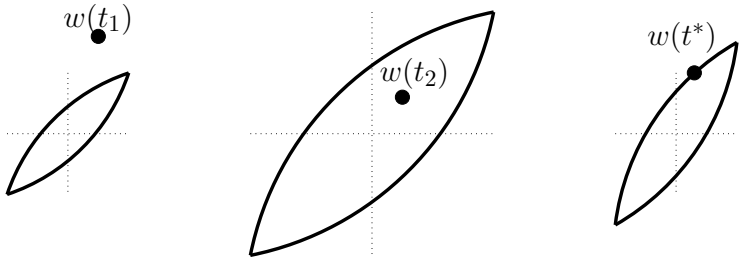

Fig. 4.1: (a) At time t_1, the problem is infeasible as the point, w, is outside the reachable set. (b) At some time $t_2 > t_1$, the point, w, is in the interior of the reachable set and the problem is feasible. (c) At the minimum time, t^*, such that $t_1 < t^* < t_2$, the point, w, is on the boundary of the reachable set.

We now study the following minimum time problem.

$$\begin{aligned} \min \quad & J = \textstyle\int_{t_0}^{t_f} 1 \, dt && \text{(P2)} \\ \text{subj. to} \quad & \dot{x}(t) = Ax(t) + Bu(t) && \text{(F1)} \\ & x(t_0) = x_0, \;\; x(t_f) = x_f && \text{(F2)} \\ & u(t) \in U_2 = \{\omega : g(\omega) \leq \rho_1\} && \text{(F3)} \end{aligned}$$

We refer to the optimal control problem as P2 and the problem of only satisfying the constraints F1-F3 as the feasibility problem, which is convex. As before, the necessary

conditions state that if (x, u) is optimal for P2 then there exist a scalar $p_0 \in \{0, 1\}$ and a function $p : [t_0, t_f] \to \mathbb{R}^n$ such that the following hold.

$$0 \neq (p_0, p) \tag{4.15}$$

$$0 = p_0 + p(t)^T(Ax(t) + Bu(t)) \tag{4.16}$$

$$\dot{p}(t) = -A^T p(t) \tag{4.17}$$

$$u(t) \in \arg\min_{\omega \in U_2} p(t)^T B\omega \tag{4.18}$$

Lemma 4.4. *Let u be a solution of P2. If (A, B) is controllable, then $g(u(t)) = \rho_1$ almost everywhere.*

Proof. If (A, B) is controllable, then $p^T(t)B \neq 0$ almost everywhere (see the proof of Corollary 4.1) and the optimal point is on the boundary of the feasible set, i.e., $g(u(t)) = \rho_1$ almost everywhere. □

With these facts about reachable sets and minimum time problems, the main theorem regarding problem P0 can be stated and proved.

Theorem 4.4. *Consider P0 and assume fixed final time. Assume P1 is not a lossless convexification of P0. If (A, B) is controllable, then there exists an optimal control u for P0 such that $g(u(t)) = \rho_1$ almost everywhere obtained by solving a sequence of convex problems.*

Proof. By assumption, P1 is not a lossless convexification for P0 and (A, B) is controllable. It follows from Corollary 4.2 that an optimal control u for P0 satisfies $g(u(t)) = \rho_1$ almost everywhere. Because U_2 is compact, convex, and $0 \in \text{int } U_2$, Lemma 4.3 indicates that reachable sets generated by U_2 are continuous, compact, convex, and expanding such that any point on the boundary of a reachable set must be reached in minimum time. We now consider two cases.

Case 1: If the final time is the minimum final time, then $w_f \in \partial\mathcal{R}(t_0, t_f, U_2)$ and Lemma 4.4 implies that any feasible control u satisfies $g(u(t)) = \rho_1$ almost everywhere. Therefore, one must solve a single instance of the convex feasibility problem F1-F3 on $[t_0, t_f]$.

Case 2: If the final time is greater than the minimum time, then $w_f \in \text{int } \mathcal{R}(t_0, t_f, U_2)$ since the reachable set is expanding. By definition of interior, $\exists \epsilon > 0$ such that $\forall w_1 \in B_\epsilon(0)$ the point $w_f - w_1 \in \text{int } \mathcal{R}(t_0, t_f, U_2)$. From closedness, convexity, and continuity (see Lemma 12.3 of [72]), $\exists \delta > 0$ such that $\forall t_1 \in B_\delta(t_0)$ the point $w_f - w_1 \in \text{int } \mathcal{R}(t_1, t_f, U_2)$.

Consider a function $v_1 : [t_0, t_1] \to \partial U_2$ and let w_1 and t_1 satisfy

$$w_1 = \int_{t_0}^{t_1} \Phi^{-1}(t, t_1) B v_1(t) dt, \tag{4.19}$$

which can always be done by making t_1 sufficiently close to t_0. That is, $w_1 \in \mathcal{R}(t_0, t_1, \partial U_2)$. If t_1 is increased to t_f and $w_f - w_1$ never leaves the reachable set, then v_1 is an optimal control for P0 since $\forall t \in [t_0, t_f], g(v_1(t)) = \rho_1$, which results in the least possible objective value.

If the point $w_f - w_1$ does leave the reachable set, then at the time t_1 when the point is on the boundary of the reachable set, there exists a minimum time control to $w_f - w_1$ denoted $u_1 : [t_1, t_f] \to \partial U_2$. It follows that the control $u : [t_0, t_f] \to \partial U_2$ given by

$$u(t) = \begin{cases} v_1(t), & t_0 \leq t < t_1 \\ u_1(t), & t_1 \leq t \leq t_f \end{cases} \tag{4.20}$$

is optimal for P0 since $\forall t \in [t_0, t_f], g(u(t)) = \rho_1$, which results in the least possible objective value.

By incrementally increasing t_1, introducing a perturbing function $v_1 : [t_0, t_1] \to \partial U_2$, solving the convex feasibility problem F1-F3 from the perturbed point to the final point for u_1, and checking if $u_1(t) \in \partial U_2$, the optimal control u for P0 is obtained. □

The proof of Theorem 4.4 is constructive and indicates that a line search for t_1, selection of a perturbing control v_1, and solution of a convex constrained problem for u_1 yields the optimal control. This is similar to free final time problems where a line search for t_f is required. Lastly, since any v_1 satisfying $g(v_1(t)) = \rho_1$ works, it is clear that optimal solutions are non-unique. A specific algorithm for finding an optimal control is given below.

4.6 Solution Procedure

This section summarizes the algorithm constructed in the proof of Theorem 4.4 and method used to solve the feasibility problem F1-F3. Given a control u on $[t_0, t_f]$, a measure of how close its magnitude is to ρ_1 is given by the following formula.

$$E(u, t_0, t_f) = \int_{t_0}^{t_f} ||g(u(t)) - \rho_1||\, dt \tag{4.21}$$

The line search algorithm to solve P0 when Theorem 4.4 applies is now given.

Algorithm 1 (Based on Theorem 4.4)

Initialization

Choose a $v \in \mathbb{R}^m$ such that $g(v) = \rho_1$.

Choose a $t_1 \in (t_0, t_f)$.

Choose a tolerance $\epsilon > 0$.

Set $t_{min} = t_0$ and $t_{max} = t_f$.

Repeat

1. Define $v_1(t) = v$ on $[t_0, t_1]$.
2. Compute $x(t_1)$ generated by v_1.
3. Solve F1-F3 from $x(t_1)$ to x_f to find u_1 on $[t_1, t_f]$.

4a. If F1-F3 is infeasible,

set $t_{max} = t_1$ and $t_1 = \frac{1}{2}(t_{min} + t_{max})$

return to 1.

4b. If F1-F3 is feasible and $E(u_1, t_1, t_f) > \epsilon$,

set $t_{min} = t_1$ and $t_1 = \frac{1}{2}(t_{min} + t_{max})$

return to 1.

4c. If F1-F3 is feasible and $E(u_1, t_1, t_f) \leq \epsilon$,

output v_1 and u_1 as an optimal control

quit.

To numerically solve the convex feasibility problem F1-F3, it is discretized and constraints are enforced at the nodes resulting in a second-order cone program that can be solved using interior-point methods. We use a simple discretization method, which is summarized below.

The time domain $[t_0, t_f]$ is uniformly discretized into $N+1$ nodes separated by Δt. The states at time t_i are denoted by $x[i]$ and they exist at all nodes $i = 1, ..., N+1$. The controls at time t_i are denoted by $u[i]$ and they exist at nodes $i = 1, ..., N$. The controls are held constant over every interval. The system dynamics are discretized using the fundamental matrix resulting in

$$x[i+1] = A_d x[i] + B_d u[i], \quad i = 1, ..., N. \tag{4.22}$$

The discrete system matrices A_d and B_d are given by

$$A_d = e^{A\Delta t}, \quad B_d = \int_0^{\Delta t} e^{A\tau} B d\tau. \tag{4.23}$$

The boundary conditions are enforced at the initial and final nodes.

$$x[1] = x_0, \quad x[N+1] = x_f \tag{4.24}$$

The control constraints are enforced at nodes 1 to N.

$$|| \, u[i] \, || \leq \rho_1, \quad \forall \, i = 1, ..., N \tag{4.25}$$

Eqs. (4.22)-(4.25) represent a finite-dimensional second-order cone program that can be solved using commercially available solvers.

4.7 Examples

In this section, the algorithm is demonstrated on a simple double integrator and a harmonic oscillator system. A Mars powered descent guidance example is then solved in a sample-and-hold scheme to emulate a real guidance system. Problems are solved using the

Gurobi [73] solver with a MATLAB interface [74].

4.7.1 Double Integrator

Consider the following problem with double integrator dynamics and an annular control constraint. The problem fits into the definition of P0 and is mathematically described below.

$$\begin{aligned}
\min \quad & J = \int_{t_0}^{t_f} ||u(t)|| \, dt \\
\text{subj. to} \quad & \dot{x}_1(t) = x_2(t) \\
& \dot{x}_2(t) = u(t) \\
& x_1(t_0) = 1, \;\; x_1(t_f) = 0 \\
& x_2(t_0) = 1, \;\; x_2(t_f) = 0 \\
& 1 \leq ||u(t)|| \leq 6
\end{aligned}$$

Recognizing $g(u(t)) = ||u(t)||$ and $\ell(g(u(t)) = g(u(t))$, the standard relaxation P1 can be stated.

$$\begin{aligned}
\min \quad & J = \int_{t_0}^{t_f} \Gamma(t) \, dt \\
\text{subj. to} \quad & \dot{x}_1(t) = x_2(t) \\
& \dot{x}_2(t) = u(t) \\
& x_1(t_0) = 1, \;\; x_1(t_f) = 0 \\
& x_2(t_0) = 1, \;\; x_2(t_f) = 0 \\
& 1 \leq \Gamma(t) \leq 6 \\
& ||u(t)|| \leq \Gamma(t)
\end{aligned}$$

According to Theorem 4.2, the above convexification will hold if $F(t_f) > G(t_f)$, where $F(t_f)$ and $G(t_f)$ are defined by Eq. (4.11). Fig. 4.2 shows the the difference $F(t_f) - G(t_f)$ as a function of the final time t_f. By solving the problem, it was determined that the minimum time is approximately 1.016 time units and the optimal time is approximately 2.1

time units. The difference is positive between the minimum and optimal times and negative for times greater than the optimal time. Consistent with Theorems 4.2 and 4.3, numerical tests demonstrate that the standard convexification holds when the difference is positive.

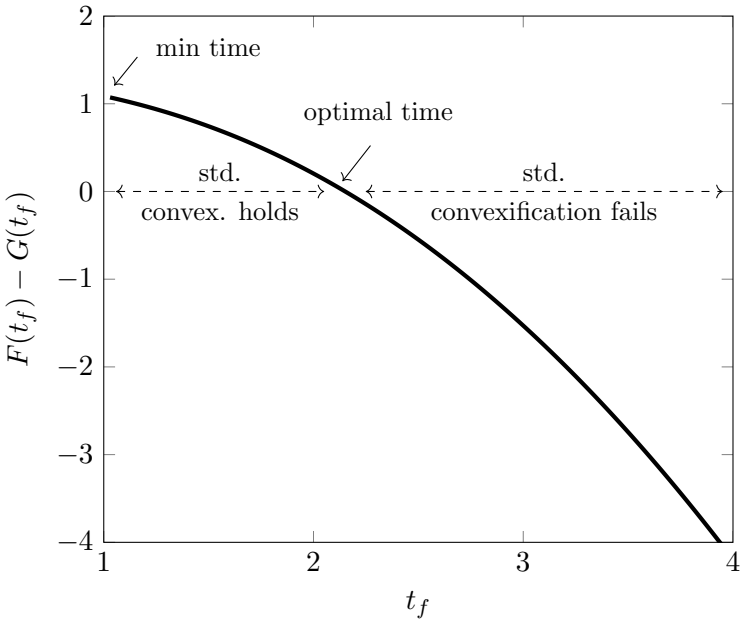

Fig. 4.2: The quantity $F - G$ is positive and convexification holds for final times between the minimum time and the optimal time of about 2.1 time units. For larger times, the difference is negative and convexification fails.

For a final time of $t_f = 5$ time units, standard convexification fails. With $t_f = 5$, Algorithm 1 is used to solve the problem. According to Theorem 4.4, since the system is controllable, the optimal control u satisfies $||u(t)|| = 1$ almost everywhere. To demonstrate non-uniqueness, two solutions are generated using the perturbing functions $v_1(t) = 1$ on $[0, 0.42]$ and $v_1(t) = -1$ on $[0, 2.38]$, respectively. In each case, the feasibility problem F1-F3 is solved to find the optimal control after the perturbing period. Figures 4.3-4.5 shows the states, controls, and reachable set.

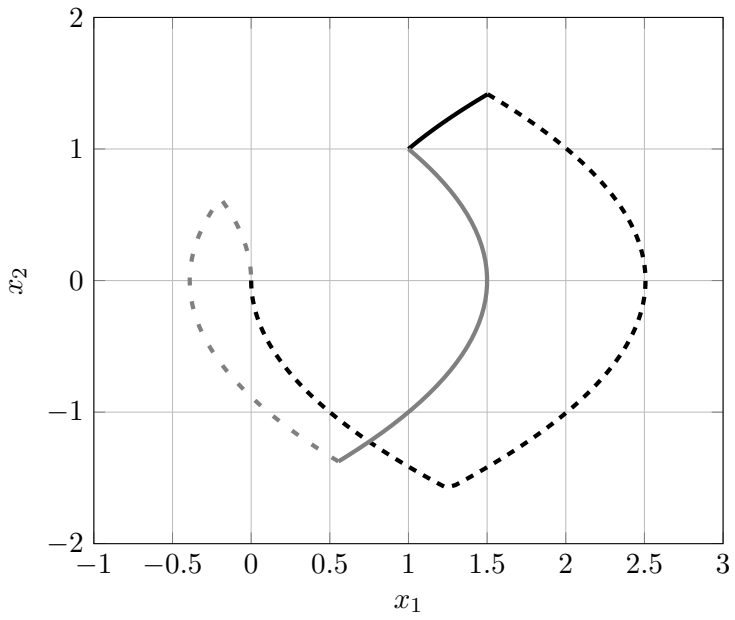

Fig. 4.3: State trajectories in phase plane. The solid black curve corresponds to the $v_1(t) = 1$ solution. The gray curve corresponds to the $v_1(t) = -1$ solution. After the perturbing periods, a minimum time control $u_1(t)$ is computed that satisfies $||u_1(t)|| = 1$. The state then follows the so-called switching curve to reach the origin.

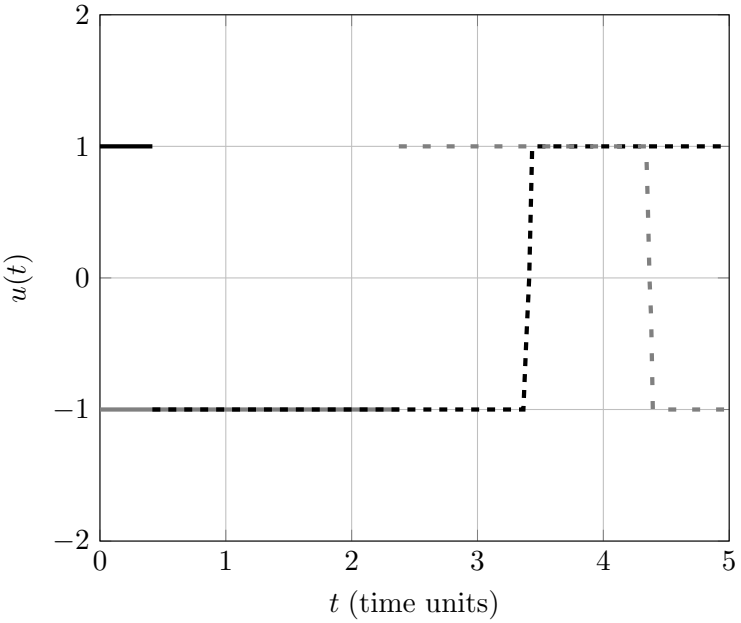

Fig. 4.4: The solid lines correspond to the perturbing controls $v_1(t)$. The dashed lines correspond to the minimum time control $u_1(t)$. Color scheme is the same as Fig. 4.3.

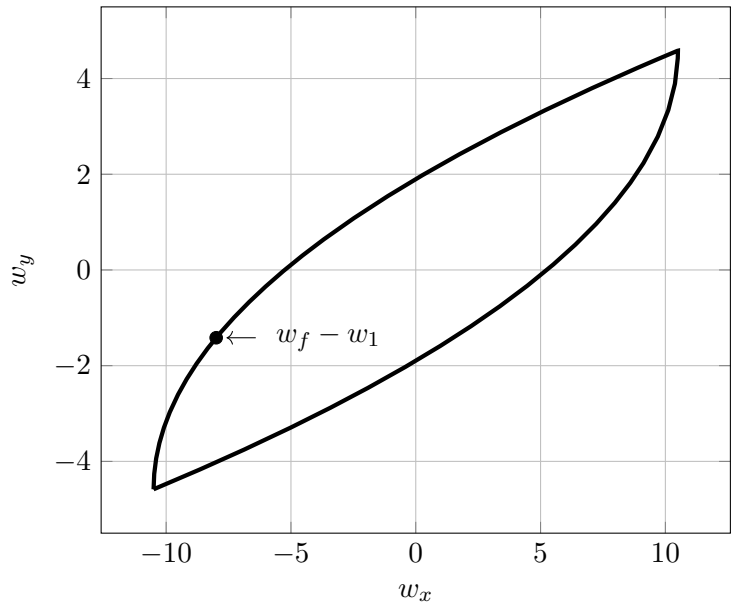

Fig. 4.5: Reachable set, $\mathcal{R}(t_1, t_f, U_2)$, for $t_1 = 0.42$ and $t_f = 5$ time units ($v_1(t) = 1$ case). As required, the point $w_f - w_1$ lies on the boundary of the set.

For both cases, Algorithm 1 was initialized with a guess of $t_1 = 2.5$. It turns out that both cases required the solution of seven second-order cone programs. On a laptop with 2.2 GHz processor, each program required about 0.2 seconds to solve for a total solution time of about 1.4 seconds.

4.7.2 Harmonic Oscillator

Consider the following problem with harmonic oscillator dynamics and an annular control constraint. The problem fits into the definition of P0 and is mathematically described

below.

$$
\begin{aligned}
\min \quad & J = \int_{t_0}^{t_f} ||u(t)|| \, dt \\
\text{subj. to} \quad & \dot{x}_1(t) = x_2(t) \\
& \dot{x}_2(t) = -x_1(t) + u(t) \\
& x_1(t_0) = 2, \;\; x_1(t_f) = 0 \\
& x_2(t_0) = 0, \;\; x_2(t_f) = 0 \\
& 1 \leq ||u(t)|| \leq 3
\end{aligned}
$$

Given below is the standard, convex relaxation to the problem.

$$
\begin{aligned}
\min \quad & J = \int_{t_0}^{t_f} \Gamma(t) \, dt \\
\text{subj. to} \quad & \dot{x}_1(t) = x_2(t) \\
& \dot{x}_2(t) = -x_1(t) + u(t) \\
& x_1(t_0) = 2, \;\; x_1(t_f) = 0 \\
& x_2(t_0) = 0, \;\; x_2(t_f) = 0 \\
& 1 \leq \Gamma(t) \leq 3 \\
& ||u(t)|| \leq \Gamma(t)
\end{aligned}
$$

Fig. 4.6 shows the variation of the difference $F(t_f) - G(t_f)$ with the final time t_f. By solving the problem, it was determined that the minimum time is approximately 1.51 time units and the optimal time is approximately 2 time units. The difference is positive between the minimum and optimal times. Consistent with Theorems 4.2 and 4.3, numerical tests demonstrate that the standard convexification holds when the difference is positive.

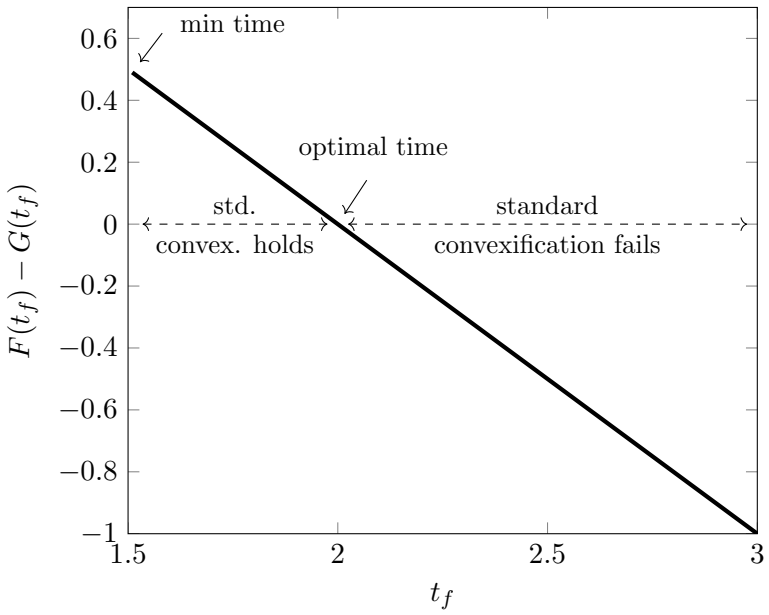

Fig. 4.6: The quantity $F - G$ is positive and convexification holds for final times between the minimum time and the optimal time of about 2 time units. For larger times, the difference is negative and convexification fails.

For a final time of $t_f = 5$ time units, standard convexification fails. With $t_f = 5$ time units, Algorithm 1 is used to solve the problem. According to Theorem 4.4, since the system is controllable, the optimal control $u(t)$ satisfies $||u(t)|| = 1$ almost everywhere.

Upon using the perturbing function $v_1(t) = 1$ on $[0, 3.65]$ and solving the feasibility problem F1-F3 to find the optimal control after the perturbing period, we find the optimal control $u(t)$. Figures 4.7 - 4.9 shows the states, controls, and the reachable set.

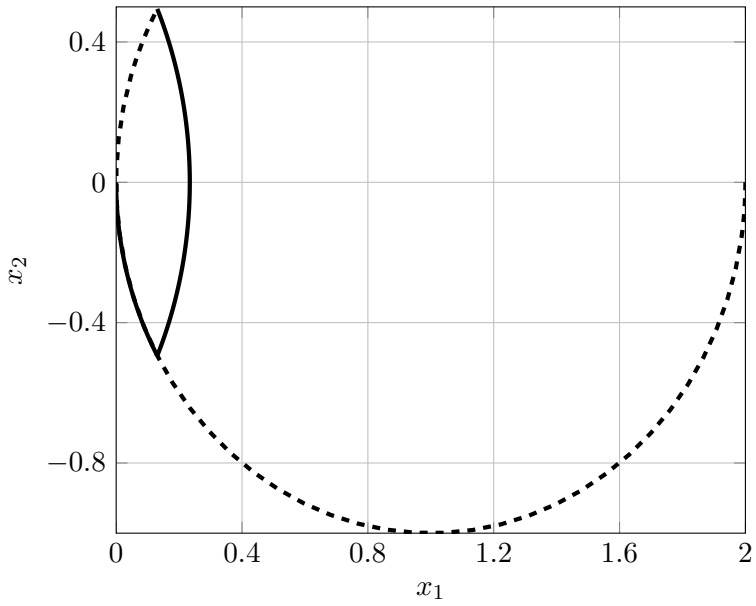

Fig. 4.7: State trajectory in phase plane. The dashed black curve corresponds to the $v_1(t) = 1$ solution. After the perturbing period, a minimum time control $u_1(t)$ is computed that satisfies $||u_1(t)|| = 1$. The state then follows the so-called switching curve to reach the origin.

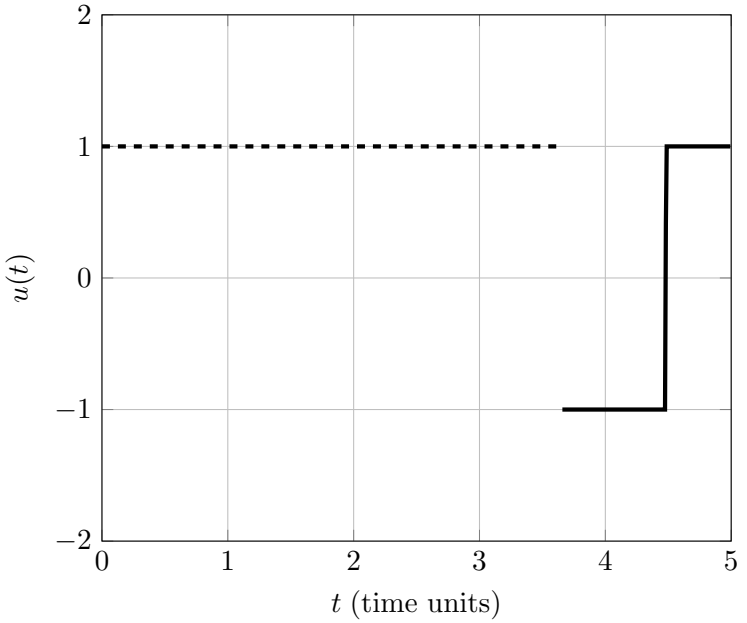

Fig. 4.8: Control trajectory. The dashed line corresponds to the perturbing control $v_1(t)$. The solid line corresponds to the minimum time control, $u_1(t)$.

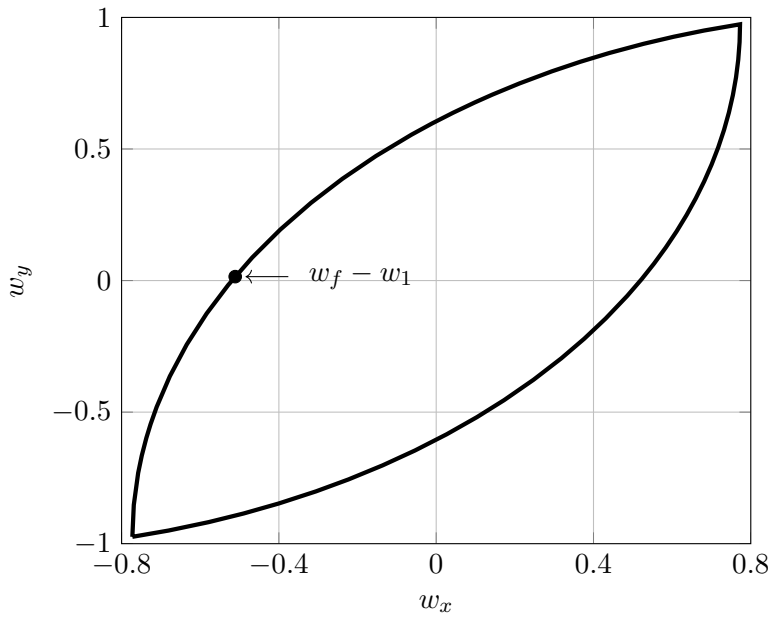

Fig. 4.9: Reachable set, $\mathcal{R}(t_1, t_f)$, for $t_1 = 3.65$ and $t_f = 5$ time units. As required, the point $w_f - w_1$ lies on the boundary of the set.

For this case, Algorithm 1 was initialized with a guess of $t_1 = 2.5$ and it required the solution of seven second-order cone programs. On a laptop with 2.2 GHz processor, each program required about 0.2 seconds to solve for a total solution time of about 1.4 seconds.

4.7.3 Mars Powered Descent Guidance

As a final example, consider a Mars powered descent guidance problem. Because the landing mission starts at a low altitude, it is assumed that the gravitational field is uniform. Aerodynamic forces are not considered since they are negligible compared to the propulsive and gravitational accelerations during powered descent. An illustration of the problem is given in [1].

The dynamics of the spacecraft are given by the following equations

$$\ddot{r}(t) = g + \frac{T(t)}{m(t)}, \tag{4.26}$$

$$\dot{m}(t) = -\alpha ||T(t)||, \tag{4.27}$$

where $r(t) \in \mathbb{R}^3$ is the position vector of the spacecraft relative to the target, $g \in \mathbb{R}^3$ is the constant gravitational vector, $T(t) \in \mathbb{R}^3$ is the net thrust vector, $m(t) \in \mathbb{R}$ is the spacecraft mass, and $\alpha \in \mathbb{R}$ is a positive constant that defines the fuel consumption rate. The net thrust is bounded by

$$0 < \rho_1 \leq ||T(t)|| \leq \rho_2, \tag{4.28}$$

which defines a non-convex set of feasible controls. Additional nonlinearities are present because of the nonlinearity of Eqs. (4.26) and (4.27). To remove these nonlinearities, the following variable transformations are introduced.

$$u := \frac{T}{m}, \quad \sigma := \frac{||T||}{m}, \quad \text{and} \quad z := \ln(m) \tag{4.29}$$

Upon defining the quantities

$$\mu_1(t) = \rho_1 e^{-\tilde{z}(t)} \quad \text{and} \quad \mu_2(t) = \rho_2 e^{-\tilde{z}(t)} \tag{4.30}$$

where

$$\tilde{z}(t) = \begin{cases} \ln(m_{wet} - \alpha\rho_2 t), & m_{wet} - \alpha\rho_2 t \geq m_{dry} \\ \ln(m_{dry}), & \text{otherwise} \end{cases}, \tag{4.31}$$

a second-order cone program can be formed that approximates the problem of interest [1].

$$
\begin{aligned}
\min \quad & J = \textstyle\int_0^{t_f} \sigma(\tau)\, d\tau \\
\text{subj. to} \quad & \dot{r}(t) = v(t) \\
& \dot{v}(t) = u(t) + g \\
& \dot{z}(t) = -\alpha\sigma(t) \\
& ||u(t)|| \leq \sigma(t) \\
& \mu_1(t)\Big[1 - \big[z(t) - \tilde{z}(t)\big] + \tfrac{1}{2}\big[z(t) - \tilde{z}(t)\big]^2\Big] \\
& \qquad \leq \sigma(t) \leq \mu_2(t)\Big[1 - \big[z(t) - \tilde{z}(t)\big]\Big] \\
& \ln(m_{wet} - \alpha\rho_2 t) \leq z(t) \leq \ln(m_{wet} - \alpha\rho_1 t) \\
& m(0) = m_{wet}, \;\; r(0) = r_0, \;\; \dot{r}(0) = \dot{r}_0 \\
& r(t_f) = \dot{r}(t_f) = 0
\end{aligned}
$$

The following parameters are used to solve the problem.

$$
\begin{aligned}
& r_0 = [1500, 0, 2000]^T \text{ m} \\
& \dot{r}_0 = [-75, 0, 100]^T \text{ m/s} \\
& g = [-3.7114, 0, 0]^T \text{ m/s}^2 \\
& m_{dry} = 1505 \text{ kg}, m_{wet} = 2110 \text{ kg} \\
& I_{sp} = 225 \text{ s}, \alpha = 5.09 \cdot 10^{-4} \text{ s/m} \\
& \rho_1 = 13.151 \text{ kN}, \rho_2 = 19.727 \text{ kN}
\end{aligned}
\tag{4.32}
$$

Through numerical tests, the problem has a minimum time of 45 seconds and an optimal time of 52 seconds. Tests indicate that the standard convexification holds for final times between 45 seconds and 72 seconds, and it fails thereafter. To demonstrate our results, the final time is set at $t_f = 90$ seconds and it is known that the optimal solution will have thrust magnitude equal to ρ_1 almost everywhere.

To emulate a practical guidance implementation, the problem is solved in a sample-and-hold manner. In each call to guidance, the feasibility problem is solved. If the control solution has magnitude ρ_1 at each node, the control at the current node is accepted and passed to the simulation. Otherwise, a perturbing control with magnitude ρ_1 is introduced and passed to the simulation. This process is repeated every one second from 90 seconds down to 1 second. The resulting state and control trajectories are shown in Figs. 4.10 to 4.12. The problems were solved on a laptop with a 2.2 GHz processor. Each call to guidance requires the solution of one second-order cone program. On average, the solution time was 0.25 seconds.

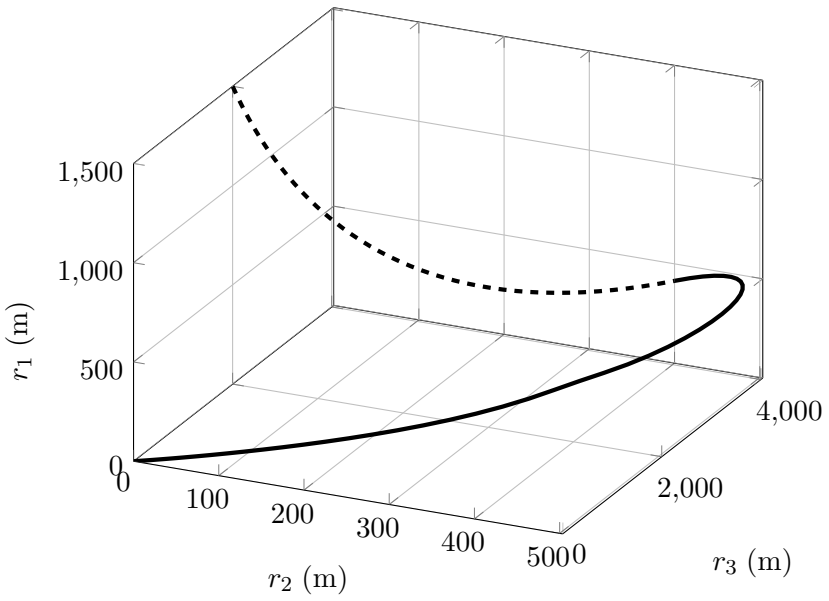

Fig. 4.10: The spacecraft's initial position is at the tip of the dashed curve. The dashed curve indicates the perturbed portion of the trajectory. After 43 seconds, a minimum time control lands the spacecraft at the desired point (indicated by the solid curve).

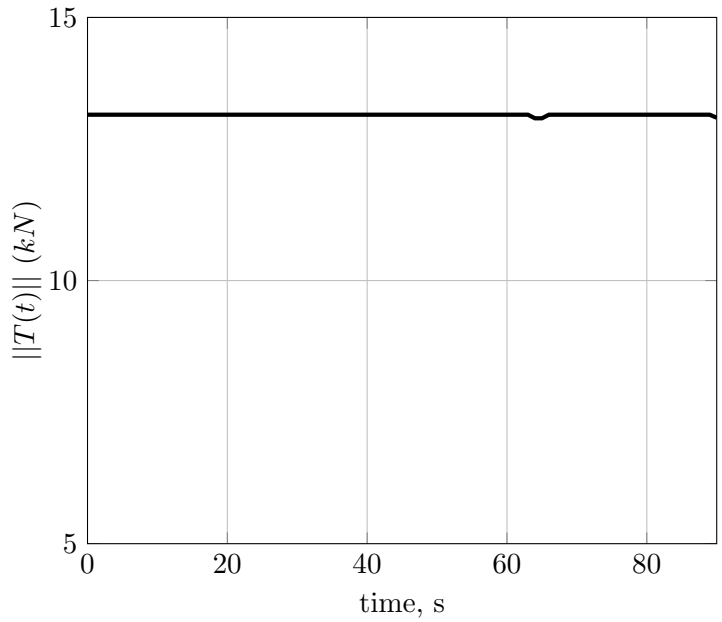

Fig. 4.11: The thrust magnitude is constant at the lower bound of $\rho_1 = 13.151$ kN.

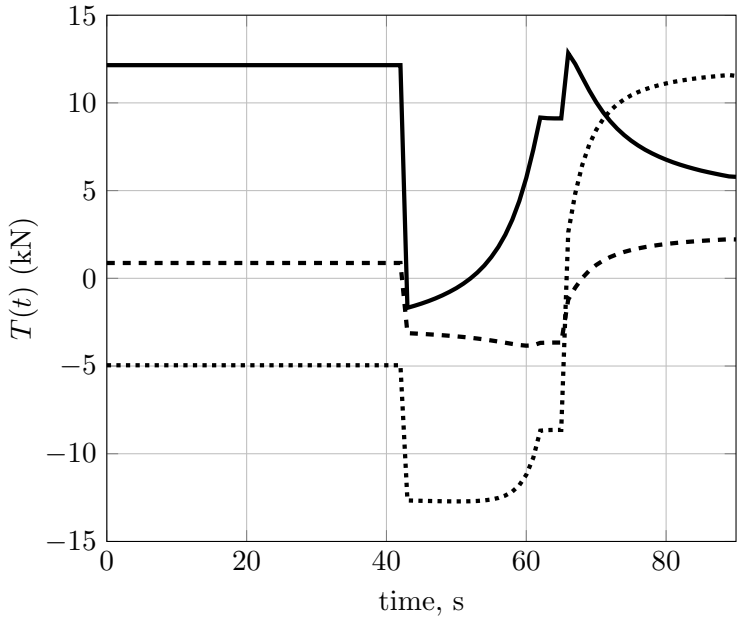

Fig. 4.12: The three components of thrust are shown as a function of time.

4.8 Proof for Lossless Convexification in Finite Dimensions

This section attempts to provide a proof for lossless convexification of a problem of type P0 in finite dimensions. Consider the following discrete-time minimum energy problem

$$\begin{aligned} \min \quad & J = \sum_{i=1}^{N} u_i^T u_i \\ \text{subj. to} \quad & x_{i+1} = Ax_i + Bu_i, \quad i = 1, ..., N \\ & x_1 = x_0, \;\; x_{N+1} = x_f \\ & \rho_1 \leq ||u_i|| \leq \rho_2, \quad i = 1, ..., N. \end{aligned}$$

Let $x_i \in \mathbb{R}^n$ and $u_i \in \mathbb{R}^m$. Recognizing that $g(u_i) = ||u_i||$ and $\ell(g(u_i)) = (g(u_i))^2 = u_i^T u_i$, the standard relaxation P1 can be stated as below.

$$\begin{aligned} \min \quad & J = \sum_{i=1}^{N} \Gamma_i^2 \\ \text{subj. to} \quad & x_{i+1} = Ax_i + Bu_i, \quad i = 1, ..., N \\ & x_1 = x_0, \;\; x_{N+1} = x_f \\ & ||u_i|| \leq \Gamma_i, \qquad i = 1, ..., N \\ & \rho_1 \leq \Gamma_i \leq \rho_2, \quad i = 1, ..., N. \end{aligned}$$

The Hamiltonian and Lagrangian functions are defined as follows

$$H_i = p^0 \Gamma_i^2 + p_{i+1}^T (Ax_i + Bu_i) \tag{4.33}$$

$$L_i = H_i + \alpha_i (u_i^T u_i - \Gamma_i^2) + \beta_i (\rho_1 - \Gamma_i) + \gamma_i (\Gamma_i - \rho_2) \tag{4.34}$$

The costate and stationary conditions are

$$p_i = \frac{\partial H_i}{\partial x_i} = A^T p_{i+1} \tag{4.35}$$

$$0 = \frac{\partial L_i}{\partial u_i} = B^T p_{i+1} + 2\alpha_i u_i \tag{4.36}$$

$$0 = \frac{\partial L_i}{\partial \Gamma_i} = 2p^0\Gamma_i - 2\alpha_i\Gamma_i - \beta_i + \gamma_i. \tag{4.37}$$

Suppose $\exists\ i$ such that $u_i^T u_i < \Gamma_i$. Then,

$$\alpha_i = 0, \quad \Gamma_i = \rho_1, \quad \gamma_i = 0, \tag{4.38}$$

$$0 = B^T p_{i+1}, \quad 2p^0\rho_1 = \beta_i. \tag{4.39}$$

The adjoint system is then given by the equations

$$\begin{aligned} p_i &= A^T p_{i+1} \\ 0 &= B^T p_{i+1} \end{aligned} \tag{4.40}$$

Observability of the discrete system given by Eq. (4.40) can be determined using simple rank tests [75–77]. Now, if the adjoint system is observable and $B^T p_{i+1} = 0$ for $i = 1, ..., n$, then $p_i = 0\ \forall\ i = 1, ..., N$. However, we cannot guarantee that the condition $B^T p_{i+1} = 0$ holds for $i = 1, ..., n$. Hence, the proof for convexification cannot be done in finite dimensions.

4.9 Conclusions

This work presented new convexification results including a sufficient condition for the standard convexification to hold for both free and fixed final time problems, a sufficient condition for the standard convexification to hold for all final times between the minimum time and the optimal time, and a perturbation technique to solve the general fixed time problem as a sequence of convex programs when the final time is greater than the optimal time. In short, the perturbation technique works as follows: perturb the initial point, solve a feasibility problem to the final point, and repeat until convexification works (so that

the control is on the boundary of the control set almost everywhere), which is guaranteed to happen. This results in a globally minimizing control. The perturbation technique has practical applications as demonstrated in the Mars landing example. In each call to guidance, the problem was solved in less than one second without customization, suggesting that the new perturbation technique is suitable for real-time guidance applications.

CHAPTER 5
APPLICATION TO MARS ASCENT GUIDANCE

5.1 Introduction

This chapter analyzes three guidance strategies for the second stage of the Mars Ascent Vehicle (MAV). One of the guidance laws is computational and based on the developments in the previous chapter. One goal is to test the law (which assumes linear dynamics) in the nonlinear ascent setting. This chapter evaluates the performance of the proposed computational guidance law in nominal and Monte Carlo settings, and a comparison of the results to those with the traditional Q-guidance (NASA's current choice) and a variant of the Powered Explicit Guidance (referred herein as LVLH-guidance).

NASA marked the beginning of its Mars Sample Return (MSR) campaign with the launch of the Mars 2020 Perserverance rover. The rover, upon landing at the Jezero Crater, will spend the next six years collecting Martian surface samples and preparing them for collection and return to Earth. In 2026, a Mars Ascent Vehicle (MAV) will be launched from Earth, stowed upon a Sample Retrieval Lander (SRL). Upon arrival at Mars, a Sample Fetch Rover (SFR), housed inside the lander collects the deposited samples and inserts them into the Orbiting Sample (OS), which is the payload for the MAV. The MAV then launches from the surface and upon reaching a target orbit, ejects the OS, which will then be captured and returned to Earth by the Earth Return Orbiter (ERO) [78].

The target orbit is a 343 km circular orbit with an inclination of 25°. However, an absolute lower bound of 300 km and a soft upper bound of 375 km is needed to interface with the ERO. Also, an eccentricity of less than 0.006 and a semi-major axis of $\pm$ 9 km are desired [79]. The solid configuration MAV consists of two stages, each equipped with a Solid Rocket Motor (SRM). The first stage SRM launches the MAV from the Jezero Crater (18.43° N 77.50° E) using an open-loop guidance scheme based on altitude. Following the

first stage cut off, the MAV coasts on a ballistic trajectory with an apoapse of 343 km and an inclination of 25°. As the vehicle approaches the apoapse, second stage guidance targets are loaded and closed-loop guidance calculations are performed continuously. Based on an ignition trigger, the second stage SRM, which has a burn time of 24.45 seconds, is then ignited to perform the circularization manuever. This work focuses on the performance of potential ignition triggers and the second stage guidance strategies with an objective to increase payload capacity, reduce fuel cost, and improve orbit insertion accuracy.

Traditional guidance laws have been simple – making many assumptions so that desired controls can be calculated in real-time onboard a basic flight computer. Assumptions typically include constant gravity, perfect state knowledge, and negligible aerodynamics. Examples of such "analytical guidance" schemes include Apollo lunar descent guidance [24–26,59], Iterative Guidance Mode (IGM) for Saturn V ascent [60,61], and Powered Explicit Guidance (PEG) for Shuttle [62,63]. In this work, the traditional Q-guidance as described in [80] and a PEG-like guidance (LVLH-guidance) as described in [81] are used to establish baselines for comparison.

Computational guidance schemes for Mars entry, descent, and landing (EDL) were first developed in 2005 at the Jet Propulsion Laboratory (JPL) by staff members Behçet Açıkmeşe and Scott Ploen [1,41,57]. They formulated the landing problem as a non-convex optimization problem, transformed it to a convex form, and solved it using convex solvers. This technology made it on-board the flight computer for abort situations but was never needed [12,82]. Computational guidance for ascent has not received the same attention and is an ongoing area of work.

However, it must be noted that since the LVLH-guidance provides an analytical solution to the nonlinear ascent problem, its performance is expected to be better than the proposed computational guidance law. To summarize, the current work focuses on formulating the second stage MAV ascent guidance problem as an optimal control problem, transforming it into a convex form, and comparing its performance to the Q-guidance and LVLH-guidance schemes. The main contributions of this work are:

1. Establishment of burn time, time of ignition, and configuration type of the SRM as critical factors that affect the performance of a computational guidance scheme (See Section 5.7.3).

2. Introduction of an alternative ignition trigger (called box-trigger) for Q-guidance with improved dispersion performance and mass reduction (See Section 5.7.1).

3. Establishment of LVLH-guidance with uhat-trigger as a guidance scheme with best performance results (See Section 5.7.2).

The chapter is organized as follows. Section 5.2 introduces the mathematical notations used. In Section 5.3, equations of motion for the vehicle are described. Section 5.4 discusses the coordinate transformations used. Section 5.5 gives a detailed description of the different guidance laws. The different ignition triggers are discussed in Section 5.6 followed a comparison of their performance results in Section 5.7. Section 5.8 dicusses the potential benefits of possible trigger changes. Finally, Section 5.9 concludes the chapter.

5.2 Nomenclature for the Chapter

The following is a partial list of notation used; $\mathbb{R}$ is the set of real numbers; $\mathbb{R}^n$ is the n-dimensional real vector space; $||v||$ is the 2-norm of the vector v and the time derivative of a function is denoted with an over-dot, i.e. $dx(t)/dt = \dot{x}(t)$.

5.3 Equations of Motion

The nonlinear equations of motion for the vehicle are written in a local vertical local horizontal (LVLH) frame shown in Figure 5.1. The equations assume a non-rotating spherical primary body and have been derived using spherical coordinates – (r, ϕ, λ). The radius is given by $r = R + y$ where R is the radius of the planet. ϕ is the longitude and λ is the latitude. The quantities x and y are the in-plane curvilinear distance and altitude; u

and v are the in-plane horizontal and vertical velocity components; and z and w are the out-of-plane curvilinear distance and velocity components.

$$\begin{aligned}
\dot{x} &= Ru/r \\
\dot{y} &= v \\
\dot{z} &= Rw/r \\
\dot{u} &= \tau\cos\theta\cos\psi + (uv/r)\tan(z/R) - uv/r + a_x \\
\dot{v} &= \tau\sin\theta - g + u^2/r + w^2/r + a_y \\
\dot{w} &= \tau\cos\theta\sin\psi - (u^2/r)\tan(z/R) - vw/r + a_z
\end{aligned} \tag{5.1}$$

The gravitational constant is denoted by μ and the gravitational acceleration is given by $g = \mu/r^2$. Also, τ is the thrust acceleration T/m; θ is the thrust pitch angle; and ψ is the thrust yaw angle. For operation at constant thrust, $T = \beta V_e$ where β is the propellant mass flow rate and V_e is the exhaust velocity. The mass equation can be integrated to obtain $m = m_0 - \beta t$ so that the mass equation can be eliminated from the problem. Thus, $\tau = -V_e/(t - \alpha)$ where $\alpha = m_0/\beta$.

Perturbing accelerations are captured componentwise in a_x, a_y, and a_z. Perturbations can include higher-order gravitational affects and atmospheric drag based on an exponential atmospheric model.

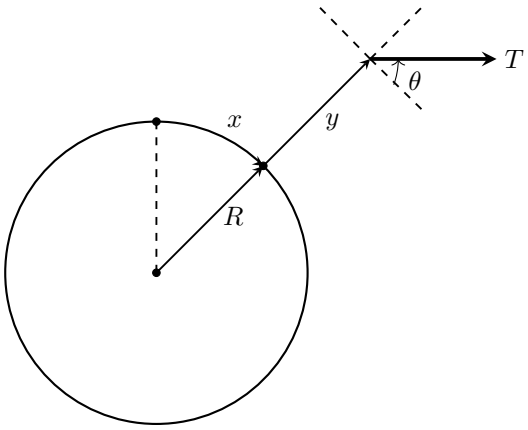

Fig. 5.1: LVLH reference frame.

However, since the current work is focused on the relatively short duration of powered flight during the second burn near apoapse, primary perturbations are not dynamic but related to the vehicle (mass and deliverable delta-v) and ignition trigger logic. As such, several simplifying assumptions can be made. First, it is observed that $y/R << 1$ so that $r \approx R$ and $g \approx \mu/R^2$. Second, the out-of-plane components z and w are sufficiently small that z/R and w/R can be neglected. This is true because the plane change is done during the first burn. Third, during thrusting arcs, $uv/R << T/m$ so that the third term in the $\dot{u}$ equation can be neglected. Fourth, the perturbing accelerations are neglected. The resulting equations are given by

$$\begin{aligned}
\dot{x} &= u \\
\dot{y} &= v \\
\dot{z} &= w \\
\dot{u} &= \tau \cos\theta \cos\psi \\
\dot{v} &= \tau \sin\theta - g + u^2/r \\
\dot{w} &= \tau \cos\theta \sin\psi
\end{aligned} \tag{5.2}$$

5.4 Coordinate Transformations

Given inertial position and velocity vectors $r_0 \in \mathbb{R}^3$ and $v_0 \in \mathbb{R}^3$, the LVLH components can be found using the equations:

$$\hat{r} = r_0/||r_0|| \tag{5.3a}$$

$$\phi = \tan^{-1}(\hat{r}_2, \hat{r}_1) \tag{5.3b}$$

$$\lambda = \sin^{-1}(\hat{r}_3) \tag{5.3c}$$

$$x = R\phi \tag{5.3d}$$

$$y = ||r_0|| - R \tag{5.3e}$$

$$z = R\lambda \tag{5.3f}$$

$$[v, u, w]^\top = T^\top v_0 \tag{5.3g}$$

T is the rotation matrix given by

$$T = \begin{bmatrix} \cos\phi\cos\lambda & -\sin\phi & -\cos\phi\sin\lambda \\ \sin\phi\cos\lambda & \cos\phi & -\sin\phi\sin\lambda \\ \sin\lambda & 0 & \cos\lambda \end{bmatrix}. \tag{5.4}$$

where ϕ is the longitude and λ is the latitude.

5.5 Guidance Laws

In this section, we discuss the three guidance laws that have been implemented and compared in this study – 1) Q-guidance (analytic in nature), 2) LVLH-guidance (analytic in nature and a PEG variant), and 3) SOCP-guidance (computational in nature). Q-guidance is NASA's current choice. Q-guidance and LVLH-guidance have a long history of space-use whereas something similar to SOCP-guidance has only been recently used by SpaceX. The third guidance requires the solution of a second-order cone program (SOCP) – hence the name.

5.5.1 Q-guidance

Q-guidance or Cross Product Steering (CPS) is a guidance technique which is fuel optimal for constant gravity fields [83] and very nearly optimal for non-constant gravity fields [84, 85]. The guidance law is based on the concept of "velocity-to-be-gained"

$$v_g = v_r - v \tag{5.5}$$

where $v \in \mathbb{R}^3$ is the inertial velocity of the vehicle, and $v_r \in \mathbb{R}^3$ is the velocity required to satisfy a set of stated mission objectives. In other words, v_r is the velocity that the vehicle would have if it coasts on a trajectory to reach the desired target. By intuition, any steering law that drives v_g to zero will be successful but may not be optimal. The differential equation for v_g can be found by differentiating Eq. (5.5) with respect to time.

We know

$$\dot{v} = g(r) + a_T \tag{5.6}$$

where $g(r) \in \mathbb{R}^3$ is the gravitational vector corresponding to the current vehicle position $r \in \mathbb{R}^3$, and $a_T \in \mathbb{R}^3$ is the thrust acceleration acting on the vehicle. Recalling that v_r is a function of r and time t, the time derivative of velocity-to-be-gained can be written in the form

$$\dot{v}_g = \frac{\partial v_r}{\partial t} + \frac{\partial v_r}{\partial r} v - g(r) - a_T \tag{5.7}$$

Substituting $v = v_r - v_g$ into Eq. (5.7) yields

$$\dot{v}_g = \frac{\partial v_r}{\partial t} + \frac{\partial v_r}{\partial r} v_r - \frac{\partial v_r}{\partial r} v_g - g(r) - a_T \tag{5.8}$$

Noting that v_r is the velocity of the vehicle on a coasting trajectory,

$$\frac{\partial v_r}{\partial t} + \frac{\partial v_r}{\partial r} v_r = g(r) \tag{5.9}$$

Hence, Eq. (5.8) becomes

$$\dot{v}_g = -\frac{\partial v_r}{\partial r} v_g - a_T \tag{5.10}$$

The term $\frac{\partial v_r}{\partial r} v_g$ is often labeled as Q and the guidance scheme is referred to as Q-guidance.

According to Battin [80], an effective way to drive all three components of v_g to zero simultaneously is to align the time of rate of change of v_g with itself. This insight results from the analysis of a constant gravity scenario of the problem. Mathematically, this is equivalent to choosing a_T such that

$$\dot{v}_g \times v_g = 0. \tag{5.11}$$

By introducing the notation

$$p = -\frac{\partial v_r}{\partial r} v_g = -Q v_g \tag{5.12}$$

Eq. (5.10) can be written as

$$\dot{v}_g = p - a_T. \tag{5.13}$$

The steering law is then equivalent to choosing a_T such that

$$a_T \times v_g = p \times v_g \tag{5.14}$$

Postmultiplying Eq. (5.14) by v_g and using the identity $(a \times b) \times c = (a \cdot c)b - (b \cdot c)a$ yields

$$(a_T \cdot v_g)v_g - ||v_g||^2 a_T = (p \cdot v_g) - ||v_g||^2 p. \tag{5.15}$$

Dividing by $||v_g||^2$ and denoting $i_g = v_g/||v_g||$ gives

$$a_T = p + (q - p \cdot i_g)i_g \tag{5.16}$$

where $q = a_T \cdot i_g$. The scalar quantity q can be calculated by squaring both sides of Eq. (5.16).

$$\begin{aligned} a_T^T a_T &= p^T p + 2(q - p \cdot i_g)p^T i_g + (q - p \cdot i_g)^2 \\ ||a_T||^2 &= ||p||^2 + 2q(p \cdot i_g) - 2(p \cdot i_g)^2 + q^2 - 2q(p \cdot i_g) + (p \cdot i_g)^2 \\ &= ||p||^2 + q^2 - (p \cdot i_g)^2 \end{aligned} \tag{5.17}$$

Therefore, we have

$$q = \left\{||a_T||^2 - ||p||^2 + (p \cdot i_g)^2\right\}^{\frac{1}{2}}. \tag{5.18}$$

Note that in Eq. (5.18), $||a_T||$ must be sufficiently large for q to be real. In other words, if $||a_T||$ is not sufficiently large, it will not be possible to align the vector v_g with its derivative. However, for rockets with burn times that are short (24.45 seconds in the current problem), no difficulty is encountered with this guidance scheme.

Since the MAV ascent problem assumes a constant thrust, the thrust acceleration magnitude $||a_T||$ can be computed at each time instant. Thus, Eq. (5.18) can be used to

calculate q and then Eq. (5.16) to compute a_T. The calculation of v_r and Q depends on the target orbit. Since in our case, the target orbit is circular, the expression for v_r is given by

$$v_r = \sqrt{\frac{\mu}{||r||}} i_n \times i_r \tag{5.19}$$

where i_n is the unit normal to the target orbital plane, i_r is the unit vector in the direction of vehicle's current position r, and μ is the gravitational constant for Mars. However, by using this approach to drive v_g to zero, one could control the shape and orientation of the final orbit, but no direct control of the radius of the orbit is possible [80].

By rewriting Eq. (5.19) as

$$v_r = S_n r \sqrt{\frac{\mu}{||r||^3}} \tag{5.20}$$

with

$$S_n = \begin{bmatrix} 0 & -n_z & n_y \\ n_z & 0 & -n_x \\ -n_y & n_x & 0 \end{bmatrix} \tag{5.21}$$

where n_x, n_y, and n_z are the direction cosines of i_n, we obtain

$$Q = \sqrt{\frac{\mu}{||r||^3}} S_n (I - \tfrac{3}{2} i_r i_r^T) \tag{5.22}$$

5.5.2 LVLH-guidance

The LVLH-guidance law was developed by David G. Hull and Matthew W. Harris in 2012 [81]. The guidance scheme is fuel optimal for the free final time transfer of a rocket between two fixed points under the assumptions of constant thrust, quasiplanar flight in the neighborhood of a spherical primary body, and small thrust angles. Due to the assumptions imposed, the equations of motion for the vehicle are described by Eq.(5.2).

For constant thrust, the problem of minimizing fuel consumption is the same as minimizing flight time if the engine can be shutoff. The engine cannot be shutoff early, however,

there is flexibility in the ignition time. Hence, we consider a minimum time problem.

$$J = t_f \tag{5.23}$$

For the moment, we set the initial time to zero, and all of the initial states are specified. The final time is free, and all of the final states are specified except for the downrange, x_f, which is free. Since the final time cannot actually be free, we will subsequently choose the ignition time to match the desired u_f, but this is not part of the optimal control analysis.

Solution of the optimal control problem begins with the formation of the Hamiltonian and the endpoint function

$$\begin{aligned} H &= \lambda_1 u + \lambda_2 v + \lambda_3 w + \lambda_4 \tau \cos\theta \cos\psi + \lambda_5(\tau \sin\theta - g_m + u^2/r_m) + \lambda_6 \tau \cos\theta \sin\psi \\ G &= t_f + \nu_2(y_f - y_{f_s}) + \nu_3(z_f - z_{f_s}) + \nu_4(u_f - u_{f_s}) + \nu_5(v_f - v_{f_s}) + \nu_6(w_f - w_{f_s}). \end{aligned} \tag{5.24}$$

The differential equations for the multipliers are derived from the condition $\dot{\lambda} = -H_x^T$ and are given by

$$\begin{aligned} &\dot{\lambda}_1 = 0, \quad \dot{\lambda}_2 = 0, \quad \dot{\lambda}_3 = 0 \\ &\dot{\lambda}_4 = -2\lambda_5 u/r_m, \quad \dot{\lambda}_5 = -\lambda_2, \quad \dot{\lambda}_6 = -\lambda_3. \end{aligned} \tag{5.25}$$

With the exception of λ_4, these equations can be integrated to obtain

$$\begin{aligned} &\lambda_1 = \text{Const}, \quad \lambda_2 = \text{Const}, \quad \lambda_3 = \text{Const} \\ &\lambda_5 = -\lambda_2 t + C_2, \quad \lambda_6 = -\lambda_3 t + C_3 \end{aligned} \tag{5.26}$$

where C_2 and C_3 denote constants of integration. Because of the boundary conditions $\lambda_f = G_{x_f}^T$ and $H_f = -G_{t_f}$, it is seen that $\lambda_1 = 0$ and that $H_f = -1$.

The optimal controls are obtained from the condition $H_u^T = 0$ which leads to

$$\begin{aligned} H_\theta &= -\lambda_4 \tau \sin\theta \cos\psi + \lambda_5 \tau \cos\theta - \lambda_6 \tau \sin\theta \sin\psi = 0 \\ H_\psi &= -\lambda_4 \tau \cos\theta \sin\psi + \lambda_6 \tau \cos\theta \cos\psi = 0. \end{aligned} \tag{5.27}$$

From the latter, it is seen that

$$\lambda_4 \tan\psi - \lambda_6 = 0 \tag{5.28}$$

so the former can be rewritten as

$$(\lambda_4 \cos\psi + \lambda_6 \sin\psi)\tan\theta - \lambda_5 = 0. \tag{5.29}$$

The solution of these equations involves a sign ambiguity that can be resolved by applying the Legendre-Clebsch condition or equivalently

$$H_{\theta\theta} \geq 0, \quad H_{\psi\psi} \geq 0, \quad H_{\theta\theta}H_{\psi\psi} - H_{\theta\psi}^2 \geq 0. \tag{5.30}$$

Consequently, if it is assumed that $\cos\theta > 0$, which is logical for ascent, the optimal thrust yaw angle is given by

$$\sin\psi = \frac{-\lambda_6}{\sqrt{\lambda_4^2 + \lambda_6^2}}, \quad \cos\psi = \frac{-\lambda_4}{\sqrt{\lambda_4^2 + \lambda_6^2}} \tag{5.31}$$

and the optimal thrust pitch angle becomes

$$\sin\theta = \frac{-\lambda_5}{\sqrt{\lambda_4^2 + \lambda_5^2 + \lambda_6^2}}, \quad \cos\theta = \frac{\sqrt{\lambda_4^2 + \lambda_6^2}}{\sqrt{\lambda_4^2 + \lambda_5^2 + \lambda_6^2}}. \tag{5.32}$$

Based on the results from Q-guidance, we assume that both thrust angles are small for lunar ascent so that a zeroth-order approximation ($\sin\phi \approx \phi, \cos\phi \approx 1$) is reasonable. Note that $\cos\psi$ is expected to be positive so that λ_4 must be negative, and $\sqrt{\lambda_4^2} = -\lambda_4$. Hence, the equations for the controls can be rewritten as

$$\begin{aligned} \sin\psi &= \frac{\lambda_6/\lambda_4}{\sqrt{1+(\lambda_6/\lambda_4)^2}}, & \cos\psi &= \frac{1}{\sqrt{1+(\lambda_6/\lambda_4)^2}} \\ \sin\theta &= \frac{\lambda_5/\lambda_4}{\sqrt{1+(\lambda_5/\lambda_4)^2+(\lambda_6/\lambda_4)^2}}, & \cos\theta &= \frac{\sqrt{1+(\lambda_6/\lambda_4)^2}}{\sqrt{1+(\lambda_5/\lambda_4)^2+(\lambda_6/\lambda_4)^2}} \end{aligned} \tag{5.33}$$

indicating that the small angle approximations are

$$(\lambda_6/\lambda_4)^2 << 1, \quad (\lambda_5/\lambda_4)^2 << 1. \tag{5.34}$$

Finally, after the small angle assumptions are made, the controls are given by

$$\sin\psi = \lambda_6/\lambda_4, \quad \cos\psi = 1, \quad \sin\theta = \lambda_5/\lambda_4, \quad \cos\theta = 1. \tag{5.35}$$

Next, the state equations are combined with the control and multiplier equations to obtain the following differential equations for a two-point boundary value problem (TP-BVP):

$$\begin{aligned} \dot{x} &= u, \quad \dot{u} = \tau \\ \dot{y} &= v, \quad \dot{v} = \tau[(-\lambda_2 t + C_2)/\lambda_4] - g_m + u^2/r_m \\ \dot{z} &= w, \quad \dot{w} = \tau[(-\lambda_3 t + C_3)/\lambda_4] \\ \dot{\lambda}_4 &= -2(-\lambda_2 t + C_2)u/r_m. \end{aligned} \tag{5.36}$$

The solution process begins by integrating the $\dot{u}$, $\dot{x}$, and $\dot{\lambda}_4$ equations. The results for u and x are given by

$$u = u_0 - V_e \ln(1 - t/\alpha) \tag{5.37}$$

$$x = x_0 + u_0 t + V_e(\alpha - t)\ln(1 - t/\alpha) + V_e t. \tag{5.38}$$

Then, with u from Eq. (5.37), the $\dot{\lambda}_4$ equation leads to

$$\begin{aligned} \lambda_4 &= C_1 - (2u_0/r_m)(-\lambda_2 t^2/2 + C_2 t) \\ &- (V_e\lambda_2/(2r_m)[2(t^2 - \alpha^2)\ln(1 - t/\alpha) - 2\alpha t - t^2] \\ &- (2V_e C_2/r_m)[(\alpha - t)\ln(1 - t/\alpha) - t] \end{aligned} \tag{5.39}$$

where $\alpha = m_0/\beta$ and C_1 is the initial value ($t_0 = 0$) of λ_4.

At this point, it is seen that the unknowns $\lambda_2, C_2, \lambda_3, C_3$ can be divided by C_1, and the need for the final condition $H_f = -1$ is eliminated. Division by C_1 is denoted by an over bar. Hence, Eq. (5.39) becomes

$$\begin{aligned} \bar{\lambda}_4 &= 1 - (2u_0/r_m)(-\bar{\lambda}_2 t^2/2 + \bar{C}_2 t) \\ &- (V_e \bar{\lambda}_2/(2r_m)[2(t^2 - \alpha^2)\ln(1 - t/\alpha) - 2\alpha t - t^2] \\ &- (2V_e \bar{C}_2/r_m)[(\alpha - t)\ln(1 - t/\alpha) - t], \end{aligned} \tag{5.40}$$

where $\bar{\lambda}_4$ is a function of $t, \bar{\lambda}_2, \bar{C}_2$ The remaining equations of motion are rewritten as

$$\begin{aligned} &\dot{y} = v, \quad \dot{v} = \tau(\bar{\lambda}_5/\bar{\lambda}_4) - g_m + [u_0 - V_e \ln(1 - t/\alpha)]^2/r_m \\ &\dot{z} = w, \quad \dot{w} = \tau(\bar{\lambda}_6/\bar{\lambda}_4) \end{aligned} \tag{5.41}$$

where

$$\bar{\lambda}_5 = -\bar{\lambda}_2 t + \bar{C}_2, \quad \bar{\lambda}_6 = -\bar{\lambda}_3 t + \bar{C}_3. \tag{5.42}$$

Solution of the $\dot{v}$ and $\dot{y}$ equations involves the first and second integrals of τ which lead to the modified thrust integrals $J'(t_f, \bar{\lambda}_2, \bar{C}_2)$, $L'(t_f, \bar{\lambda}_2, \bar{C}_2)$, $Q'(t_f, \bar{\lambda}_2, \bar{C}_2)$, and $S'(t_f, \bar{\lambda}_2, \bar{C}_2)$ (Appendix: A). Also needed are the first and second integrals of the centrifugal acceleration u^2/r_m. These integrals, denoted $F(t_f)$ and $G(t_f)$, can be obtained analytically by substituting the already known u (Appendix: B). Then, the v and y equations become

$$\begin{aligned} v &= -v_0 - \bar{\lambda}_2 \widehat{J}' + \bar{C}_2 \widehat{L}' - g_m t + \widehat{F} \\ y &= -y_0 - v_0 t - \bar{\lambda}_2 \widehat{Q}' + \bar{C}_2 \widehat{S}' - g_m t^2/2 + \widehat{G}, \end{aligned} \tag{5.43}$$

where the over hat denotes the corresponding integral evaluated at t instead of t_f. Similarly, the $\dot{w}$ and $\dot{z}$ equations can be integrated to obtain

$$\begin{aligned} w &= w_0 - \bar{\lambda}_3 \widehat{J}' + \bar{C}_3 \widehat{L}' \\ z &= z_0 + w_0 t - \bar{\lambda}_3 \widehat{Q}' + \bar{C}_3 \widehat{S}'. \end{aligned} \tag{5.44}$$

At this point, the prescribed boundary conditions are applied to obtain the equations to be solved for the unknown constants $t_f, \bar{\lambda}_2, \bar{C}_2, \bar{\lambda}_3, \bar{C}_3$ using the definitions

$$\begin{aligned} V_x &= u_f - u_0 \\ V_y &= v_f - v_0 + g_m t_f - F, \quad Y = y_f - y_0 - v_0 t_f + g_m t_f^2/2 - G \\ V_z &= w_f - w_0, \quad Z = z_f - z_0 - w_0 t_f. \end{aligned} \tag{5.45}$$

First, Eq. (5.37) applied at the final time can be solved for t_f as

$$t_f = \alpha[1 - \exp(-V_x/V_e)]. \tag{5.46}$$

Then, Eq. (5.43) can be rewritten as

$$\begin{aligned} V_y &= -\bar{\lambda}_2 J'(t_f, \bar{\lambda}_2, \bar{C}_2) + \bar{C}_2 L'(t_f, \bar{\lambda}_2, \bar{C}_2) \\ Y &= -\bar{\lambda}_2 Q'(t_f, \bar{\lambda}_2, \bar{C}_2) + \bar{C}_2 S'(t_f, \bar{\lambda}_2, \bar{C}_2). \end{aligned} \tag{5.47}$$

For known values of V_y and Y, these equations can be solved iteratively for $\bar{\lambda}_2$ and $\bar{C}_2$. Finally, Eq. (5.44) can be applied at t_f and solved analytically for $\bar{\lambda}_3$ and $\bar{C}_3$ as

$$\begin{aligned} \bar{\lambda}_3 &= (V_z S' - Z L')/(L'Q' - J'S') \\ \bar{C}_3 &= (V_z Q' - Z J')/(L'Q' - J'S'). \end{aligned} \tag{5.48}$$

In conclusion, there are only two implicit equations to be solved to obtain the five unknowns.

Finally, the approximate optimal controls are obtained from Eq. (5.33) as

$$\begin{aligned} \sin\psi &= (-\bar{\lambda}_2 t + \bar{C}_2)/\bar{\lambda}_4, \quad \cos\psi = 1 \\ \sin\theta &= (-\bar{\lambda}_3 t + \bar{C}_3)/\bar{\lambda}_4, \quad \cos\theta = 1. \end{aligned} \tag{5.49}$$

However, in a simulation, the controls should be calculated as in Eq. (5.33) with a bar over each multiplier. This ensures that sine squared plus cosine squared equals one.

Based on other analysis, we know that $\bar{\lambda}_4$ is very nearly equal to one, so that an approximate solution with $\bar{\lambda}_4 = 1$ is possible. The effect of this assumption is that the

modified thrust integrals become the standard thrust integrals which are functions of the final time only. Hence, the equations to be solved for the unknown constants become the following:

$$\begin{aligned} V_x &= L \\ V_y &= -\bar{\lambda}_2 J + \bar{C}_2 L, \quad Y = -\bar{\lambda}_2 Q + \bar{C}_2 S \\ V_z &= -\bar{\lambda}_3 J + C_3 L \quad Z = -\bar{\lambda}_3 Q + \bar{C}_3 S. \end{aligned} \tag{5.50}$$

The V_x equation can be solved for the final time

$$t_f = \alpha[1 - \exp(-V_x/V_e)] \tag{5.51}$$

as before. Given t_f, the thrust integrals are known so that the V_y and Y equations can be solved for $\bar{\lambda}_2$ and $\bar{C}_2$ as follows:

$$\begin{aligned} \bar{\lambda}_2 &= (V_y S - Y L)/(LQ - JS) \\ \bar{C}_2 &= (V_y Q - Y J)/(LQ - JS). \end{aligned} \tag{5.52}$$

Finally, the V_z and Z equations can be solved for $\bar{\lambda}_3$ and $\bar{C}_3$, that is,

$$\begin{aligned} \bar{\lambda}_3 &= (V_z S - Z L)/(LQ - JS) \\ \bar{C}_3 &= (V_z Q - Z J)/(LQ - JS). \end{aligned} \tag{5.53}$$

Note that the solution is completely analytical in that no quadratures or iterations are necessary.

With $\bar{\lambda}_4 = 1$, the optimal controls are obtained from Eq. (5.33) as

$$\begin{aligned} \sin\psi &= \frac{\bar{\lambda}_6}{\sqrt{1+\bar{\lambda}_6^2}}, & \cos\psi &= \frac{1}{\sqrt{1+\bar{\lambda}_6^2}} \\ \sin\theta &= \frac{\bar{\lambda}_5}{\sqrt{1+\bar{\lambda}_5^2+\bar{\lambda}_6^2}}, & \cos\theta &= \frac{\sqrt{1+\bar{\lambda}_6^2}}{\sqrt{1+\bar{\lambda}_5^2+\bar{\lambda}_6^2}}. \end{aligned} \tag{5.54}$$

In a practical implementation, the final time t_f is not free and the final downrange velocity constraint on u cannot be met exactly. Thus, an effective trigger for LVLH-guidance must ignite the second-stage to minimize error in the downrange velocity.

5.5.3 SOCP-guidance

To do real-time optimization within guidance, the underlying optimization problems must be solvable by numerical methods that offer convergence guarantees. One of the more general classes of problem for which such solvers exist are second-order cone programs (SOCPs). Notably, SOCPs are convex and they can be solved to global optimality in polynomial time. The optimization problem formulated in the LVLH-guidance section is not convex because of the nonlinear dynamics and annular thrust magnitude constraint. Relaxation techniques exist to transform the annular constraint, but there are no similar workarounds for nonlinear dynamics. One must either make an approximation to induce convexity or rely on nonlinear solvers that do have the needed convergence guarantees. Here, convexity is induced by approximating the u^2/r term – ignoring it is too big of an assumption – by a linearly time varying estimate denoted $\hat{u}_r$. Hence the dynamics are given by

$$\begin{aligned} \dot{x} &= u \\ \dot{y} &= v \\ \dot{z} &= w \\ \dot{u} &= \tau_x \\ \dot{v} &= \tau_y - g + \hat{u}_r \\ \dot{w} &= \tau_z \end{aligned} \tag{5.55}$$

where the thrust components have now been used in place of the thrust angles. The equations are linear and time-varying because of the $\hat{u}_r$ term. Once ignition occurs, the burn time is fixed. The goal is to minimize error in the final state while adhering to the above equations of motion and constant thrust magnitude constraint. Mathematically, the objective is

$$J = (y_f - y_d)^2 + (z_f - z_d)^2 + \cdots + (w_f - w_d)^2 \tag{5.56}$$

where the subscript f denotes the value at the final time and subscript d denotes the desired

value at the final time. In the LVLH frame, the final x position is free since it represents downrange position (analogous to anomaly in the orbital elements). Several formulations have been investigated. For example, hard constraints can be imposed to force the final orbital elements within their feasible region. However, doing so might make the optimization problem infeasible particularly as the time-to-go approaches zero. In an attempt to balance performance with numerical stability, the objective given in Eq. (5.56) is chosen.

Constant thrust is assumed so that thrust acceleration τ is known but time-varying. The control constraint is

$$\tau_x^2 + \tau_y^2 + \tau_z^2 = \tau^2 \tag{5.57}$$

which must hold pointwise in time. This constraint is non-convex and presents the main challenge in solving the optimal control problem. Based on the results from the chapter 4, the following simple relaxation is proposed.

$$\tau_x^2 + \tau_y^2 + \tau_z^2 \leq \tau^2 \tag{5.58}$$

This weaker constraint is convex but may not yield feasible solutions. However, because the system is controllable with zero thrust in the interior of the control set, the reachable set is expansive and any minimum time solution will satisfy the constraint with equality. The fixed final time may not correspond to the minimum time. But one may apply feasible (but otherwise arbitrary) controls during the time difference to achieve optimal controls (refer back to Theorem 4.4). Hence, the numerical optimization problem is solvable as a SOCP.

The resulting optimization model is a continuous time optimal control problem. To couple with a solver, a basic discretization is applied by assuming a zero-order hold on the controls. This is appropriate since guidance issues zero-order hold commands to the control system. Because of linearity, the discretization is exact. The problem is then parsed using YALMIP and solved using Gurobi. Theoretically, the LVLH-guidance thrust angles vary linearly with time as do the SOCP-guidance thrust angles. Using a first-order hold in these guidance implementations may improve the results, but this was not performed in order to

be consistent with the Q-guidance scheme.

5.6 Ignition Triggers

Ignition triggers determine the starting time/location of the circularization burn. Under nominal conditions, the lowest-energy point to perform this maneuver is at the apoapse of the ballistic trajectory. However, in the presence of dispersions such as initial mass variations or SRM performance/delta-v variations, burning at apoapse causes large discrepencies in final semi-major axis and eccentricity [78,86]. As such, the second stage SRM is designed such that it carries excess delta-v to account for such off-nominal conditions or intrinsic solid motor performance variations.

For circularization at apoapse, approximately 1,689 m/s of delta-v is required. The second stage SRM can deliver 1,696 m/s of delta-v. Thus, the nominal case carries 7 m/s of excess delta-v. This is shown graphically in Figure 5.2. The dashed horizontal line corresponds to the available delta-v. The dotted vertical line identifies the point of apoapse. The solid curve identifies the required delta-v as a function of time.

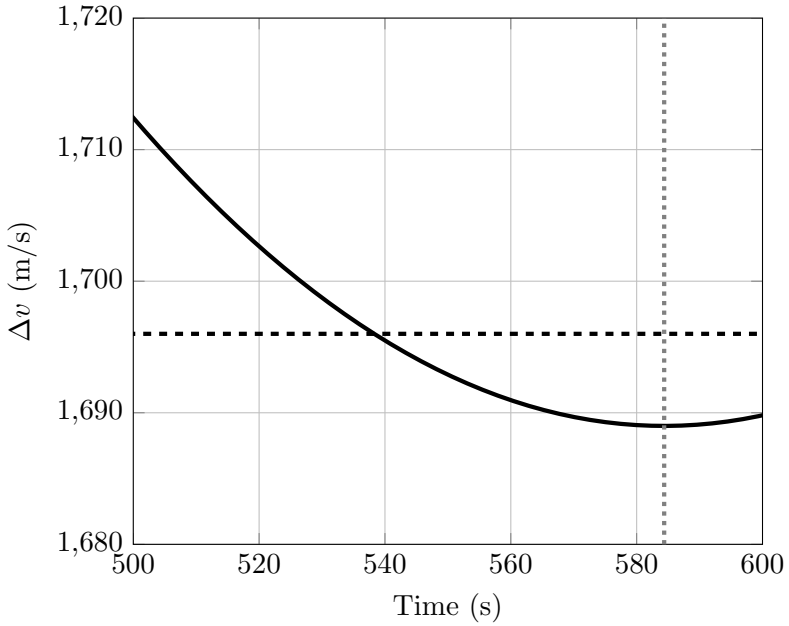

Fig. 5.2: Required Δv vs. time

To account for this excess energy, a trigger logic must be implemented to ignite the second stage SRM at some point prior to the apoapse while minimizing the dispersions in final semi-major axis and eccentricity. That is, the burn should be intentionally performed at a sub-optimal point/time. A practical implementation requires closed-loop guidance calculations to be continuously performed as the vehicle approaches the apoapse. Three ignition triggers are analyzed in this work – 1) Q-trigger (NASA's current choice), 2) Box-trigger, and 3) uhat-trigger.

5.6.1 Q-trigger

This trigger was developed by NASA and is based in Q-guidance. The approach of implementating the trigger along with Q-guidance is collectively termed Simple Cross-product Steering (SXS) by NASA [86]. According to this trigger logic, ignition should occur when the magnitude of the velocity-to-be-gained vector (v_g) computed onboard matches the predicted onboard delta-v capability of the SRM.

Thus, the trigger aims at finding the time t_{ig} after the current mission elapsed time t, such that ignition occurs at $t_b = t + t_{ig}$. This requires solving the equation

$$f(t_{ig}) = ||v_g(t_{ig})|| - v_{cap}, \tag{5.59}$$

where v_{cap} is the predicted onboard delta-v capability of the SRM. The solution can be found using the Newton-Raphson method, where t_{ig} can be iterated in the following fashion

$$t_{ig_{k+1}} = t_{ig_k} - \frac{f(t_{ig})}{\dot{f}(t_{ig})} = t_{ig_k} - \frac{\big(||v_g(t_{ig})|| - v_{cap}\big)}{\big(\frac{\partial ||v_g||}{\partial t_{ig}}\big)}. \tag{5.60}$$

Note that the partial of $||v_g||$ with respect to time in Eq. (5.60) can be written as

$$\frac{\partial ||v_g||}{\partial t} = i_g \cdot \frac{\partial v_g}{\partial t} \tag{5.61}$$

The computations are performed in a guidance target frame (i_x, i_y, i_z), which shares similarities to the LVLH frame. The vector i_y represents the out-of-plane component, and is

defined as the anti-parallel direction to the angular momentum vector of the target orbit ,i.e., $i_y = -i_n$. The radial component i_x is represented by the current inertial position vector projected onto the target plane.

$$i_x = \frac{r - (r \cdot i_y)}{||r - (r \cdot i_y||} \tag{5.62}$$

Finally, the downrage component i_z completes the right-handed coordinate system. Now, the partial of the vector v_g with repect to time in Eq. (5.61) is given by

$$\frac{\partial v_g}{\partial t} = -\frac{\mu}{||v_r||||r||^2}[i_r \cdot v]i_z - ||v_r||\frac{(v \cdot i_z)}{(r \cdot i_x)}i_x + \frac{\mu}{||r||^3}r \tag{5.63}$$

The derivation for Eq. (5.63) is given in Appendix: D.

5.6.2 Box-trigger

This trigger makes use of the following logic – as the vehicle approaches apoapse, 1) guidance calculations are performed at each time instant t assuming that the ignition time is t, i.e., $t_b = t$, followed by 2) a computation for the estimates of final semi-major axis and eccentricity, and 3) activating the trigger instantly if the final values meet the predefined mission objectives. Because the trigger activates when the state first enters the apoapse-eccentricity box, we call it the box-trigger. A key advantage of the trigger is that it replaces the Newton iterations in the Q-trigger with an integration. Moreover, the trigger is applicable to all guidance schemes discussed in Section 5.5.

5.6.3 uhat-trigger

As noted in Section 5.5.2, an effective trigger for LVLH-guidance must ignite the second-stage to minimize error in the downrange velocity u. We call such a trigger the uhat-trigger since it is based on an estimate of u. The trigger logic can be summarized as follows – as the vehicle approaches the apoapse, at each time instant t,

1. Compute $\bar{\lambda}_2, \bar{C}_2, \bar{\lambda}_3, \bar{C}_3$ using Eq. (5.52)-(5.53).

2. Compute $\bar{\lambda}_5$ and $\bar{\lambda}_6$ $\forall\ t \in [0, t_f]$, where $t_f = 24.45$ seconds.

3. Compute $\sin\psi, \cos\psi, \sin\theta$, and $\cos\theta$ using Eq. (5.54) $\forall\ t \in [0, t_f]$.

4. Integrate the $\dot{u}$ equation in Eq. (5.2) using a standard quadrature technique such as the trapezoidal rule to find the estimate $\hat{u}$.

5. Activate the trigger if $\hat{u} \geq u_d$, where the u_d is the desired downrange velocity.

Thus, the computation of $\hat{u}$ involves one quadrature and the trigger is iteration free. Hence, there are no convergence concerns. Aside from the fact that u must be estimated, this trigger logic is optimal for LVLH-guidance law.

5.7 Performance Comparison

This section compares the performance of the different guidance schemes discussed in Section 5.5 coupled with the different ignition triggers discussed in Section 5.6. The performance is evaluated under both nominal and off-nominal (Monte Carlo) settings.

5.7.1 Q-guidance Performance

To establish a baseline for comparison, NASA's current guidance choice Q-guidance is implemented along with the current ignition trigger (Q-trigger) logic for energy management (required to bleed the excess delta-v capability). Note that while Q-guidance is analytic Q-trigger is not as it requires Newton iterations. Nominal pitch and yaw angles are shown in Figures 5.3 and 5.4 respectively.

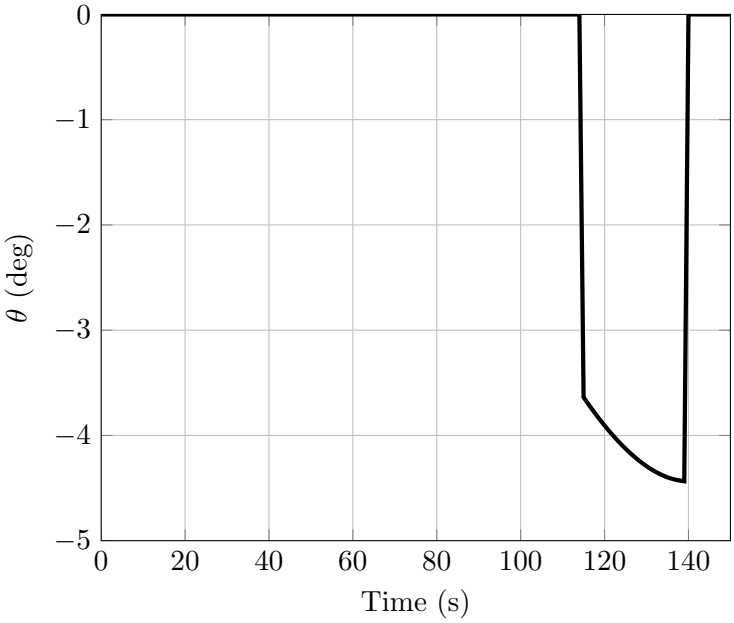

Fig. 5.3: Thrust pitch angle using Q-guidance.

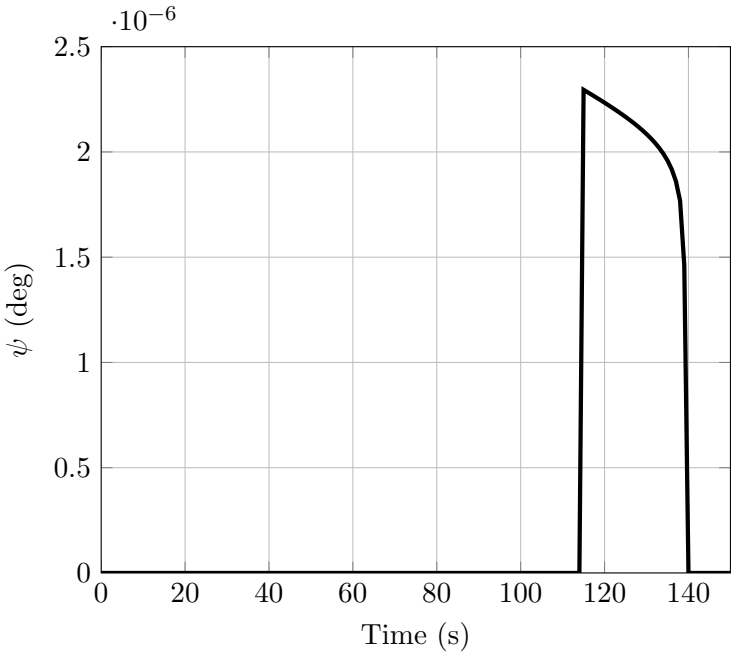

Fig. 5.4: Thrust yaw angle using Q-guidance.

After the second burn, the orbit has been successfully circularized. The semi-major axis, eccentricity, and inclination are below and within tolerances specified by NASA.

```
sma = 3.445340870281458e+05 km
ecc = 0.001312904482567
inc = 24.999996433414527 deg
```

To verify that the Q-guidance implemented in this work is similar to that of NASA's, normally distributed mass at launch and stage-2 delta-v capacity are introduced, and the results are compared. These distributions have a 3σ range of about 1 kg and 1 percent respectively. It is observed that the mass dispersions place the final orbit semi-major axis within a range of about 80 km and the delta-v dispersions place the final orbit semi-major axis within a range of about 60 km. NASA reports 1-D sensitivities of 90 km and 75 km, respectively, and notes that these are an order of magnitude greater than other parameter affects [78]. The dispersion for each case are shown in Figures 5.5 and 5.6.

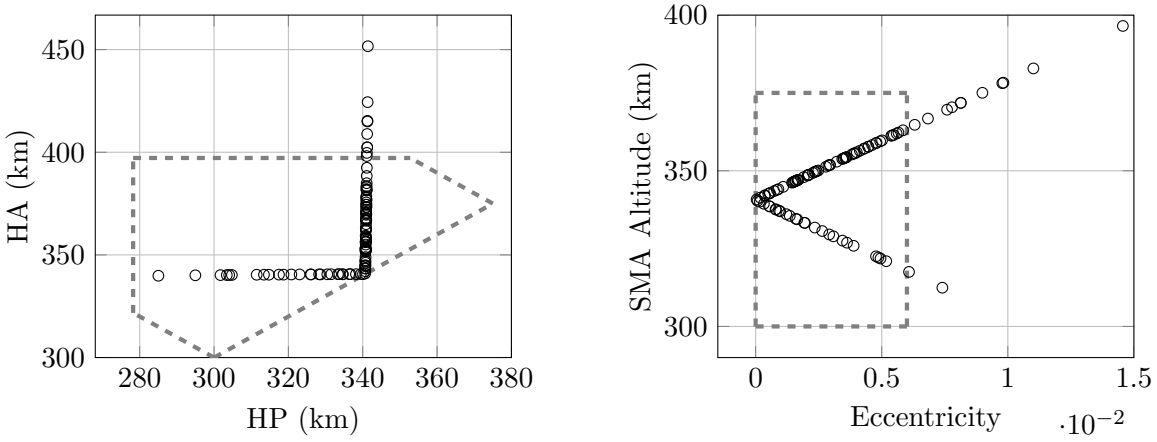

Fig. 5.5: Final orbital elements for mass dispersions. The boxes denote the feasible region defined by NASA.

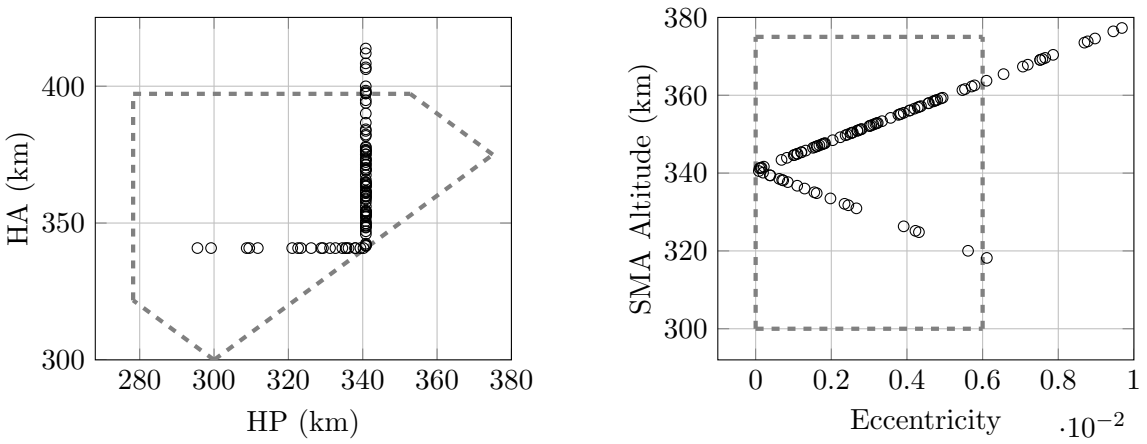

Fig. 5.6: Final orbital elements for delta-v dispersions. The boxes denote the feasible region defined by NASA.

It is evident from the number of points outside of the feasible regions in Figures 5.5 and 5.6 that the 3σ limits on mass and delta-v must be reduced to ensure feasibility with high probability. When they are reduced to 1/3 kg and 1/3 percent, the final orbital elements are well within the feasible region as seen in Figure 5.7. Given our under-prediction of the 1-D sensitivities, these dispersion levels will be used for comparison with other guidance laws in the upcoming sections. Although not shown, 99% of the cases were within the feasible region when the mass dispersion was increased to 1/2 kg.

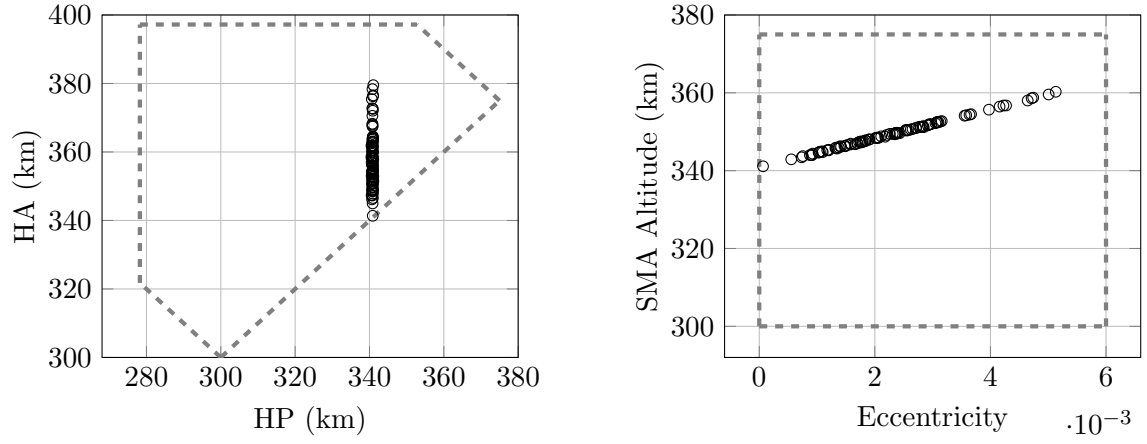

Fig. 5.7: Reducing 3σ dispersion levels to 1/3 kg and 1/3 percent places the final orbital elements well within the feasible region.

Based on these plots, it appears that the Q-trigger is primarily associated with the periapsis altitude since dispersions are mostly vertical in the left-hand plot. As such, the eccentricity dispersions are larger than required and exceed 0.004.

The final orbital elements using Q-guidance with the box-trigger are shown in Figure 5.8, in which it is evident the dispersions are tighter. The trigger has the affect of distributing the dispersion along lines of constant apoapsis and periapsis, and decreasing the dispersions in periapsis and eccentricity.

Although testing has not been done in high fidelity simulations, the box-trigger may provide an opportunity to reduce the excess delta-v (and hence mass) carried for the second-stage and weaken the navigation requirements.

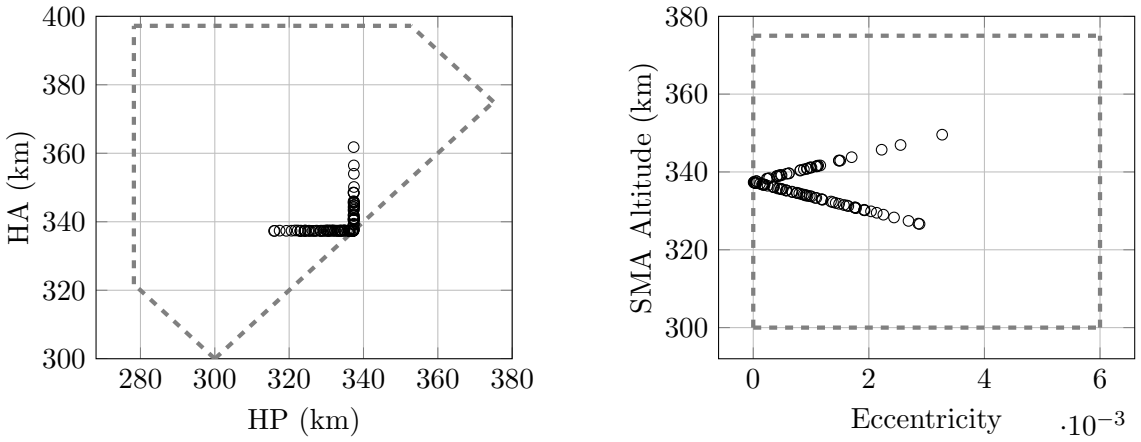

Fig. 5.8: Changing from the Q-trigger to the box-trigger reduced dispersion levels by about half in eccentricity and apoapsis altitude. Additionallly, the box-trigger is analytic.

5.7.2 LVLH-guidance Performance

Now we provide performance results for LVLH-guidance in the nominal case (without dispersions). For this study, an analytic version of LVLH-guidance with the uhat-trigger was implemented. The resulting thrust pitch and yaw angles are shown in Figures 5.9 and 5.10 respectively.

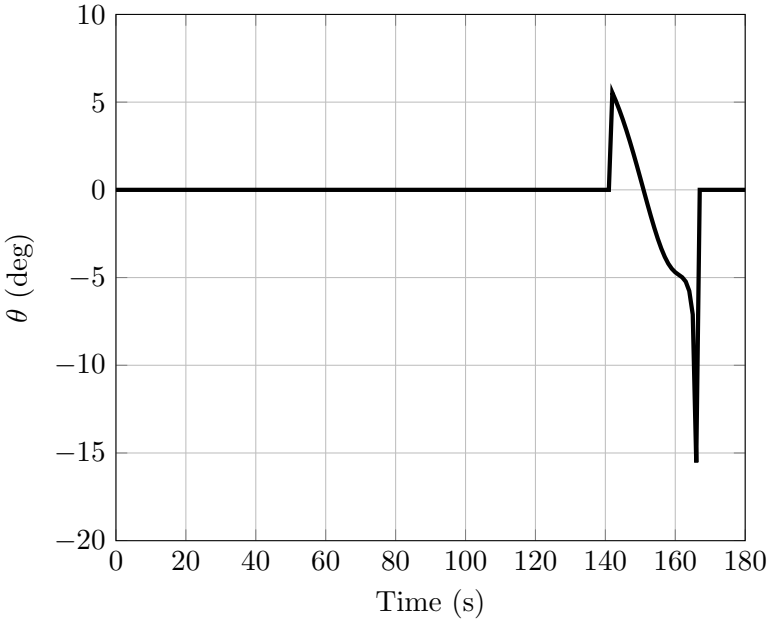

Fig. 5.9: Thrust pitch angle using LVLH-guidance.

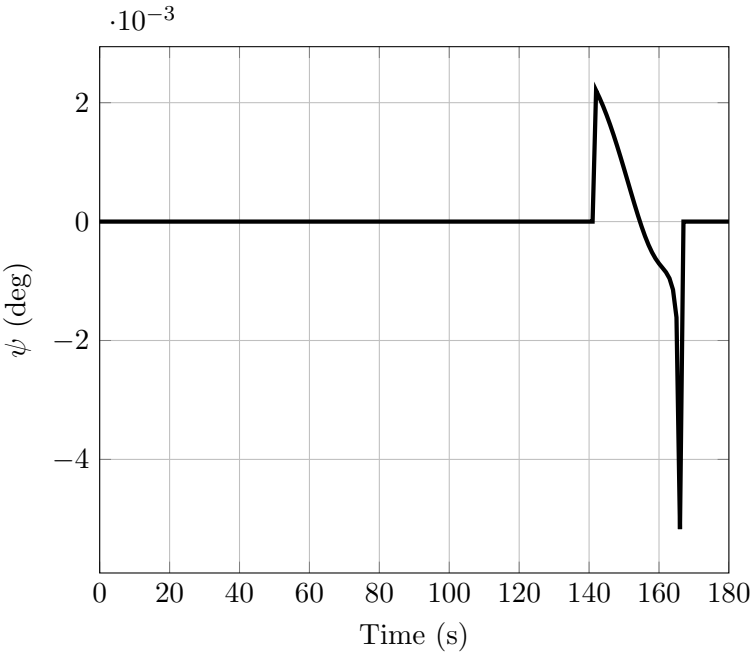

Fig. 5.10: Thrust yaw angle using LVLH-guidance.

After the second burn, the orbit has been successfully circularized. The semi-major axis, eccentricity, and inclination are below and within tolerances specified by NASA.

```
sma = 3.448382806278444e+05 km
ecc = 5.089799571866628e-04
inc = 25.000002551429098 deg
```

Two importants observations can be made. First, in the nominal case, both Q-guidance and the LVLH-guidance perform equally well. Second, the LVLH-guidance naturally offers some energy management as it has a nearly symmetric burn angle with both positive and negative values in both pitch and yaw.

Now, similar dispersions as those used in Q-guidance with 3σ levels of 1/3 kg for mass and 1/3 percent for delta-v capacity are introduced. The final orbital elements are shown in Figure 5.11, and it is evident that LVLH-guidance performance is about the same as Q-guidance with the box-trigger.

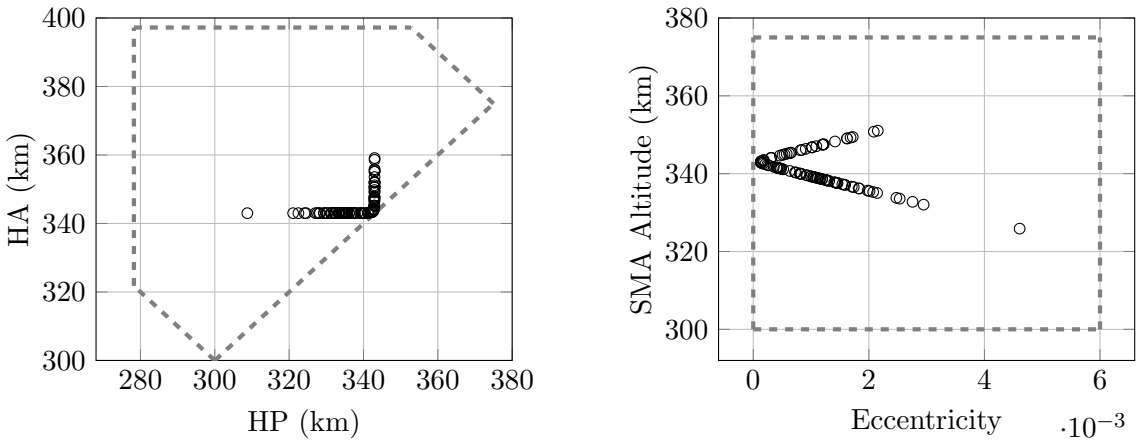

Fig. 5.11: Final orbital elements dispersions for LVLH-guidance using the uhat-trigger. Performance is similar to Q-guidance using the box-trigger

This analysis indicates that LVLH-guidance using the uhat-trigger is a solid competitor to Q-guidance using the box-trigger and that both perform better than Q-guidance with the Q-trigger. However, note that this conclusion is based on a relatively low fidelity simulation and dispersions on the most sensitive parameters. Hence, further analysis by NASA in high

fidelity simulations with additional dispersions is needed to conclude which guidance and trigger are best.

5.7.3 SOCP-guidance Performance

The computational guidance scheme also naturally bleeds energy and matches the desired final conditions in both nominal and off-nominal cases. Thrust pitch and yaw angles for the nominal case are shown in Figures 5.12 and 5.13 respectively.

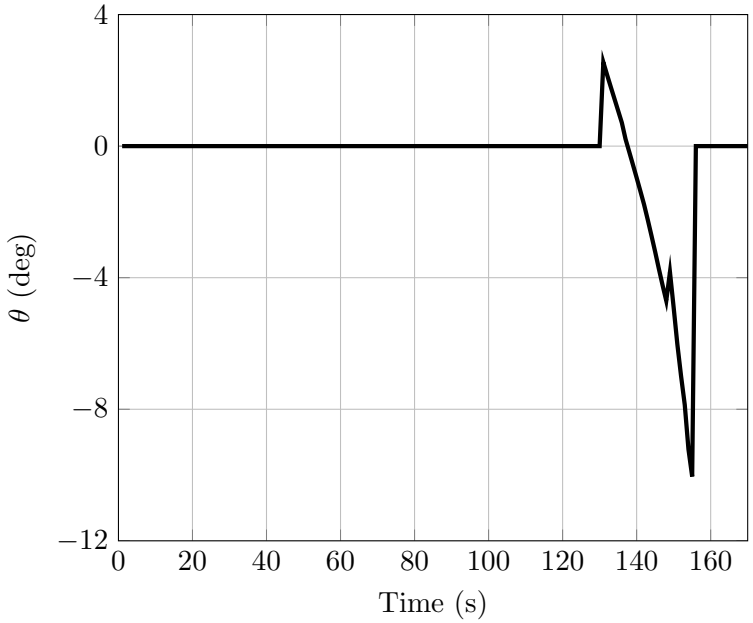

Fig. 5.12: Thrust pitch angle using SOCP-guidance.

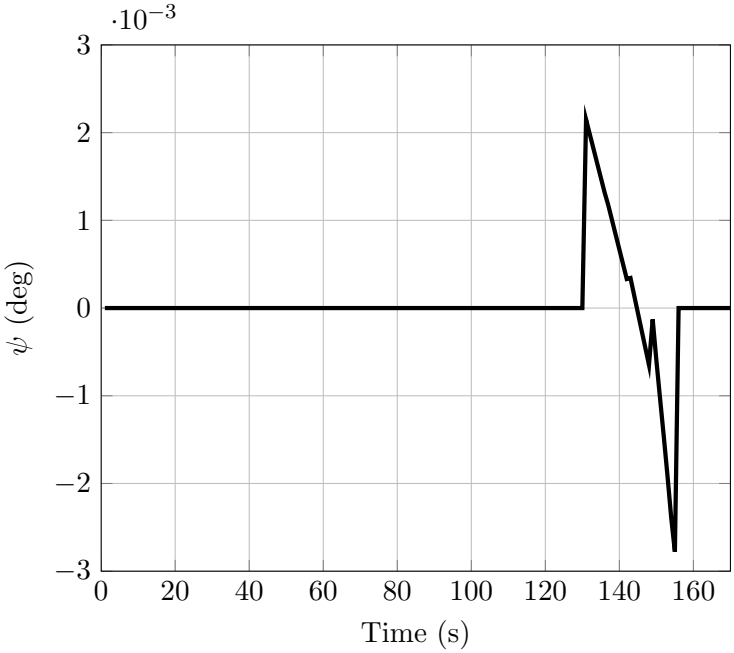

Fig. 5.13: Thrust yaw angle using SOCP-guidance.

The final conditions meet specifications.

```
sma = 3.447602502201293e+05 km
ecc = 7.640199463441428e-04
inc = 24.999998329235272 deg
```

In each call to guidance, the computational guidance algorithm solves a second-order cone program. The average solution time is 0.17 seconds. Previous work indicates that solve times on RAD hard flight computers are 2-3 orders of magnitude slower; however, a customized algorithm accelerates solve time by an order of magnitude. Hence, estimated solve time on a flight computer is approximately one second, which is appropriate for guidance applications.

Next, similar dispersions as those used in Q-guidance and LVLH-guidance with 3σ levels of 1/3 kg for mass and 1/3 percent for delta-v capacity are introduced. The final orbital elements are shown in Figure 5.14. Results are similar when using either the uhat-trigger or box-trigger, and it is evident that SOCP-guidance performance is about the same

as Q-guidance with the Q-trigger but worse than the other guidance methods presented.

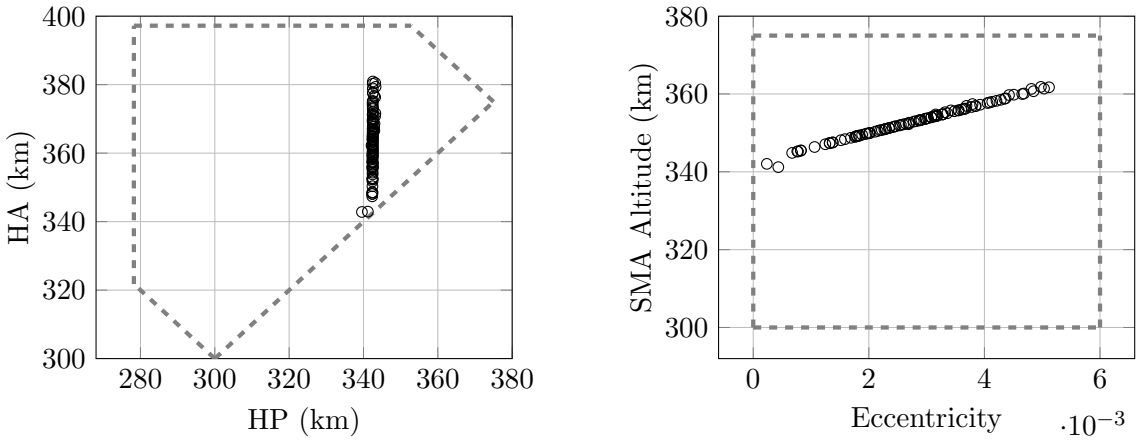

Fig. 5.14: Final orbital elements dispersions for SOCP-guidance using the box-trigger. Performance is similar to Q-guidance using the Q-trigger.

Although not further explored, the study suggests that a different trigger exist for SOCP-guidance that will distribute the dispersions along periapsis and apoapsis. In any case, the current analysis do not warrant the results to be significantly different than those presented for Q-guidance or LVLH-guidance. It seems that the short, fixed burn time and non-throttleable engine have eliminated the degrees of freedom that a computational guidance algorithm could leverage for benefit.

5.8 Possible Benefits of Guidance or Trigger Changes

In this section, we briefly discuss possible benefits of changing triggers or guidance laws. Refer to Figures 5.5 and 5.6 to see the independent effects of mass and delta-v dispersions on the final orbital elements using Q-guidance with the Q-trigger (both in the current NASA plan). There are many instances outside of the feasible region and the combined effects are worse. By switching to the box-trigger, about 95% of the cases are feasible. This is shown in Figure 5.15.

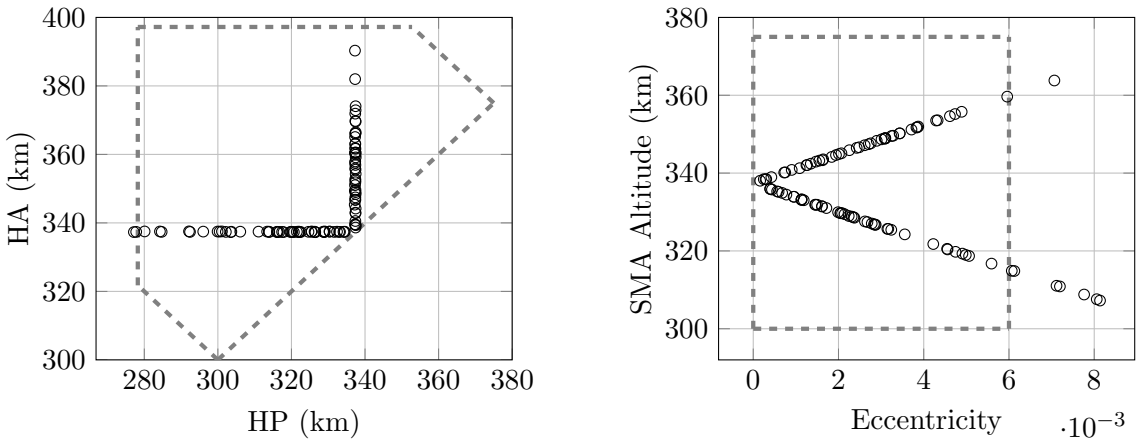

Fig. 5.15: Final orbital elements dispersions for Q-guidance using the box-trigger. As in Figures 5.5 and 5.6, the 3σ levels are 1 kg and 1 percent. Based on these simulations, the box-trigger improves Q-guidance.

We now investigate possible reductions in mass. Refer to Figure 5.7 to see Q-guidance performance using the Q-trigger with 3σ dispersions of 1/3 kg and 1/3 percent, respectively for mass and stage-2 delta-v capacity. These are with the nominal delta-v capacity of 1,696 m/s. Even at higher dispersion levels, using Q-guidance with the box-trigger can reduce the nominal delta-v while maintaining a high probability of being in the feasible region. This is shown in Figure 5.16 with a nominal delta-v capacity of 1,690 m/s.

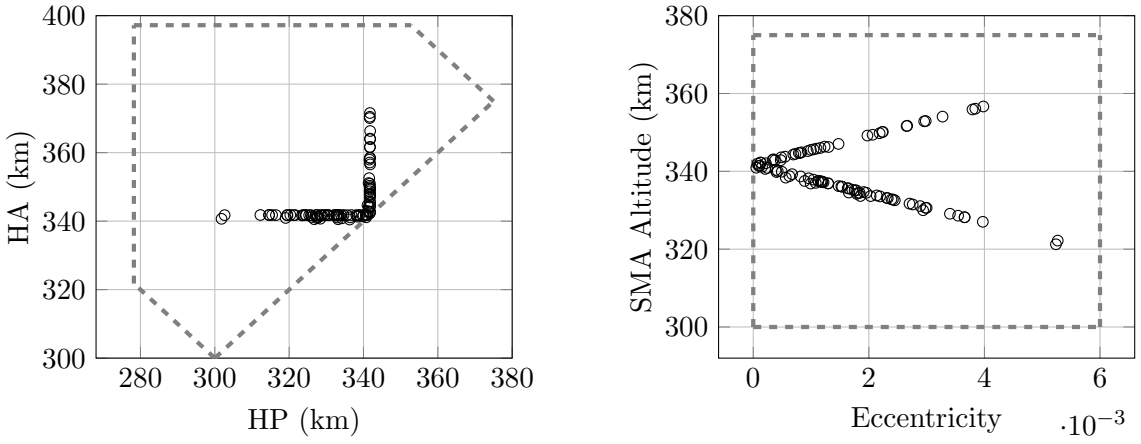

Fig. 5.16: Final orbital elements dispersions for Q-guidance using the box-trigger and a nominal delta-v of 1,690 m/s. The 3σ levels are 1 kg and 1/2 percent on mass and delta-v.

Lastly, similar statements can be made about LVLH-guidance using the uhat-trigger as performance is similar to Q-guidance with the box-trigger. Based on analysis, the LVLH-guidance with the uhat-trigger is a guidance scheme that demands further consideration. It is theoretically the best since it matches five of six states in guidance and attempts to match the sixth in the trigger logic. It also performs better in Monte Carlo analyses compared to the other guidance schemes.

5.9 Conclusions

Given the short duration of the second burn, all guidance approaches behave about the same in nominal circumstances and they are all sensitive to the trigger (ignition) logic. Monte Carlo analyses have focused on the three most sensitive parameters: mass at launch, stage-2 delta-v, and trigger logic. Results indicate that Q-guidance and LVLH-guidance have different thrust profiles but similar dispersions in the final orbit. Because it relies on a lower fidelity dynamic model, SOCP-guidance has a thrust profile similar to LVLH-guidance but has higher dispersion levels in the final orbit. Notably, changing the Q-guidance trigger to box-trigger reduces the final orbit dispersions compared to NASA's current approach (Q-trigger). Further, the box-trigger does not require Newton iterations. LVLH-guidance and its trigger perform the best and are the most simple. A hypothesis was that SOCP-guidance would offer improved fuel and dispersion performance. However, it seems that the short duration of the second burn, sensitivity to the trigger time, and selection of a solid (non-throttleable) rocket negates much of the hypothesized improvements.

CHAPTER 6
STRONG OBSERVABILITY AS A SUFFICIENT CONDITION FOR NON-SINGULARITY IN OPTIMAL CONTROL WITH MIXED CONSTRAINTS

6.1 Introduction

This chapter analyzes a class of finite horizon optimal control problems with linear time-varying dynamics defined on a smooth manifold with a mixed constraint (a constraint involving both the state and control) and additional control constraints. The main contribution of the chapter is the identification of sufficient conditions for non-singularity of optimal control for this particular class of problems. In particular, it is shown that strong observability of the dual system is sufficient for there to be no non-degenerate intervals on which the control is always in the interior of its constraint set. Singular solutions are characterized as zero directions for the dual system, and they are easy to calculate for linear time-invariant systems. Knowing an optimal control is on the boundary simplifies controller design, enables exact and approximate relaxations, and helps to choose an appropriate numerical method.

Motivation for this work is real-time control of mechanical and aerospace systems that are highly constrained by operational, environmental, and mission constraints. One such problem is the atmospheric reentry of the space shuttle [38–40]. As previously stated in Section 2.2, the heating constraint is a mixed constraint that is a function of the states and the control. Another particularly relevant example is that of planetary descent [1, 41]. The spacecraft is powered with a chemical propulsion system that provides thrust magnitudes between a non-zero lower bound and an upper bound, and the mission requires the spacecraft to approach the landing site at a specific angle. Such constraints on the thrust levels, commonly referred to as "annular constraints", make the problem non-convex. Also, state constraints such as the glide slope constraint introduce additional complexity to the

problem. Proving non-singularity enables a convex relaxation as described in Section 6.7.

The importance of non-singularity and controllability/observability in optimal control is evident in the seminal work of Pontryagin [21]. They showed that controllability is related to non-singularity, uniqueness, and regularity of the control [21]. For time optimal problems, they used normality (a controllability-like concept) to show when controls are on the boundary of a parallelepiped constraint [21]. Normality has been used more generally to show when controls are at the extreme points of a constraint set [87]. Similar results have been provided for other classes of problems [88]. We view this work as a continuation of such results.

Key to our results are a recent statement of a maximum principle on manifolds with mixed constraints [53] and a recent test for strong observability of linear-time varying systems with non-zero feedthrough matrix [89]. This test enables one to practically check the sufficient condition. Strong controllability and strong observability are dual concepts and the primal system being strongly controllable is equivalent to the dual system being strongly observable [47]. There are numerous tests for strong observability of linear time-invariant systems and means for characterizing their zeros and zero directions. One way to characterize zeros of time-varying systems is by transformation. As an example, Wu [90] introduces transformations for invariable systems. In Theorem 6.1, we introduce a time transformation technique that is sufficient for time-varying systems to have the same zeros and zero directions as a time-invariant system. Hence, the time-varying system is said to be "effectively" time-invariant.

The requirement for non-singularity is related to the idea of lossless convexification. The results herein subsume those of Harris and Açıkmeşe [16] as they focused on annularly constrained problems in Euclidean space. Moreover, their method of proof required a specific coordinate representation. Our proof is coordinate independent leveraging only the concepts of strong observability, the weakly unobservable subspace, and the cotangent space.

The main contributions of the chapter are the following:

1. Sufficient conditions for linear time-varying systems to be "effectively" time-invariant for the purpose of determining strong observability (see Theorem 6.1).

2. Sufficient conditions for non-singular optimal control of systems evolving on a smooth manifold subject to mixed constraints and additional control constraints (see Theorem 6.2).

3. Sufficient conditions for non-singular optimal control of systems defined on $\mathbb{R}^n$ subject to an explicit linear state constraint, mixed constraints, and additional control constraints (see Section 6.5.1).

4. Application of the results to time optimal and fuel optimal control problems (see Sections 6.6-6.7).

The chapter is organized as follows. Section 6.2 introduces the mathematical notation. Section 6.3 describes the primary problem of interest, which is an optimal control problem on a manifold with additional mixed constraints and control constraints. This section also includes the assumptions imposed on the problem and a geometric motivation for the current work. Section 6.4 presents some of the linear systems theory concepts crucial to the mathematical analysis of the problem. A new time transformation technique is also presented here. The main results are presented in Section 6.5, which states the sufficient conditions for non-singularity. Sections 6.6 and 6.7 apply the results to minimum time and minimum fuel problems. In Section 6.8, we present a time-transformation example. In Section 6.9, a discussion on how singular solutions can be charaterized as zeros for time-invariant systems is provided. Finally, Section 6.10 concludes the chapter.

6.2 Nomenclature for the Chapter

The topic of this chapter is optimal control of a dynamical system evolving on a smooth manifold. A topological k-dimensional manifold X is a topological space which is Hausdorff, second-countable, and such that for every $x \in X$ there is a neighborhood $U \subset X$ containing

x that is homeomorphic to $\mathbb{R}^k$ via the coordinate map $\varphi : U \to \mathbb{R}^k$. The pair (U, φ) is called a coordinate chart. Two charts (U, φ) and (V, ψ) are smoothly compatible if either $U \cap V = \emptyset$ or $\psi \circ \varphi$ is a diffeomorphism. A family of smoothly compatible charts whose domain covers X is a smooth atlas for X. A smooth k-dimensional manifold X is a topological manifold with a smooth atlas. Any open subset $X' \subset X$ is a submanifold of X. For any point $x \in X$, the tangent and cotangent spaces at x of X are denoted $T_x X$ and $T_x^* X$. The tangent and cotangent bundles are denoted TX and T^*X. A dynamical system on X is characterized by a continuous mapping $f : \mathbb{R} \times X \times \mathbb{R}^m \to TX$ such that $f(t, x, u) \in T_x X$ and which is smooth with respect to (t, x).

The following is a partial list of notation used: $\mathcal{C}^k(I)$ is the set of k-times continuously differentiable maps on I; $\mathbb{C}$ is the set of complex numbers; $\mathbb{R}$ is the set of real numbers; $\mathbb{R}_+$ is the set of non-negative real numbers; $\mathbb{R}^n$ is the set of real n-tuples; $\mathcal{CL}_\infty^+$ is the set of continuous, uniformly bounded functions over the set of non-negative real numbers; $\mathcal{CL}_\infty^>$ is the set of functions $v \in \mathcal{CL}_\infty^+$ such that $||v(t)||$ does not decay to zero as $t \to \infty$; a condition is said to hold almost everywhere (a.e.) in the interval $[a, b]$ if the set of points in $[a, b]$ where this condition fails to hold is measure zero; a map x is identically zero if it is zero for every point in its domain and denoted $x \equiv 0$; an over-dot denotes the the time derivative of a function, i.e. $dx(t)/dt = \dot{x}(t)$; the partial of ϕ with respect to vector $x \in \mathbb{R}^n$ is denoted $\nabla_x \phi$ and is a column vector; im A is the image of A; int S is the interior or set S; ∂S is the boundary of set S; the extreme points of a set S are those that cannot be written as convex combinations of other points in S and denoted ex(S).

6.3 Problem Description

In this section, we introduce the primary problem of interest, which is an optimal control problem defined on a smooth manifold X subject to a mixed constraint and additional

control constraints. It is labeled as P0.

$$\begin{aligned} \min \quad & J = \phi(t_f, x_f) + \int_{t_0}^{t_f} \ell(w(t))\, dt \\ \text{subj. to} \quad & \dot{x}(t) = A(t)x(t) + B(t)u(t) \\ & y(t) = C(t)x(t) + D(t)u(t) \\ & u(t) \in U(w(t)) \\ & w(t) \in W \\ & x(t_0) = x_0 \in X,\ x(t_f) \in X_f. \end{aligned} \tag{P0}$$

The initial time is t_0. The final time is t_f. They form a non-degenerate interval $I = [t_0, t_f] \subset \mathbb{R}_+$. The system state is an absolutely continuous function $x : I \to \mathbb{R}^n$ that evolves on a smooth manifold X with dynamics $f(t, x(t), u(t)) = A(t)x(t) + B(t)u(t)$. The system matrices are $A, B \in \mathcal{C}^{2n-3}(I)$. The initial state is the point $x_0 \in X$ and the final state is the point $x(t_f) \in X_f$, which is a submanifold of X. The terminal constraint can also be written in the functional form $\psi(t_f, x(t_f)) = 0$.

The control input $u : I \to \mathbb{R}^m$ belongs to the set of bounded measurable functions. It is pointwise constrained to the set $U(w(t)) = \{u \in \mathbb{R}^m : g(u, w(t)) \leq 0\}$. The set is parameterized by a second control $w : I \to \mathbb{R}$ where $w(t) \in W = \{w \in \mathbb{R} : s(w) \leq 0\}$. The reason for having the second control will become evident in Section 6.7 where the results of this chapter are connected with results from chapter 4. The function $y : I \to \mathbb{R}^r$ is given. The mixed constraint is given by $h(t) = C(t)x(t) + D(t)u(t) - y(t) = 0$. The matrices $C, D \in \mathcal{C}^{2n-2}(I)$. The smooth terminal cost function is $\phi : \mathbb{R}_+ \times X \to \mathbb{R}$ and the smooth integral cost function is $\ell : \mathbb{R} \to \mathbb{R}$. The objective is to minimize the sum of the terminal and the integral costs. The final time can be free or fixed.

A special case of this problem has a minimum time objective, dynamics in $\mathbb{R}^n$, no mixed constraint, and a bounded control of the form $||u|| \leq \rho$. This special case has been studied extensively, and it is well known that a sufficient condition for the control to (almost) always be on the boundary of the control set is controllability [88]. It is also well documented that a

sufficient condition for the control to (almost) always be at an extreme point of the control set is normality [21, 87]. The primary purpose of this paper is to develop a generalized sufficient condition that applies to P0. The challenge in doing so is described below, and it is also seen why generalizing the normality condition cannot be done without additional strong assumptions.

For visual purposes, consider the case with a two-dimensional control ($m = 2$) and one-dimensional mixed constraint ($r = 1$). Suppose U is the polyhedral set shown in Fig. 6.1. At a given instant of time, the mixed constraint $D(t)u(t) = y(t) - C(t)x(t)$ appears as a line cutting through U. The line can translate and/or rotate with time. As such, the admissible control set at this time instant is the line segment $\overline{ab}$.

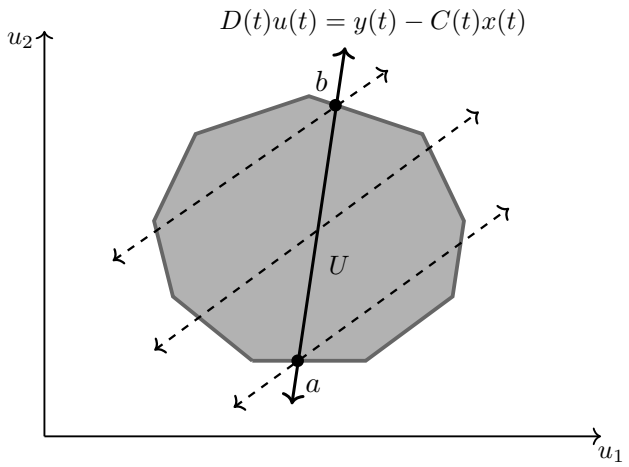

Fig. 6.1: The admissible set of controls is the line segment $\overline{ab}$. The dashed lines indicate lines of constant cost for the pointwise objective $\lambda^T(t)B(t)u(t)$.

For a control u to be optimal, it must minimize the Hamiltonian pointwise in time, i.e.,

$$\begin{aligned} u(t) &\in \arg\min \ \lambda^T(t)B(t)u(t) \\ \text{subj. to} \quad & D(t)u(t) = y(t) - C(t)x(t), \ u(t) \in U. \end{aligned} \tag{6.1}$$

In Fig. 6.1, the dashed lines represent the contours of constant cost for the pointwise objective $\lambda^T Bu$. The optimal point will be at a or b provided those contours are not parallel to

$\overline{ab}$. If the contours are parallel to $\overline{ab}$, the optimal point is anywhere along $\overline{ab}$ and hence in the interior of U. Because the contours of constant cost depend on λ and because the mixed constraint depends on x, neither of which are known a priori, proving that the contours are never parallel to the mixed constraint seems unlikely. However, a sufficient condition is given in Theorem 6.2 requiring strong observability of the adjoint system and indicating that singular solutions correspond to system zeros. Relevant background from linear system theory is provided in Section 3.

To show that the control is always at an extreme point, the line segment $\overline{ab}$ must always pass through an extreme point of U. For polyhedral U, this means that the line segment cannot translate, i.e., $y(t) - C(t)x(t)$ must remain constant over the whole trajectory. This assumption is too strong for the applications in mind. Alternatively, if ex $U = \partial U$ then being at the extreme points is the same as being on the boundary, and the aforementioned theorem applies.

6.4 Linear Systems Theory

Important concepts from linear systems theory include system zeros, strong observability, and various tests for strong observability of LTI and LTV systems. In this section, the linear system of interest $\Sigma = (A, B, C, D)$ is defined on $\mathbb{R}_+$ and is given by:

$$\begin{aligned} \dot{x}(t) &= A(t)x(t) + B(t)u(t), \quad x(t_0) = x_0 \\ y(t) &= C(t)x(t) + D(t)u(t) \end{aligned} \tag{6.2}$$

where $x(t) \in \mathbb{R}^n$, $u(t) \in \mathbb{R}^m$, and $y(t) \in \mathbb{R}^p$.

Definition 6.1. *A point x_0 is called weakly unobservable if there exists an input function u such that the corresponding output function satisfies $y \equiv 0$. The set of all weakly unobservable points at t_0 is denoted $\mathcal{V}(\Sigma, t_0)$.*

Definition 6.2. *A system Σ is called strongly observable if for every input function u the output $y \equiv 0$ implies $x \equiv 0$, i.e., $\mathcal{V}(\Sigma, \cdot) \equiv 0$.*

The point x_0 is also called a zero state direction and the associated input u is a zero control direction. The zeros and zero directions are related to the observability properties of the system. For LTV systems, we give precise definitions of zeros and zero directions and a tool to determine them using the $\mathcal{W}$-transform as reported by O'Brien [91].

Definition 6.3. *A function q is a transmission zero for Σ if there exist an initial state x_0 and an input direction $r \in \mathcal{CL}_\infty^>$ such that the output of Σ is zero for all $t \geq 0$ when the input is $r(t)\phi_q(t,0)$, where ϕ_q is the scalar transition function for $q(t)$.*

Definition 6.4. *A function q is an ordinary zero for Σ if there exist an initial state x_0 and a constant input direction r such that the output of Σ is zero for all $t \geq 0$ when the input is $r\phi_q(t,0)$, where ϕ_q is the scalar transition function for $q(t)$.*

Definition 6.5. *Suppose that Σ has an impulse response function g. The directional $\mathcal{W}$-transform of Σ with respect to a function q in the direction r is defined as*

$$\hat{\Sigma}(q(.), r(.), t) = \int_{-\infty}^{t} g(t,\tau) r(\tau) \phi_q(\tau, t) d\tau \tag{6.3}$$

whenever the integral converges.

Using the $\mathcal{W}$–transform, the transmission zeros and ordinary zeros of a time–varying system can be determined. The result is taken from Corollary 23 of the paper by O'Brien [91].

Lemma 6.1. *Suppose that*

$$\bar{x}_0 = \int_{-\infty}^{0} \Phi_{A-qI}(0,\sigma) B(\sigma) r(\sigma) d\sigma \tag{6.4}$$

is well defined for a given q and a direction $r \in \mathcal{CL}_\infty^>$. Then, q is a transmission zero for Σ with a direction r and an initial state x_0 if and only if

$$\hat{\Sigma}(q(.), r(.), t) = C(t) \Phi_{AU-qI}(t,0) \tilde{x}_0 \tag{6.5}$$

where $\tilde{x}_0 = \bar{x}_0 - x_0$.

While the above lemma provides a test for zeros and zero directions, it is challenging to use as a synthesis tool. Proving the non-existence of zeros can be done with a rank test provided $D(t)$ is a constant rank matrix. For constant rank matrices, we have the following decomposition.

Lemma 6.2. *Let $G : \mathbb{R}_+ \to \mathbb{R}^{n\times n}$ such that $G \in \mathcal{C}^\ell(\mathbb{R}_+)$ and* rank $G(t) \equiv g$. *Then there exist matrix-valued maps $L, R \in \mathcal{C}^\ell(\mathbb{R}_+)$ that are non-singular for all t such that*

$$L(t)G(t)R(t) = \begin{bmatrix} I_g & 0 \\ 0 & 0 \end{bmatrix} \tag{6.6}$$

where I_g is the g-dimensional identity matrix [92].

Suppose that $p = m$ such that $D(t)$ is square with constant rank d. (This dimensionality can always be achieved by adding rows of zeros in the output equation or adding columns of zeros to the $B(t)$ and $D(t)$ matrices.) From the above lemma, there exist non-singular $L(t)$ and $R(t)$ matrices associated with $D(t)$. Define

$$\hat{B}(t) = B(t)R(t) = [\hat{B}_1(t)\ \hat{B}_2(t)] \tag{6.7}$$

where $\hat{B}_1(t) \in \mathbb{R}^{n\times d}$ and $\hat{B}_2(t) \in \mathbb{R}^{n\times(p-d)}$. Define

$$\hat{C}(t) = L(t)C(t) = \begin{bmatrix} \hat{C}_1^T(t) & \hat{C}_2^T(t) \end{bmatrix}^T \tag{6.8}$$

where $\hat{C}_1(t) \in \mathbb{R}^{d\times n}$ and $\hat{C}_2(t) \in \mathbb{R}^{(p-d)\times n}$. Lastly, define

$$\hat{A}(t) = A(t) - \hat{B}_1(t)\hat{C}_1(t). \tag{6.9}$$

Lemma 6.3. *Suppose that $D(t)$ is a constant rank matrix. The system $\Sigma = (A, B, C, D)$ is strongly observable if and only if $\hat{\Sigma} = (\hat{A}, \hat{B}_2, \hat{C}_2)$ is strongly observable [89].*

A simple rank test now applies to $\hat{\Sigma}$ involving the observability and invertibility matrices, $Q(t)$ and $W(t)$, respectively. The observability matrix is characterized by

$$Q(t) = [C_1^T(t), \ldots, C_n^T(t)]^T \tag{6.10}$$

where

$$\begin{aligned} C_1(t) &= \hat{C}_2(t) \\ C_{\mu+1}(t) &= \dot{C}_\mu(t) + C_\mu(t)\hat{A}(t) \text{ for } \mu = 1, \ldots, n-1. \end{aligned} \tag{6.11}$$

The invertibility matrix is characterized by

$$W(t) = \begin{bmatrix} 0 & 0 & \cdots & 0 \\ B_{10}(t) & 0 & \cdots & 0 \\ B_{20}(t) & B_{21}(t) & \cdots & 0 \\ \vdots & \vdots & \ddots & \vdots \\ B_{n-1,0}(t) & B_{n-1,1}(t) & \cdots & B_{n-1,n-2}(t) \end{bmatrix} \tag{6.12}$$

where

$$\begin{aligned} B_{\mu+1,\mu}(t) &= \hat{C}_2(t)\hat{B}_2(t) \quad \text{for } 0 \le \mu \le n-1 \\ B_{\mu+1,0}(t) &= C_{\mu+1}(t)\hat{B}_2(t) + \dot{B}_{\mu 0}(t) \quad \text{for } 1 \le \mu \le n-1 \\ B_{\mu+1,\nu}(t) &= B_{\mu,\nu-1}(t) + \dot{B}_{\mu\nu}(t) \quad \text{for } 1 \le \nu < \mu \le n-1 \end{aligned} \tag{6.13}$$

Lemma 6.4. *The system $\hat{\Sigma} = (\hat{A}, \hat{B}_2, \hat{C}_2)$ is strongly observable if and only if*

$$\text{rank}[Q(t)\ W(t)] = \text{rank} \begin{bmatrix} I_n & 0 \\ Q(t) & W(t) \end{bmatrix} \tag{6.14}$$

for all $t \in \mathbb{R}_+$ except a nowhere dense subset and where I_n is the n-dimensional identity matrix [93].

The synthesis of zeros, zero directions, and strong observability is much simpler for time-invariant systems. For LTI systems, the system matrix is given by

$$P_\Sigma(\lambda) = \begin{bmatrix} \lambda I_n - A & -B \\ C & D \end{bmatrix} \tag{6.15}$$

where $\lambda \in \mathbb{C}$.

Definition 6.6. *A time-invariant system Σ has a transmission zero $\lambda \in \mathbb{C}$ if there exist $u_0 \neq 0 \in \mathbb{R}^m$ and $x_0 \in \mathbb{R}^n$ such that*

$$P_\Sigma(\lambda) \begin{bmatrix} x_0 \\ u_0 \end{bmatrix} = 0 \tag{6.16}$$

The zero λ defines an input $u_0 e^{\lambda t}$ and an initial state x_0 such that the corresponding output of Σ will be zero for all t [47].

Analogous to time-varying systems, the point x_0 is a zero state direction and u_0 is a zero control direction. They are now easy to find when they exist since one must simply check the null space of $P_\Sigma(\lambda)$.

The non-existence of zeros and zero directions is equivalent to strong observability. There are numerous equivalent tests for LTI systems [47].

Lemma 6.5. *The following statements are equivalent to strong observability of time-invariant Σ:*

(i) $\mathcal{V}(\Sigma) = 0$.

(ii) $(C + DF,\ A + BF)$ *is observable for all* F.

(iii) $\operatorname{rank} P_\Sigma(\lambda) = n + \operatorname{rank} [B^T\ D^T]^T$ *for all* $\lambda \in \mathbb{C}$.

(iv) the Smith form of P_Σ is equal to the constant matrix

$$Q = \begin{bmatrix} I & 0 \\ 0 & 0 \end{bmatrix}. \tag{6.17}$$

(v) the rank test in Lemma 6.4 holds.

Given the simplicity of these tests and the characterization of zeros for LTI systems, we provide a new result in Theorem 6.1 stating when LTV systems are "effectively" time-invariant.

Theorem 6.1. *Suppose there exists a linear time-varying system system* $\Sigma_1 = (A(t), B(t), C(t), D(t))$ *and a linear time-invariant system* $\Sigma_2 = (A, B, C, D)$. *If* Σ_2 *is strongly observable and there exists a* $F(t)$ *such that the following relations hold*

$$\begin{aligned} B(t) &= B \\ D(t) &= D \\ A(t) &= A + BF(t) \\ C(t) &= C + DF(t) \end{aligned} \tag{6.18}$$

then Σ_1 *is strongly observable.*

Proof. Suppose Σ_2 is strongly observable and $\Sigma_1 = (A + BF(t), B, C + DF(t), D)$ is not strongly observable. Let (x, u) be zero directions for Σ_1 with $x \not\equiv 0$. This implies

$$\begin{aligned} \dot{x}(t) &= (A + BF(t))x(t) + Bu(t) \\ 0 &= (C + DF(t))x(t) + Du(t) \end{aligned} \tag{6.19}$$

Introducing $v(t) = u(t) + F(t)x(t)$, Equation (6.19) becomes

$$\begin{aligned} \dot{x}(t) &= Ax(t) + Bv(t) \\ 0 &= Cx(t) + Dv(t) \end{aligned} \tag{6.20}$$

Equation (6.20) defines Σ_2. Hence, $x \equiv 0$, which is a contradiction. □

Example: Consider the time-varying system with

$$A = \left[\begin{array}{cc:cc} & & 1 & 0 \\ & 0_{2\times 2} & 0 & 2 \\ \hdashline -1 & 0 & & \\ 0 & -2 & & 0_{2\times 2} \end{array}\right], \quad B = 0_{4\times 1},$$

$$C(t) = \left[\begin{array}{c:cc} & 1+t & \sin t \\ 0_{2\times 2} & & \\ & 2t & 1+2\sin t \end{array}\right], \quad D = \begin{bmatrix} 1 \\ 2 \end{bmatrix}.$$

According to Theorem 6.1, the above system is strongly observable if there exists a strongly observable time-invariant system (A, B, C, D) and a $F(t)$ such that Eq. (6.18) is satisfied. Let A, B, and D equal those above with

$$C = \left[\begin{array}{c:c} 0_{2\times 2} & I_{2\times 2} \end{array}\right] \quad \text{and} \quad F(t) = \begin{bmatrix} 0 & 0 & t & \sin t \end{bmatrix}.$$

It is easily verified that (A, B, C, D) is strongly observable and that the two systems are equal using $F(t)$. This implies the time-varying system is strongly observable, which can be confirmed using the rank test described in Lemma 6.4.

We conclude this section with a modified definition of strong observability for systems in a subspace $S \subset \mathbb{R}^n$.

Definition 6.7. *A system is strongly observable on subspace $S(t) \subset \mathbb{R}^n$ if the intersection of the weakly unobservable subspace with S is zero, i.e.*

$$\mathcal{V}(\Sigma, t) \cap S(t) \equiv 0. \tag{6.21}$$

6.5 Mathematical Results

In this section, we analyze Problem P0 in an effort to understand when the optimal controls are on the boundary of the control set. In some contexts, controls belonging to the interior of the control set are called singular, and so the conditions obtained here

are sufficient conditions for non-singularity of optimal control problems on manifolds with mixed constraints. They are generalizations of well-known results involving observability for problems without mixed constraints. In the absence of the mixed constraints, they reduce to the well known results [21, 87, 88, 94].

Two cases of P0 are analyzed here. First, we consider the case where the system intrinsically evolves on a smooth manifold, and secondly, when the system does not intrinsically evolve on a manifold but is subjected to an explicit linear state constraint. In both cases, we provide results for time-invariant and time-varying systems. We define the system in P0 as $\Sigma = (A, B, C, D)$.

Definition 6.8. *The problem is said to be time-invariant if Σ, y, and ψ do not depend on time. Otherwise, the problem is time-varying.*

The Hamiltonian, Lagrangian, and endpoint functions are defined for P0 as given below.

$$H = p_0\ell(w) + p^T(Ax + Bu) \tag{6.22}$$

$$L = H + \nu^T(Cx + Du - y) + \mu^T g(u, w) + \eta^T s(w) \tag{6.23}$$

$$G = p_0\phi + \xi^T\psi. \tag{6.24}$$

The sufficient conditions for the optimal control to be on the boundary of its control set are now stated.

Assumption 6.1. *The dual linear system $\Sigma^\top = (-A^T, -C^T, B^T, D^T)$ is strongly observable on the cotangent space $T^*_{x(t)}X$ for all $t \in [t_0, t_f]$.*

Assumption 6.2. *At least one of the following holds:*

a) the problem is time-invariant and

$$\ell(w(t)) + \nabla_{t_f}\phi(t_f, x_f) \neq 0 \text{ for all } t \in [t_0, t_f].$$

b) the problem is time-varying, $C(t) = 0$, and the matrix

$$T = \left[\begin{array}{c|c} -\ell(w(t_f)) - \nabla_{t_f}\phi(t_f, x_f) & -\nabla_{t_f}\psi(t_f, x_f) \\ \hline \nabla_{x_f}\phi(t_f, x_f) & \nabla_{x_f}\psi(t_f, x_f) \end{array}\right]$$

is full column rank.

Theorem 6.2. *If Assumption 6.1 and Assumption 6.2 hold, then there are no non-degenerate time intervals $\mathcal{I} = [\tau_1, \tau_2]$ where $u(t) \in \text{int } U \ \forall t \in \mathcal{I}$.*

Proof. Assuming that an extremal solution exists, the relevant necessary conditions (as per Theorem 3.2) are given by

$$p_0 \in \{0, 1\} \qquad (p_0, p(t)) \neq 0 \qquad \forall t \in [t_0, t_f] \tag{6.25}$$

$$\dot{x}(t) = Ax(t) + Bu(t) \tag{6.26}$$

$$\dot{p}(t) = -A^T p(t) - C^T \nu(t) \tag{6.27}$$

$$0 = B^T p(t) + D^T \nu(t) + \mu \nabla_u g \tag{6.28}$$

a) Suppose the system $\Sigma^\top$ is strongly observable on $T^*_{x(t)}X$ for all t and the problem is time-invariant with $\ell(w(t)) + \nabla_{t_f}\phi \neq 0$. Suppose there exists a non-degenerate interval $\mathcal{I} = [\tau_1, \tau_2] \in [t_0, t_f]$ where $u(t) \in \text{int } U \ \forall t \in \mathcal{I}$. Then, on this interval $\mu = 0$ because of complementary slackness. This results in the linear system

$$\begin{aligned} \dot{p}(t) &= -A^T p(t) - C^T \nu(t), \ p(t) \in T^*_{x(t)}X \\ 0 &= B^T p(t) + D^T \nu(t). \end{aligned} \tag{6.29}$$

Since $p(t) \in T^*_{x(t)}X$, strong observability on $T^*_{x(t)}X$ implies $p(\tau_1) = 0$. Also, because the problem is time-invariant, the Hamiltonian is a constant $\forall t \in [t_0, t_f]$ and $\nabla_{t_f}\psi(t_f, x_f) = 0$. Therefore, the constant value of the Hamiltonian is

$$H(\tau_1) = -p_0 \nabla_{t_f}\phi(t_f, x_f) \tag{6.30}$$

This implies that

$$-p_0\nabla_{t_f}\phi(t_f,x_f) = p_0\ell(w(\tau_1)) + p^T(\tau_1)(Ax(\tau_1)+Bu(\tau_1)) \tag{6.31}$$

This means p_0 must be zero since $\ell(w(\tau_1)) + \nabla_{t_f}\phi(t_f,x_f) \neq 0$. This contradicts the non-triviality condition. Hence, there are no non-degenerate time intervals $\mathcal{I} \subset [t_0,t_f]$ where the optimal control $u(t) \in \text{int } U \ \forall t \in \mathcal{I}$.

b) Suppose the system $\Sigma^\top$ is strongly observable on $T^*_{x(t)}X$, the problem is time-varying, $C(t) = 0$, and the matrix T is full rank. Suppose there exists a non-degenerate interval $\mathcal{I} = [\tau_1,\tau_2] \in [t_0,t_f]$ where $u(t) \in \text{int } U \ \forall t \in \mathcal{I}$. With $C(t) = 0$, Eq. (6.27) becomes

$$\begin{aligned} \dot{p}(t) &= -A^T p(t),\ p(t) \in T^*_{x(t)}X \\ 0 &= B^T p(t) + D^T \nu(t) \end{aligned} \tag{6.32}$$

Again, strong observability on $T^*_{x^*(t)}X$ implies $p(\tau_1) = 0$. Since $p(\cdot)$ is the solution of a homogeneous system, $p(t) = 0 \ \forall t \in [t_0,t_f]$. Hence $p(t_f) = 0$. As a result, we have $H = p_0\ell(w(t)) \ \forall t \in [t_0,t_f]$. Now the transversality conditions result in the following system of equations

$$-p_0\ell(w(t_f)) - p_0\nabla_{t_f}\phi(t_f,x_f) = \xi^T\nabla_{t_f}\psi(t_f,x_f) \tag{6.33}$$

$$p_0\nabla_{x_f}\phi(t_f,x_f) + \xi^T\nabla_{x_f}\psi(t_f,x_f) = 0 \tag{6.34}$$

Since the matrix T is full rank, $p_0 = 0$, which contradicts the non-triviality condition. Therefore, there are no non-degenerate time intervals $\mathcal{I} \subset [t_0,t_f]$ where the optimal control $u(t) \in \text{int } U \ \forall t \in \mathcal{I}$. □

Remark 6.1. *The theorem states that there are no intervals with the control in the interior rather than the stronger statement that the control is almost always on the boundary. This is because the definition of strong observability requires zero output everywhere. Furthermore, in Lemma 6.4, it is possible to construct infinitely differentiable systems for which*

the exceptional set has positive measure.

6.5.1 Problem with Explicit Linear State Constraint

It is not uncommon in engineering problems for the system to evolve in $\mathbb{R}^n$ and be constrained to a manifold X. Such a problem is considered in this section. The system dynamics are given by $f : \mathbb{R}\times\mathbb{R}^n\times\mathbb{R}^m \to \mathbb{R}^n$, where $f(t, x(t), u(t)) = A(t)x(t)+B(t)u(t)$ and the state is restricted to evolve on a linear manifold, i.e., $x(t) \in X = \{\gamma : E\gamma = z\}$, where E is a constant matrix and z is a constant – both given. The problem is mathematically described below and is labeled as P1.

$$
\begin{aligned}
\min \quad & J = \phi(t_f, x_f) + \int_{t_0}^{t_f} \ell(w(t))\, dt \qquad \text{(P1)}\\
\text{subj. to} \quad & \dot{x}(t) = A(t)x(t) + B(t)u(t)\\
& y(t) = C(t)x(t) + D(t)u(t)\\
& z = Ex(t)\\
& g(u(t), w(t)) \le 0\\
& s(w(t)) \le 0\\
& x(t_0) = x_0,\ \psi(t_f, x_f) = 0.
\end{aligned}
$$

The strategy in this section is to transform P1 back to P0 so that there is no explicit manifold constraint and the system intrinsically evolves on one. To do so, differentiate the state constraint $z = Ex(t)$ w.r.t. time.

$$E\dot{x}(t) = 0 \tag{6.35}$$

The parallel projection of $\dot{x}$ is given by

$$\dot{x}_{||}(t) = E^T(EE^T)^{-1}E\dot{x}(t) \tag{6.36}$$

such that the orthogonal projection is

$$\dot{x}_\perp(t) = A(t)x_\perp(t) + B(t)u(t) - E^T(EE^T)^{-1}E\big(A(t)x_\perp(t) + B(t)u(t)\big) \tag{6.37}$$

Defining the following quantities

$$\begin{aligned} F &= I - E^T(EE^T)^{-1}E \\ \bar{A}(t) &= FA(t) \\ \bar{B}(t) &= FB(t) \end{aligned} \tag{6.38}$$

allows the above differential equation to be rewritten as

$$\dot{x}_\perp(t) = \bar{A}x_\perp(t) + \bar{B}u(t) \tag{6.39}$$

for which $x_\perp(t)$ evolves on the manifold. Secondly, we use Eq. (6.35) to rewrite the state constraint as a mixed constraint

$$0 = EA(t)x_\perp(t) + EB(t)u(t) \tag{6.40}$$

When this mixed constraint holds, the (A, B) and $(\bar{A}, \bar{B})$ systems are the same. Thus, the original mixed constraint is augmented as

$$\bar{y}(t) = \bar{C}(t)x_\perp(t) + \bar{D}(t)u(t) \tag{6.41}$$

where

$$\bar{y}(t) = \begin{bmatrix} y(t) \\ 0 \end{bmatrix}, \bar{C}(t) = \begin{bmatrix} C(t) \\ EA(t) \end{bmatrix}, \bar{D}(t) = \begin{bmatrix} D(t) \\ EB(t) \end{bmatrix} \tag{6.42}$$

Problem P1 can now be written in the form P2.

$$\begin{aligned} \min \quad & J = \phi(t_f, x_f) + \int_{t_0}^{t_f} \ell(w(t))\, dt \\ \text{subj. to} \quad & \dot{x}(t) = \bar{A}(t)x(t) + \bar{B}(t)u(t) \\ & \bar{y}(t) = \bar{C}(t)x(t) + \bar{D}(t)u(t) \\ & g(u(t), w(t)) \leq 0 \\ & s(w(t)) \leq 0 \\ & x(t_0) = x_0,\ \psi(t_f, x_f) = 0. \end{aligned} \tag{P2}$$

Problem P2 now has the form of Problem P0. Assumptions 6.1 and 6.2 and Theorem 6.2 now apply to the barred linear system. If those assumptions are satisfied, then there are no non-degenerate intervals for which the optimal control in P1 is in the interior of its set.

Remark 6.2. *Checking that the system is strongly observable on the cotangent space at each time can be difficult, in general, since doing so requires one to know the optimal state trajectory. However, when the manifold is linear, the cotangent space is constant and the check is straightforward.*

Testing for strong observability can be done using Lemma 6.1, Lemma 6.3, Lemma 6.4, Lemma 6.5, or Theorem 6.1. Furthermore, if the dual system is not strong observable, singular solutions are characterized as zeros of the system. The zeros and zero directions can be found through Lemma 6.1 or Definition 6.6. Lastly, strong observability and strong controllability are dual concepts. Hence, the requirement that the dual system be strongly observable is equivalent to one requiring the primal system be strongly controllable.

6.6 Application to Time Optimal Control

This section emphasizes the importance of the above results to time optimal control problems. It is straightforward to see that Problem P0 can be cast as a time optimal problem by setting $\phi(t_f, x_f) = t_f$ and setting the integral cost to zero. As such, the problem becomes a fairly general time optimal control problem evolving on a manifold with

additional mixed and control constraints. The same applies to problem P1 for which the dynamics are restricted to evolve on a linear manifold. Theorem 6.2 states that for time-invariant systems, the system Σ^T being strongly observable is sufficient for the optimal control to be on the boundary of the control set. This generalizes the classical results for problems in $\mathbb{R}^n$ without mixed constraints since our condition reduces to (A, B) being controllable in this setting.

Example: Consider the following minimum time problem with double integrator dynamics.

$$\begin{aligned} \min \quad & J = t_f \\ \text{subj. to} \quad & \dot{x}(t) = Ax(t) + Bu(t) \\ & 0 = Cx(t) + Du(t) \\ & ||u(t)|| \leq 5 \\ & x(t_0) = x_0,\ x(t_f) = 0. \end{aligned}$$

The system matrices are

$$A = [0\ I; 0\ 0],\ \ B = [0\ I]^T,\ \ C = [1\ 2\ 1\ 1],\ \text{and}\ D = [1\ 1].$$

The initial state is $x_0 = [1\ 1\ 1\ 1]^T$. The dual system $\Sigma^\top$ is strongly observable. One should expect an optimal control whose magnitude is always five (max thrust in nature). The problem was numerically solved using SDPT3 [7]. The control magnitude is shown in Fig. 6.2. The small blips away from five are a result of discretization as described in Appendix C.

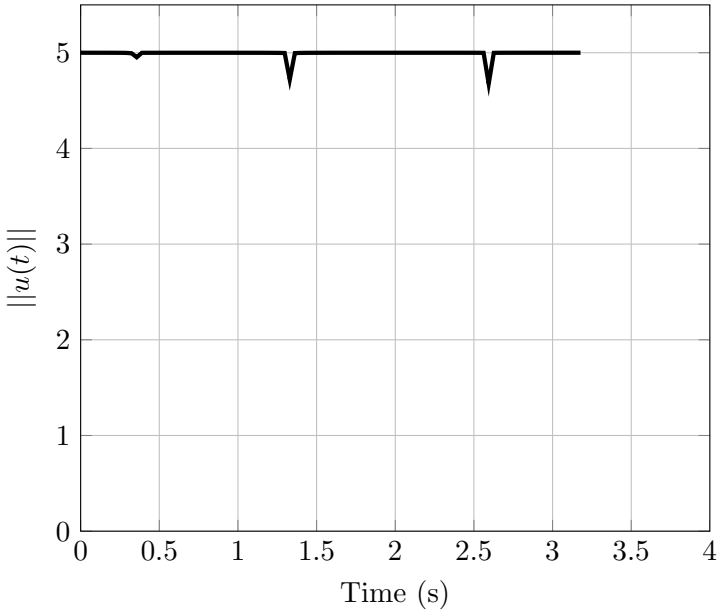

Fig. 6.2: Magnitude of a time optimal controller with a mixed constraint.

6.7 Application to Fuel Optimal Control and Connection to Prior Results

In this section, the minimum fuel planetary descent problem is solved. Chemical thrusters do not have deep throttle or reliable restart capabilities such that a non-convex, annular control constraint must be included. It is demonstrated that the results herein encompass previous "lossless convexifications" for problems with mixed constraints [16].

In the final powered decent phase of a Mars landing, the spacecraft is close enough to the surface of Mars so that (1) the gravity is assumed constant and (2) the aerodynamic forces are considered negligible compared to the thrust forces. The dynamics of the spacecraft are given by

$$\ddot{x}(t) = -g + u(t). \tag{6.43}$$

The state vector is given by x. The range, altitude, and cross range are denoted by the components x_1, x_2, and x_3, respectively. Their corresponding rates are given by x_4, x_5, and x_6, respectively. The gravity vector is assumed constant with $g = [0 \quad 3.71 \quad 0]^T$ m/s^2 and u is the control thrust acceleration. The problem is to minimize the fuel required to transfer the spacecraft from an initial state to the landing site (origin) with zero final velocity.

The spacecraft is required to approach the landing site on a 45 degree glide slope angle in the altitude/range plane.

$$x_1(t) - x_2(t) = 0. \tag{6.44}$$

The control magnitude is constrained with an upper-bound and a non–zero lowerbound. The lower bound exists since the thrusters fail to operate reliably below this bound.

$$6 \leq ||u(t)|| \leq 10 \text{ m/s}^2. \tag{6.45}$$

The annular control constraint in Eq. (6.45) makes the feasible control set non-convex. A convex relaxation proposed in [16] requires introducing a second control w and lifting the dimension of the control set to a higher dimension thereby making the set convex. The optimal solution to the relaxed problem is then optimal to the original problem provided $u(t)$ is on the boundary of $U(w(t))$.

The resulting optimal control problem is mathematically described below:

$$\begin{aligned}
\min \quad & J = \int_0^{t_f} w(t)\, dt \\
\text{subj. to} \quad & \ddot{x}(t) = -g + u(t) \\
& 0 = x_1(t) - x_2(t) \\
& ||u(t)|| \leq w(t) \\
& 6 \leq w(t) \leq 10 \\
& x(t_0) = x_0,\ x(t_f) = 0.
\end{aligned}$$

The above problem fits the definition of Problem P1 with $C = 0$, $D = 0$, and $E = [1\ -1\ 0\ 0\ 0\ 0]$. To solve this problem, we construct F, $\bar{A}$, $\bar{B}$, $\bar{C}$, and $\bar{D}$ as in Eqs. (6.38) and (6.42). If the adjoint system $\bar{\Sigma}^\top = (-\bar{A}^T, -\bar{C}^T, \bar{B}^T, \bar{D}^T)$ is strongly observable on the cotangent space $T_x^* X$, then there are no intervals where $||u(t)|| < w(t)$. Hence, the relaxation is exact and termed a lossless convexification. To verify the conditions, the weakly unobservable subspace for the adjoint system and a basis for the cotangent space

$T_x^* X$ in matrix form are calculated.

$$\mathcal{V}(\bar{\Sigma}^\top) = \begin{bmatrix} -1 \\ 1 \\ 0 \\ 0 \\ 0 \\ 0 \end{bmatrix} \qquad T_x^* X = \begin{bmatrix} \sqrt{2} & 0 & 0 & 0 & 0 \\ \sqrt{2} & 0 & 0 & 0 & 0 \\ 0 & 2 & 0 & 0 & 0 \\ 0 & 0 & 2 & 0 & 0 \\ 0 & 0 & 0 & 2 & 0 \\ 0 & 0 & 0 & 0 & 2 \end{bmatrix}$$

Hence, the requirement, $\mathcal{V}(\bar{\Sigma}) \cap T_x^* X = 0$, is satisfied and the system is strongly observable on the cotangent space. The problem is numerically solved using the Gurobi [73] solver with a MATLAB [74] interface. Fig. 6.3 shows the state trajectory. The trajectory begins at the top right, ends at the origin in the bottom left, and evolves on the 45 degree plane. The evolution on the 45 degree plane is shown in Fig. 6.4. The control magnitude is shown in Fig. 6.5. The discretization is described in Appendix C.

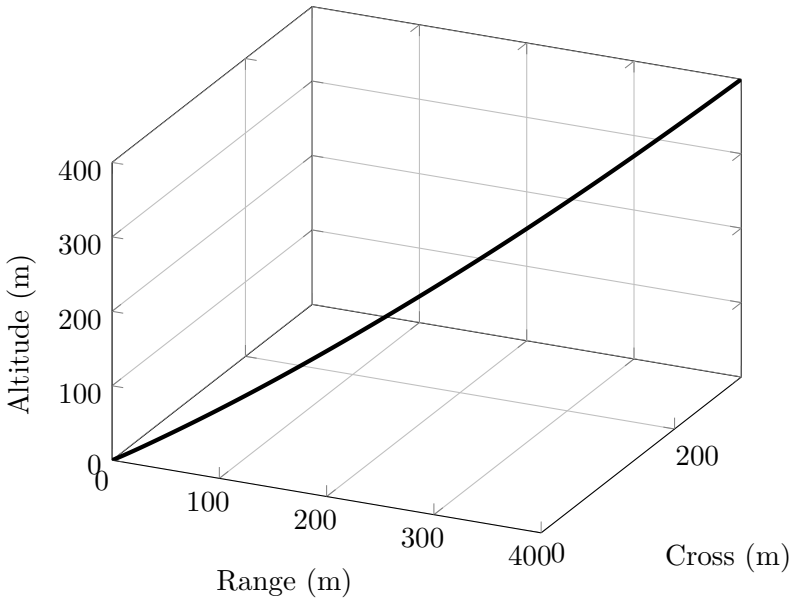

Fig. 6.3: State trajectory.

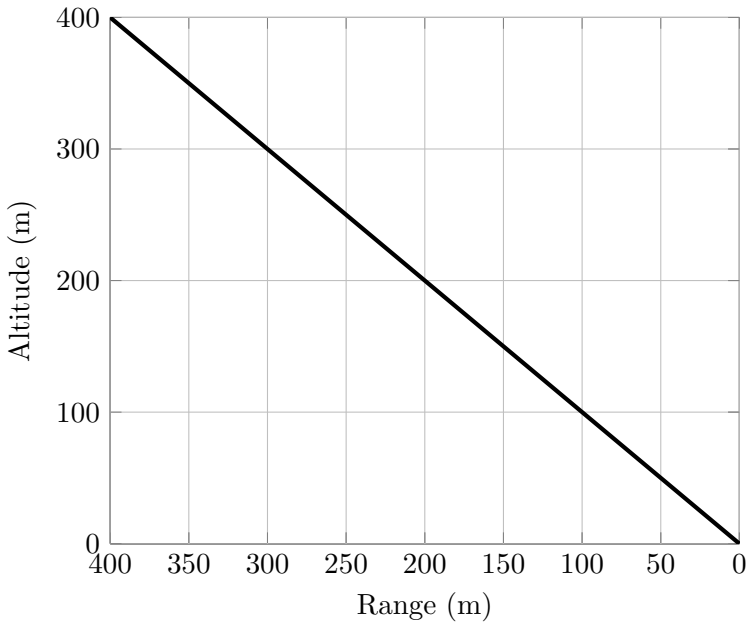

Fig. 6.4: Glide slope.

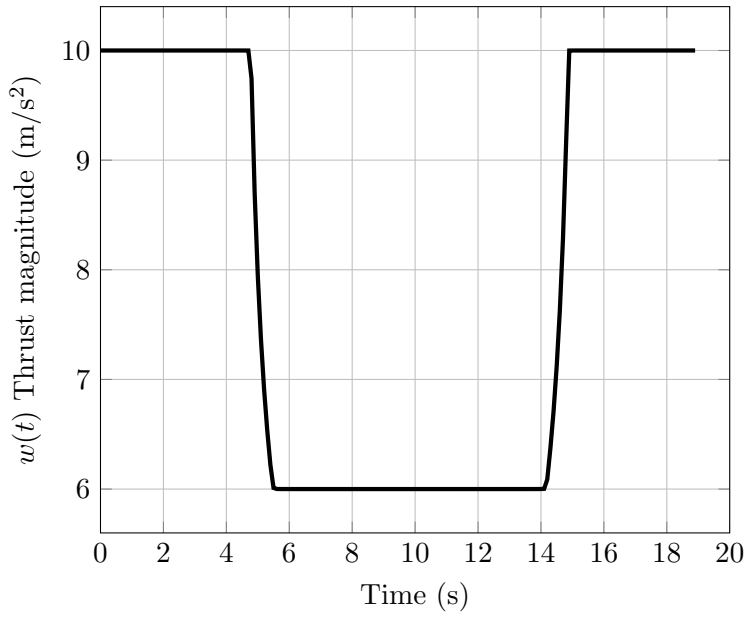

Fig. 6.5: Thrust magnitude

6.8 Time Transformation Example

In this section, a minimum time problem with coupled harmonic oscillator dynamics and time-varying control influence matrix is considered.

$$
\begin{aligned}
\min \quad & J = t_f \\
\text{subj. to} \quad & \dot{x}(t) = Ax(t) + Bu(t) \\
& 0 = Cx(t) + Du(t) \\
& ||u(t)|| \leq 5 \\
& x(t_0) = x_0,\ x(t_f) = 0.
\end{aligned}
$$

where,

$$
A = \left[\begin{array}{cc:cc} & & 1 & 0 \\ & 0_{2\times 2} & 0 & 2 \\ \hdashline -1 & 0 & & \\ 0 & -2 & & 0_{2\times 2} \end{array}\right], \quad B(t) = \left[\begin{array}{cc} 0 & 0 \\ 0 & 0 \\ \hdashline 1+t & \sin t \\ 2t & 1+2\sin t \end{array}\right],
$$

$$
C = 0_{1\times 4}, \quad D = [1 \quad 2], \quad \text{and} \quad x_0 = [10 \quad 10 \quad 1 \quad 1]^T.
$$

Note that the dual system is strongly observable as shown in the example of Theorem 6.1 in Section 6.4. As such, the optimal control will be bang-bang as shown in Fig. 6.6. Again, the blips away from five are caused by the particular discretization as described in Appendix C.

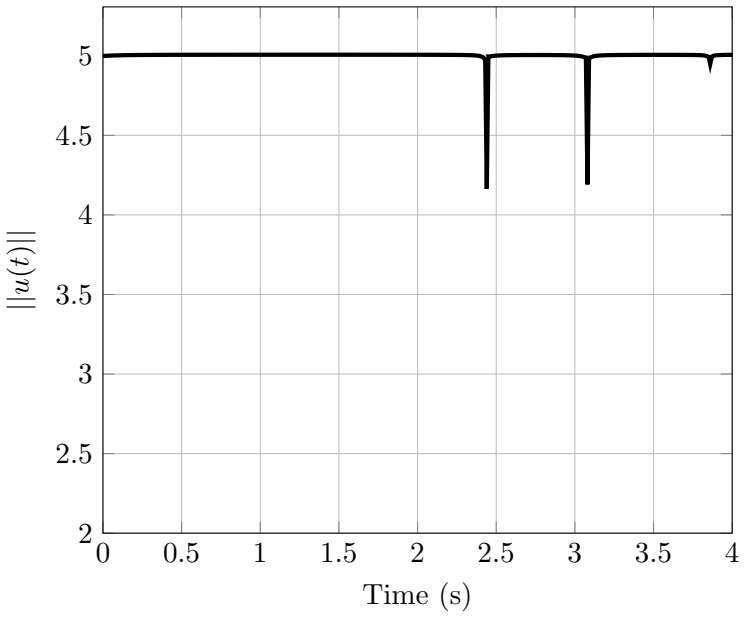

Fig. 6.6: Control magnitude

6.9 Characterizing Singular Solutions as System Zeros

According to Theorem 6.2, there are no degenerate intervals with the control in the interior for strongly controllable time-invariant systems. In other words, strongly observable adjoint systems do not permit singular solutions. In this section, we attempt to characterize the singular solutions as zeros of the system. This is done with the help of two examples.

Example 1. Consider an invertible double integrator system with

$$A = \begin{bmatrix} 0 & 1 \\ 0 & 0 \end{bmatrix}, \quad B = \begin{bmatrix} 0 \\ 1 \end{bmatrix}, \quad C = \begin{bmatrix} 1 & 2 \end{bmatrix}, \quad D = \begin{bmatrix} 1 \end{bmatrix}.$$

The adjoint system $\Sigma^\top$ that satisifies Eq. (6.29) is then given by

$$-A^T = \begin{bmatrix} 0 & 0 \\ -1 & 0 \end{bmatrix}, \quad -C^T = \begin{bmatrix} -1 \\ -2 \end{bmatrix}, \quad B^T = \begin{bmatrix} 0 & 1 \end{bmatrix}, \quad D^T = \begin{bmatrix} 1 \end{bmatrix}.$$

The adjoint system matrix can be computed as

$$P_{\Sigma^\top}(\lambda) = \begin{bmatrix} \lambda I + A^T & C^T \\ B^T & D^T \end{bmatrix} = \begin{bmatrix} \lambda & 0 & 1 \\ 1 & \lambda & 2 \\ 0 & 1 & 1 \end{bmatrix}.$$

Since the characteristic polynomial of this system is $\lambda^2 - 2\lambda + 1$, we know the system has a double root at $\lambda = 1$. The zero direction is then $[-1\ -1\ 1]^T$. Thus, for any $p(t_0) = [-\alpha\ -\alpha]^T$ and any $\nu(t) = \alpha e^{(t-t_0)}$, where $\alpha \in \mathbb{R}$, the output must be zero. This can be easily verified as follows.

Using the equation for $\dot{p}(t)$ in Eq. (6.29), we find

$$\begin{aligned} p(t) &= e^{-A^T(t-t_0)}p(t_0) - \int_{t_0}^{t} e^{-A^T(t-\tau)}C^T\nu(\tau)d\tau \\ &= \begin{bmatrix} 1 & 0 \\ t_0 - t & 1 \end{bmatrix}\begin{bmatrix} -\alpha \\ -\alpha \end{bmatrix} - \int_{t_0}^{t} \begin{bmatrix} 1 & 0 \\ \tau - t & 1 \end{bmatrix}\begin{bmatrix} 1 \\ 2 \end{bmatrix}\alpha e^{\tau} d\tau \\ &= e^{t-t_0}\begin{bmatrix} -\alpha \\ -\alpha \end{bmatrix} \end{aligned}$$

Then, the output is given by

$$B^T p(t) + D^T \nu(t) = -\alpha e^{t-t_0} + \alpha e^{t-t_0} = 0. \tag{6.46}$$

Since the system is invertible with $D = [1]$, the state equations (Eq. (**??**)) can be rewritten as

$$\begin{aligned} u(t) &= y - Cx(t) \\ \dot{x}(t) &= (A - BC)x(t) + Byu(t) = A_i x(t) + Byu(t) \end{aligned} \tag{6.47}$$

The solution to this system is

$$x(t) = e^{A_i(t-t_0)}x_0 + \int_{t_0}^{t} e^{A_i(t-\tau)}Byd\tau$$
$$= e^{t-t_0}\left[\begin{array}{c|c} (t-t_0+1) & (t-t_0) \\ \hline (t_0-t) & (t_0-t+1) \end{array}\right]x_0 + \begin{bmatrix} -te^{t_0-t} + (t_0-1)e^{t_0-t} + 1 \\ (t-t_0)e^{t_0-t} \end{bmatrix} y$$

For simplicity, we assume $y = 0$. Also, we assume that there exists a final time t_f such that the above equation holds, and a control set such that the resulting control is feasible. Now, since the system is time-invariant, the Hamiltonian is a constant. It then follows that $p^T(t)\dot{x}(t)$ is a constant, i.e.,

$$\dot{x}(t) = -e^{t-t_0}\left[\begin{array}{c|c} (t-t_0+1) & (t-t_0) \\ \hline (t_0-t) & (t_0-t+1) \end{array}\right]x_0 + e^{t-t_0}\begin{bmatrix} 1 & 1 \\ -1 & -1 \end{bmatrix} x_0$$

and by letting $x_0 = [a\ b]^T$, we have

$$p^T(t)\dot{x}(t) = \alpha(a+b) = const. \tag{6.48}$$

It can also be inferred from Eq. (6.48) that abnormal solutions occur when $a + b = 0$. The above example shows how singular costate trajectories can be computed as adjoint system zeros for both normal and abnormal solutions.

Example 2. Now, we consider the case of a non-invertible system – two integrators linked through a mixed constraint.

$$A = \begin{bmatrix} 0 & 1 \\ 0 & 1 \end{bmatrix}, \quad B = \begin{bmatrix} 1 & 0 \\ 0 & 1 \end{bmatrix}, \quad C = \begin{bmatrix} 1 & 1 \end{bmatrix}, \quad D = \begin{bmatrix} 1 & 1 \end{bmatrix}.$$

The adjoint system $\Sigma^\top$ that satisifies Eq. (6.29) is then given by

$$-A^T = \begin{bmatrix} -1 & 0 \\ 0 & -1 \end{bmatrix}, \quad -C^T = \begin{bmatrix} -1 \\ -1 \end{bmatrix}, \quad B^T = \begin{bmatrix} 1 & 0 \\ 0 & 1 \end{bmatrix}, \quad D^T = \begin{bmatrix} 1 \\ 1 \end{bmatrix}.$$

The adjoint system matrix can be computed as

$$P_{\Sigma^\top}(\lambda) = \begin{bmatrix} \lambda I + A^T & C^T \\ B^T & D^T \end{bmatrix} = \begin{bmatrix} \lambda+1 & 0 & 1 \\ 0 & \lambda+1 & 1 \\ 1 & 0 & 1 \\ 0 & 1 & 1 \end{bmatrix}.$$

It can be found that the system has a zero at $\lambda = 0$ with corresponding zero directions of $[-1 \ -1 \ 1]^T$. Thus, for any $p(t_0) = [-\alpha \ -\alpha]^T$ and any $\nu(t) = \alpha e^{(t-t_0)}$, where $\alpha \in \mathbb{R}$, the output must be zero. Following a similar analysis as in the above example,

$$\begin{aligned} p(t) &= e^{-A^T(t-t_0)}p(t_0) - \int_{t_0}^{t} e^{-A^T(t-\tau)}C^T\nu(\tau)d\tau \\ &= \begin{bmatrix} e^{t_0-t} & 0 \\ 0 & e^{t_0-t} \end{bmatrix} \begin{bmatrix} -\alpha \\ -\alpha \end{bmatrix} + \alpha(e^{t_0-t}-1) \begin{bmatrix} 1 \\ 1 \end{bmatrix} \\ &= \begin{bmatrix} -\alpha \\ -\alpha \end{bmatrix} \end{aligned}$$

Then, the output is given by

$$B^T p(t) + D^T \nu(t) = \begin{bmatrix} 1 & 0 \\ 0 & 1 \end{bmatrix} \begin{bmatrix} -\alpha \\ -\alpha \end{bmatrix} + \begin{bmatrix} 1 \\ 1 \end{bmatrix} \alpha = 0. \tag{6.49}$$

Now, since the Hamiltonian is a constant, $p^T(t)\dot{x}(t)$ is a constant, i.e.,

$$p^T(t)\dot{x}(t) = -\begin{bmatrix} \alpha & \alpha \end{bmatrix} \begin{bmatrix} x_1+u_1 \\ x_2+u_2 \end{bmatrix} = x_1+u_1+x_2+u_2 = const. \tag{6.50}$$

However, this appears to be an infinite-order singular problem for which we have do not have enough information to synthesize a solution.

In the event that the system $\Sigma^\top$ is not strongly observable, it may be possible to introduce system dynamic perturbations so that the perturbed system $\Sigma_\epsilon^\top = (-A_\epsilon^T, -C^T, B_\epsilon^T, D^T)$ is strongly observable. This is motivated by the fact that full rank matrices are dense in the metric space of all matrices with metric $||A_1 - A_0|| + ||B_1 - B_0||$. Since the solutions of ordinary differential equations vary continuously with parameters in the problem [95], the error caused by the perturbation can be made arbitarily small by reducing the size of the perturbation. This technique was introduced by Harris in [67] for non-normal linear time-invariant systems and rigorously justified by Lemma 4 in the paper.

Now, consider the following perturbed adjoint system $\Sigma_\epsilon^\top$

$$-A_\epsilon^T = \begin{bmatrix} -1 & \epsilon \\ 0 & -1 \end{bmatrix}, \quad -C^T = \begin{bmatrix} -1 \\ -1 \end{bmatrix}, \quad B_\epsilon^T = \begin{bmatrix} 1 & 0 \\ 0 & 1 \end{bmatrix}, \quad D^T = \begin{bmatrix} 1 \\ 1 \end{bmatrix}.$$

The adjoint system matrix can be computed as

$$P_{\Sigma_\epsilon^\top}(\lambda) = \begin{bmatrix} \lambda I + A^T & C^T \\ B^T & D^T \end{bmatrix} = \begin{bmatrix} \lambda+1 & \epsilon & 1 \\ 0 & \lambda+1 & 1 \\ 1 & 0 & 1 \\ 0 & 1 & 1 \end{bmatrix}.$$

The system is now strongly observable, i.e., the zeros have been eliminated. This can be verified using any of the tests listed in Lemma 6.5. For example, according to test (iii), rank $P_{\Sigma_\epsilon^\top}(\lambda) = 3 = n + \text{rank } [-C\ D]^T = 2 + 1 = 3$, for all $\lambda \in \mathbb{C}$.

6.10 Conclusions

Sufficient conditions for non-singular optimal control of systems defined on a smooth manifold with mixed constraint and additional control constraints has been presented. This was done in a geometric framework using a minimum principle for problems defined on

manifolds with mixed constraints. It was found that strong observability of the adjoint system is one key property that ensures non-singularity, and the new results generalize a particular lossless convexification result related to annularly constrained systems. It also generalizes the classic controllability/observability conditions for non-singularity in time-optimal and fuel-optimal control problems. Consequently, the main theorem applies to a number of trajectory optimization problems.

CHAPTER 7
FINAL REMARKS

The dissertation presented new developments in the field of relaxations and its applications to some of the important practical problems. In chapter 4, a relaxation technique for solving fixed final time problems between fixed points for annularly constrained systems was presented. This was done by establishing controllability as a sufficient condition for the problem to be solvable as a sequence of convex programs. In chapter 5, relaxation techniques were applied to the Mars ascent problem. This involved transforming the annular thrust acceleration magnitude constraint and approximating the nonlinear centripetal acceleration term with a linearly time-varying estimate. Chapter 6 presented sufficient conditions for non-singular optimal control for problems on a smooth manifold with a mixed constraint and additional control constraints. Each of the above is a unique contribution to the field of relaxations. However, as with any research, this work has identified areas of further interest and potential improvement.

First, the analysis in chapter 5 indicates that the selection of a solid rocket motor, an ignition trigger, and a relatively short burn time negated much of the anticipated improvements from computational guidance. It would be interesting to find how computational guidance performs for a hybrid/liquid configuration of the vehicle and for longer burn times. Also, it might be possible that there exists a different ignition trigger that maximizes SOCP-guidance performance.

Secondly, the results presented in chapter 6 required the dual system to be strongly observable on the cotangent space. For linear manifolds, performing this check is straightforward since the cotangent space is constant and does not evolve with time. However, for higher dimensional manifolds such as quadratic manifolds, this becomes a difficult task as the cotangent space evolves with time and this requires one to know the optimal state

trajectory. Further research is required on how to perform the strong observability check for systems on quadratic manifolds.

Third, earlier work has proved that the normality property of the system can be established as a sufficient condition for non-singular optimal control for problems with disconnected sets [67]. It was also proved that non-normal systems can be approximated as normal systems by introducing system dynamic perturbations [67]. However, earlier work considered systems with linear dynamics. Proving the same for nonlinear systems still remains an open challenge.

Finally, the choice to implement an analytical or a computational guidance scheme depends on the complexity of the vehicle under consideration and the mission objectives. However, successful demonstrations through the flight tests [69, 70, 82, 96] and the recent SpaceX landings [58] shows that computational guidance is a powerful tool that should be further exploited when complex actuator models are involved and when stringent mission objectives need to be met.

REFERENCES

[1] Açıkmeşe, B. and Ploen, S., "Convex programming approach to powered descent guidance for mars landing," *AIAA Journal of Guidance, Control and Dynamics*, Vol. 30, 2007, pp. 1353–1366.

[2] Lu, P. and Liu, X., "Autonomous trajectory planning for rendezvous and proximity operations by conic optimization," *Journal of Guidance, Control, and Dynamics*, Vol. 36, 2013, pp. 375–389.

[3] Schouwenaars, T., Moor, B. D., Feron, E., and How, J., "Mixed integer programming for multi-vehicle path planning," European Control Conference, 2001.

[4] Açıkmeşe, B. and Blackmore, L., "Lossless convexification for a class of optimal control problems with nonconvex control constraints," *Automatica*, Vol. 47, 2011, pp. 341–347.

[5] Boyd, S. and Vandenberghe, L., *Convex Optimization*, Cambridge University Press, 2004.

[6] Nesterov, Y. and Nemirovsky, A., *Interior-point Polynomial Methods in Convex Programming*, SIAM, 1994.

[7] Toh, K. C., Todd, M. J., and Tutuncu, R. H., "SPDT3- A matlab software package for semidefinite programming," *Optimization Methods and Software*, Vol. 11, 1999, pp. 645–681.

[8] Mattingley, J. and Boyd, S., "Cvxgen-A code generator for embedded convex optimization," *Optimization and Engineering*, Vol. 13, 2012, pp. 1–27.

[9] Chu, E., Parikh, N., Domahidi, A., and Boyd, S., "Code Generation for Embedded Second-Order Cone Programming," European Control Conference (Zurich, Switzerland), 2013.

[10] Domahidi, A., Chu, E., and Boyd, S., "ECOS: An SOCP Solver for Embedded Systems," European Control Conference (Zurich, Switzerland), 2013.

[11] Lu, P., "Introducing computational guidance and control," *Journal of Guidance, Control, and Dynamics*, Vol. 40, 2017.

[12] Blackmore, L., Açıkmeşe, B., and Scharf, D., "Minimum landing error powered descent guidance for mars landing using convex optimization," *Journal of Guidance, Control and Dynamics*, Vol. 33, 2010, pp. 1161–1171.

[13] Blackmore, L., Açıkmeşe, B., and Carson, J. M., "Lossless convexification of control constraints for a class of nonlinear optimal control problems," *Automatica*, Vol. 61, 2012, pp. 863–870.

[14] Harris, M. W. and Açıkmeşe, B., "Lossless Convexification for a Class of Optimal Control Problems with Linear State Constraints," IEEE Conferencce on Decision and Control (Florence, Italy), 2013.

[15] Harris, M. W. and Açıkmeşe, B., "Lossless Convexification for a Class of Optimal Control Problems with Quadratic State Constraints," American Control Conference (Washington, D.C.), 2013.

[16] Harris, M. W. and Açıkmeşe, B., "Lossless convexification of non-convex optimal control problems for state constrained linear systems," *Automatica*, Vol. 50, 2014, pp. 2304–2311.

[17] Sargent, R. W. H., "Optimal control," *Journal of Computaional and Applied Mathematics*, Vol. 124, 2000, pp. 361–371.

[18] Jurdjevic, V., *Geometric Control Theory*, Cambridge University Press, 1996.

[19] Young, L. C., *Lecture on the Calculus of Variations and Optimal Control Theory*, AMS Chelsea Publishing, 1969.

[20] McShane, E. J., "On multipliers for lagrange problems," *American Journal of Mathematics*, Vol. 61, 1939, pp. 809–819.

[21] Pontryagin, L. S., Boltyanskii, V. G., Gamkrelidze, R. V., and Mischenko, E. F., *The Mathematical Theory of Optimal Processes*, Gordon and Breach Science Publishers, 1986.

[22] Meditch, J., "On the problem of optimal thrust programming for a lunar soft landing," *IEEE Transactions on Automatic Control*, Vol. 9, 1964, pp. 477–484.

[23] Hull, D. G., "Thrust programs for minimum propellant consumption during the vertical take-off and landing of a rocket," *Journal of Optimization theory and Applications*, Vol. 1, 1967, pp. 53–69.

[24] Klumpp, A. R., "Apollo lunar descent guidance," *Automatica*, Vol. 10, 1974, pp. 133–146.

[25] Cherry, G. W., "A general, explicit, optimizing guidance law for rocket-propelled spaceflight," Guidance, Navigation, and Control Conference, AIAA Paper 1997-3709, 1997.

[26] D'Souza, C. S., "An optimal guidance law for planetary landing," Astrodynamics, Guidance and Control Conference, AIAA Paper 1964-0638, 1964.

[27] Liu, X., Lu, P., and Pan, B., "Survey of convex optimization for aerospace applications," *Astrodynamics*, Vol. 1, 2017, pp. 23–40.

[28] Açıkmeşe, B., Carson, J., and Blackmore, L., "Lossless convexification of nonconvex control bound and pointing constraints of the soft landing optimal control problem," *IEEE Transactions on Control Systems Technology*, Vol. 21, 2013, pp. 2104–2113.

[29] Harris, M. W. and Açıkmeşe, B., "Maximum divert for planetary landing using convex optimization," *Journal of Optimization Theory and Applications*, Vol. 162, 2013, pp. 975–995.

[30] Liu, X. and Lu, P., "Solving nonconvex optimal control problems by convex optimization," *Journal of Guidance, Control, and Dynamics*, Vol. 37, 2014, pp. 750–765.

[31] Liu, X. and Lu, P., "Robust Trajectory Optimization for Highly Constrained Rendezvous and Proximity Operations," AIAA Guidance, Navigation, and Control (GNC) Conference, AIAA 2013-4720, 2013.

[32] Pinson, R. and Lu, P., "Rapid generation of optimal asteroid powered descent trajectories," AAS/AIAA Astrodynamics Specialist Conference, AAS 15-616, 2015.

[33] Pinson, R. and Lu, P., "Trajectory design employing convex optimization for landing on irregularly shaped asteroids," AAS/AIAA Astrodynamics Specialist Conference, AIAA 2016-5378, 2016.

[34] Betts, J. T., "Survey of numerical methods for trajectory optimization," *Journal of Guidance, Control and Dynamics*, Vol. 21, 1998, pp. 193–207.

[35] Vlassenbroeck, J. and Dooren, R. V., "A chebyshev technique for solving nonlinear optimal control problems," *IEEE Transactions on Automatic Control*, Vol. 33, 1998, pp. 333–340.

[36] Hull, D. G., "Conversion of optimal control problems into parameter optimization problems," *Journal of Guidance, Control and Dynamics*, Vol. 20, 1997, pp. 57–60.

[37] Peng, J., Roos, C., and Terlaky, T., *Self-regularity: A New Paradigm for Primal-dual Interior-point Algorithms*, Princeton Series in Applied Mathematics, 2001.

[38] Kreim, H., Kugelmann, B., Pesch, H. J., and Breitner, M. H., "Minimizing the Maximum Heating of a Reentry Space Shuttle: An Optimal Control Problem with Multiple Control Constraints," *Optimal Control Applications and Methods*, Vol. 17, 1996, pp. 45–69.

[39] Bonard, B., Faubourg, L., Launay, G., and Trelat, E., "Optimal Control with State Constraints and the Space Shuttle Re–Entry Problem," *Journal of Dynamical and Control Systems*, Vol. 9, 2003, pp. 155–199.

[40] Graichen, K. and Petit, N., "Constructive Methods for Initialization and Handling Mixed State-Input Constraints in Optimal Control," *Journal of Guidance, Control, and Dynamics*, Vol. 31, 2008, pp. 1334–1343.

[41] Açıkmeşe, B. and Ploen, S. R., "A powered descent guidance algorithm for mars pinpoint landing," AIAA Guidance, Navigation, and Control Conference (San Francisco, California), 2005.

[42] Augugliaro, F., Schoellig, A. P., and D'Andrea, R., "Generation of Collision-Free Trajectories for a Quadrocopter Fleet : A Sequential Convex Programming Approach," IEEE/RSJ Int. Conf. on Intelligent Robots and Systems, 2012.

[43] Mellinger, D., Michael, N., and Kumar, V., "Trajectory Generation and Control for Precise Aggresive Maneuvers with Quadrotors," *Int. Journal of Robotics Research*, Vol. 5, 2012, pp. 664–674.

[44] Shen, S., Mulgaonkar, Y., Michael, N., and Kumar, V., "Vision–Based State Estimation and Trajectory Control Towards High–Speed Flight with a Quadrotor," Robotics: Science and Systems, 2013.

[45] Watterson, M., Liu, S., Sun, K., Smith, T., and Kumar, V., "Trajectory Optimization on Manifolds with Applications to SO(3) and R3XS2," Robotics: Science and Systems, 2018.

[46] Misra, G. and Bai, X., "Task–Constrained Trajectory Planning of Free–Floating Space-Robotic Systems using Convex Optimization," *AIAA Journal of Guidance, Control, and Dynamcis*, Vol. 40, 2017, pp. 2857–2870.

[47] Trentelman, H. L., Stoorvogel, A. A., and Hautus, M., *Control Theory for Linear Systems*, Springer, 2001.

[48] Liberzon, D., *Calculus of Variations and Optimal Control theory*, Princeton University Press, 2012.

[49] Guillemin, V. and Pollack, A., *Differential topology*, Prentice Hall, 1974.

[50] Milnor, J. W., *Topology from the Differential Viewpoint*, University Press of Virginia, 1963.

[51] Carmo, M. P. D., *Riemannian Geometry*, Birkhauser, 1992.

[52] Boothby, W. M., *An Introduction to Differentiable Manifolds and Riemannian Geometry*, Academic Press, 1986.

[53] Bonalli, R., *Optimal Control of Aerospace Systems with Control-State Constraints and Delays*, Ph.D. thesis, Sorbonne Université, UPMC University of Paris 6, ONERA –The French Aerospace Lab, Paris, France, 2018.

[54] Dmitruk, A. V., "Maximum principle for the general optimal control problem with phase and regular mixed constraints," *Computational Mathematics and Modeling*, Vol. 4, 1993, pp. 364–377.

[55] Hartl, R., Sethi, S., and Vickson, R., "A Survey of the Maximum Principles for Optimal Control Problems with State Constraints," *SIAM Review*, Vol. 37, No. 2, June 1995, pp. 181–218.

[56] Milyutin, A. A. and Osmolovskii, N. P., *Calculus of Variations and Optimal Control*, American Mathematical Society, 1998.

[57] Ploen, S. R., Açıkmeşe, B., and Wolf, A., "A comparison of powered descent guidance laws for mars pinpoint landing," AIAA Guidance, Navigation, and Control Conference (Keystone, Colorado), 2006.

[58] Blackmore, L., "Autonomous Precision Landing of Space Rockets," *The Bridge : Linking Engineering and Society (National Academy of Engineering)*, Vol. 26, 2016.

[59] Lu, P., "Theory of Fraction-Polynomial Powered Descent Guidance," *Journal of Guidance, Control, and Dynamics*, Vol. 43, 2020, pp. 398–409.

[60] Martin, D. T., Sievers, R. F., O'Brien, R. M., and Rice, A. L., "Saturn V Guidance, Navigation, and Targeting," *Journal of Spacecraft and Rockets*, Vol. 4, 1967, pp. 891–898.

[61] Chandler, D. C. and Smith, I. E., "Development of the Iterative Guidance Mode with its Applications to Various Vehicles and Missions," *Journal of Spacecraft and Rockets*, Vol. 4, 1967, pp. 898–903.

[62] McHenry, R. L., Brand, T. J., Long, A. D., Cockrell, B. F., and Thibodeau, J. R., "Space Shuttle Ascent Guidance, Navigation, and Control," *Journal of the Astronautical Sciences*, Vol. 27, 1979, pp. 1–38.

[63] Hull, D., "Optimal Guidance for Quasi-Planar Lunar Descent With Throttling," AAS/AIAA Space Flight Mechanics Meeting, AAS 11-169, 2011.

[64] Lu, P., "Augmented apollo powered descent guidance," *Journal of Guidance, Control, and Dynamics*, Vol. 42, 2019, pp. 447–457.

[65] Bixby, R. E., "A Brief History of Linear and Mixed-Integer Programming Computation," *Documenta Mathematica*, 2012, pp. 107–121.

[66] Malyuta, D. and Açıkmeşe, B., "Lossless Convexi

cation of Optimal Control Problems with Semi-continuous Inputs," IFAC World Congress 2020, 2020.

[67] Harris, M. W., "Optimal control on disconnected sets using extreme point relaxations and normality approximations," *IEEE Transactions on Automatic Control*, To Appear 2021.

[68] Dueri, D., Açıkmeşe, B., Scharf, D., and Harris, M. W., "Customized Real-time Interior-point Method for Onboard Powered Descent Guidance," *Journal of Guidance, Control and Dynamics*, Vol. 40, 2017, pp. 197–212.

[69] Açıkmeşe, B., Aung, M., Casoliva, J., Mohan, S., Johnson, A., Scharf, D., Masten, D., Scotkin, J., Wolf, A., and Regehr, M. W., "Flight testing of trajectories computed by G-FOLD: Fuel optimal large divert guidance algorithm for planetary landing," AAS/AIAA Spaceflight Mechanics Meeting, 2013.

[70] Scharf, D. P., Regehr, M. W., Dueri, D., Açıkmeşe, B., Vaughan, G. M., and Benito, J., "ADAPT: Demonstrations of onboard large-divert guidance with a resuable launch vehicle," IEEE Aerospace Conference, 2014.

[71] Açıkmeşe, B., Aung, M., Casoliva, J., Mohan, S., Johnson, A., Scharf, D., Masten, D., Scotkin, J., Wolf, A., and Regehr, M. W., "Flight testing of trajectories computed by G-FOLD: Fuel optimal large divert guidance algorithm for planetary landing," AAS/AIAA spaceflight mechanics meeting, 2013.

[72] Hermes, H. and LaSalle, J. P., *Functional Analysis and Time Optimal Control*, Academic Press, 1969.

[73] LLC, G. O., "Gurobi Optimization Reference Manual," 2019.

[74] *MATLAB 2019a*, The Mathworks, Inc., 2019.

[75] Antsaklis, P. and Michel, A., *A Linear Systems Primer*, Birkhauser, 2007.

[76] Sarachik, P. E. and Kreindler, E., "Controllability and Observability of Linear Discrete-time Systems," *International Journal of Control*, 1965.

[77] Brockett, R. W., *Finite Dimensional Linear Systems*, John Wiley and Sons, Inc., 1970.

[78] Anzalone, E., Erickson, D., Everett, J., and Powers, J., "Guidance and Navigation Challenges for a Mars Ascent Vehicle," 2020 IEEE Aerospace Conference, Big Sky, MT 2020, pp. 1–14.

[79] Yaghoubi, D. and Schnell, A., "Mars Ascent Vehicle Solid Propulsion Configuration," 2020 IEEE Aerospace Conference, Big Sky, MT 2020, pp. 1–11.

[80] Battin, R. H., *An Introduction to the Mathematics and Methods of Astrodynamics, Revised Edition*, American Institute of Aeronautics and Astronautics, 1999.

[81] Hull, D. G. and Harris, M. W., "Optimal Solutions for Quasi-Planar Ascent Over a Spherical Moon," *Journal of Guidance, Control, and Dynamics*, Vol. 35, July- August 2012, pp. 1218–1223.

[82] Carson, J. M., Açıkmeşe, B., and Blackmore, L., "Mars Ultra-Precision EDL Research Report: A Smart-Divert Capability for Powered Descent Guidance," Tech. rep., JPL Document D-66203, not cleared for external release, Jet Propulsion Laboratory, California Institute of Technology, 2010.

[83] Martin, F. H., "Closed-Loop Near-Optimum Steering for a Class of Space Missions," *AIAA Journal*, Vol. 4, No. 11, 1966, pp. 1920–1927.

[84] Laning, J. H. and Battin, R. H., "Optimum Fuel Trajectories for a Q-Type Guidance System," Tech. rep., Engineering Memorandum E-520, MIT Instrumentation Laboratory, 1956.

[85] Sokappa, B. G., "On Optimal Steering to Achieve "Required Velocity"," Tech. rep., Tech. Rep.R-491, MIT Instrumentation Laboratory, 1965.

[86] Everett, J. M., "A Generalized Guidance Approach to In-Space Solid-Propellant Vehicle Maneuvers," AAS Guidance, Navigation, and Control Conference, 2020.

[87] Berkovitz, L. D., *Optimal Control Theory*, Springer-Verlag, 1975.

[88] Athans, M. and Falb, P. L., *Optimal Control: An Introduction to the Theory and Its Applications*, McGraw-Hill, 1966.

[89] Hernandez, D., Bejarano, F. J., Davila, J., and Fridman, L. M., "On the strong observability in linear time-varying singular systems," *Automatica*, Vol. 101, 2019, pp. 60–65.

[90] Wu, M. Y., "Transformation of a Linear Time-Varying System into a Linear Time-Invariant System," *Int. J. Control*, Vol. 27, 1978, pp. 589–602.

[91] Jr, R. T. O. and Iglesias, P. A., "On the Poles and Zeros of Linear, Time-Varying Systems," *IEEE Transactions on Circuits and Systems-I: Fundamental Theory and Applications*, Vol. 48, 2001, pp. 565–577.

[92] Weiss, L. and Falb, P. L., "Dolezal's Theorem linear algebra with continuously parameterized elements, and time-varying systems," *Theory of Computing Systems*, Vol. 3, 1998, pp. 67–75.

[93] Kratz, W. and Liebscher, D., "A local characterization of observability," *Linear Algebra and Its Applications*, Vol. 269, 1998, pp. 115–137.

[94] Lee, E. B. and Markus, L., *Foundations of Optimal Control Theory*, John Wiley and Sons, Inc., 1967.

[95] Nagle, R. K., Saff, E. B., and Snider, A. D., *Fundamentals of Differential Equations and Boundary Value Problems*, Addison Wesley, 2000.

[96] Scharf, D. P., Açıkmeşe, B., Benito, J., and Casoliva, J., "Implementation and Experimental Demonstration of Onboard Powered-descent Guidance," *Journal of Guidance, Control, and Dynamics*, Vol. 40, No. 2, 2016, pp. 213–229.

APPENDICES

APPENDIX A

Thrust Integrals

The standard thrust integrals L, S, J, and Q are first and second integrals of the thrust to mass ratio τ, that is,

$$\begin{aligned} L &= \int_0^{t_f} \tau \, dt = -V_e \ln(1 - t_f/\alpha)) \\ S &= \int_0^{t_f} \int_0^t \tau \, dt \, dt = (-\alpha + t_f)L + V_e t_f \\ J &= \int_0^{t_f} \tau t \, dt = -S + t_f L \\ Q &= \int_0^{t_f} \int_0^t \tau t \, dt \, dt = -V_e t_f^2/2 + \alpha S. \end{aligned} \tag{A.1}$$

The thrust integrals are functions of t_f.

The modified thrust integrals (denoted by primes) are analogous to the ordinary thrust integrals and are defined as

$$\begin{aligned} L' &= \int_0^{t_f} \tau/\bar{\lambda}_4 \, dt, \quad S' = \int_0^{t_f} \int_0^t \tau/\bar{\lambda}_4 \, dt \, dt \\ J' &= \int_0^{t_f} \tau t/\bar{\lambda}_4 \, dt, \quad Q' = \int_0^{t_f} \int_0^t \tau t/\bar{\lambda}_4 \, dt \, dt. \end{aligned} \tag{A.2}$$

The modified thrust integrals are functions of $t_f, \bar{\lambda}_2, \bar{C}_2$. These integrals cannot be evaluated analytically because of the division by $\bar{\lambda}_4$ in the integrand. They must be evaluated numerically.

The single integrals can be evaluated using any standard quadrature technique such as the trapezoidal rule or Simpson's rule. Fortunately, double integrals can be rewritten as single integrals by applying integration by parts as

$$\int_0^{t_f} \int_0^t f(t) \, dt \, dt = t_f \int_0^{t_f} f(t) \, dt - \int_0^{t_f} t f(t) \, dt. \tag{A.3}$$

With the following definition:

$$H' = \int_0^{t_f} \tau t^2/\bar{\lambda}_4 \, dt, \tag{A.4}$$

the two double integrals can then be evaluated using three quadratures, that is,

$$S' = t_f L' - J', \quad Q' = t_f J' - H'. \tag{A.5}$$

APPENDIX B

Integrals of Centrifugal Acceleration

The centrifugal acceleration integrals F and G are the first and second integrals of the function

$$f(t) = [u_0 - V_e \ln(1 - t_f/\alpha)]^2/r_m. \tag{B.1}$$

The integrals are given by

$$\begin{aligned} F &= \textstyle\int_0^{t_f} f\ dt = (u_0^2 t_f - 2u_0 V_e I_1 + V_e^2 I_2)/r_m \\ G &= \textstyle\int_0^{t_f} \int_0^t f\ dt\ dt = (u_0^2 t_f^2/2 - 2u_0 V_e I_3 + V_e^2 I_4)/r_m \end{aligned} \tag{B.2}$$

and are functions of t_f, since the integrals I_1 through I_4 are the following functions of t_f:

$$\begin{aligned} I_1 &= -\alpha[(1 - t_f/\alpha)\ln(1 - t_f/\alpha) - (1 - t_f/\alpha) + 1] \\ I_2 &= -\alpha[(1 - t_f/\alpha)\ln^2(1 - t_f/\alpha) - 2(1 - t_f/\alpha)\ln(1 - t_f/\alpha) \\ &\quad +2(1 - t_f/\alpha) - 2] \\ I_3 &= -\alpha[I_5 - I_6 + t_f] \\ I_4 &= -\alpha[I_7 - 2I_5 + 2I_6 - 2t_f] \\ I_5 &= -\alpha[2(1 - t_f/\alpha)^2 \ln(1 - t_f/\alpha) - (1 - t_f/\alpha)^2 + 1]/4 \\ I_6 &= -\alpha[(1 - t_f/\alpha)^2 - 1]/2 \\ I_7 &= -\alpha[2(1 - t_f/\alpha)^2 \ln^2(1 - t_f/\alpha) - 2(1 - t_f/\alpha)^2 \ln(1 - t_f/\alpha) \\ &\quad +(1 - t_f/\alpha)^2 - 1]/4. \end{aligned} \tag{B.3}$$

APPENDIX C

Numerical Solution Method

To numerically solve an infinite-dimensional problem, it is converted to a finite-dimensional parameter optimization problem. This is done by discretizing the problem and enforcing the constraints at the nodes. Note that the constraints in all of the examples are first or second-order cone constraints. Therefore, the resulting problems after discretization are finite-dimensional second-order cone programs that can be solved to global optimality using the powerful interior-point methods in convex optimization [5, 7]. We use a simple discretization method which is summarized below.

The time domain $[0, t_f]$ is discretized into $N+1$ nodes separated by Δt.

$$t_i = (i-1)\Delta t, \quad i = 1, ..., N+1$$

The states at time t_i are denoted by $x[i]$ and they exist at all nodes $i = 1, ..., N+1$. The controls at time t_i are denoted by $u[i]$ and they exist at nodes $i = 1, ..., N$. The controls are held constant over every interval. The system dynamics are discretized using the fundamental matrix resulting in

$$x[i+1] = A_d x[i] + B_d u[i], \quad i = 1, ..., N$$

where A_d and B_d are matrices given by

$$A_d = e^{A\Delta t}, \quad B_d = \int_0^{\Delta t} e^{A\tau} B d\tau.$$

The integral cost can be approximated by using any numerical integration technique, e.g., trapezoidal integration:

$$\int_0^{t_f} \ell(w(t)) \approx \frac{\Delta t}{2} \sum_{i=1}^{N} \Big(\ell(w[i+1]) + \ell(w[i]) \Big).$$

All other constraints are enforced at the nodes. For example, control constraints are written as

$$||u[i]|| \leq w[i], \quad \forall\, i = 1, ..., N$$
$$\rho_1 \leq w[i] \leq \rho_2, \quad \forall\, i = 1, ..., N$$

The result is a finite-dimensional approximation to the infinite-dimensional optimal control problem.

APPENDIX D

Velocity-to-go First Order Partial

The partial of the magnitude of the velocity-to-go vector $\frac{\partial||v_g||}{\partial t}$ can be re-written as

$$\frac{\partial||v_g||}{\partial t} = i_g \cdot \frac{\partial v_g}{\partial t} \tag{D.1}$$

Noting that

$$v_g = v_r - v = ||v_r||i_z - v, \tag{D.2}$$

its derivative can be written as

$$\frac{\partial v_g}{\partial t} = \frac{\partial||v_r||}{\partial t} i_z + ||v_r|| \frac{\partial i_z}{\partial t} - \frac{\partial v}{\partial t}. \tag{D.3}$$

Now, the individual components of Eq. (D.3) are derived.

Assuming a spherical gravity model,

$$\frac{\partial v}{\partial t} = -\frac{\mu}{||r||^3} r. \tag{D.4}$$

Next,

$$\frac{\partial||v_r||}{\partial t} = \frac{\partial||v_r||}{\partial r}\frac{\partial r}{\partial t} = \frac{\partial||v_r||}{\partial r}\left(i_r \cdot \frac{\partial r}{\partial t}\right) = \frac{\partial||v_r||}{\partial r}(i_r \cdot v). \tag{D.5}$$

Noting that

$$||v_r|| = \sqrt{\mu\left(\frac{2}{||r||} - \frac{1}{a_d}\right)} \tag{D.6}$$

where a_d is the desired semi-major axis,

$$\frac{\partial||v_r||}{\partial r} = \frac{1}{2||v_r||}\left(-\frac{2\mu}{||r||^2}\right) = -\frac{\mu}{||v_r||||r||^2}. \tag{D.7}$$

Therefore, Eq. (D.3) becomes

$$\frac{\partial v_g}{\partial t} = -\frac{\mu}{||v_r||||r||^2}(i_r \cdot v)i_z + ||v_r||\frac{\partial i_z}{\partial t} + \frac{\mu}{||r||^3}r. \tag{D.8}$$

The last term to be found is $\frac{\partial i_z}{\partial t}$. Re-writing i_z as

$$i_z = \frac{r \times i_y}{||r \times i_y||}, \tag{D.9}$$

and noting the following derivatives,

$$\frac{\partial}{\partial t}(r \times i_y) = v \times i_y$$
$$\frac{\partial}{\partial t}(||r \times i_y||) = \frac{r \times i_y}{||r \times i_y||}(v \times i_y)$$

an expression for $\frac{\partial i_z}{\partial t}$ is obtained as follows

$$\frac{\partial i_z}{\partial t} = \frac{(v \times i_y)}{||r \times i_y||} - \frac{(r \times i_y)}{||r \times i_y||^2}\left(\frac{(r \times i_y)}{||r \times i_y||}(v \times i_y)\right) \tag{D.10}$$

Eq. (D.10) is further simplied using vector cross product identities. More details can be found in [86]. The resulting expression for $\frac{\partial i_z}{\partial t}$ is given by

$$\frac{\partial i_z}{\partial t} = -\frac{v \cdot i_z}{r \cdot i_x}i_x. \tag{D.11}$$

Finally, Eq. (D.8) can be written as

$$\frac{\partial v_g}{\partial t} = -\frac{\mu}{||v_r||||r||^2}[i_r \cdot v]i_z - ||v_r||\frac{(v \cdot i_z)}{(r \cdot i_x)}i_x + \frac{\mu}{||r||^3}r. \tag{D.12}$$

CURRICULUM VITAE

Sheril Avikkal Kunhippurayil

Journal Articles

- **S. Kunhippurayil**, M. Harris, O. Jansson, "Lossless Convexification of Optimal Control Problems with Annular Control Constraints," Automatica, accepted.
- **S. Kunhippurayil**, M. Harris, "Strong Observability as a Sufficient Condition for Non-singularity in Optimal Control with Mixed Constraints," Automatica, submitted.